DEVELOPMENT AND TESTING OF A LOW-COST WRIST-ELBOW REHABILITATION DEVICE

by

Seth Christopher Paul

A thesis submitted to the faculty of
The University of Utah
in partial fulfillment of the requirements for the degree of

Master of Science

Department of Mechanical Engineering

The University of Utah

May 2015

The University of Utah Graduate School

STATEMENT OF THESIS APPROVAL

The thesis of **Seth Christopher Paul**

has been approved by the following supervisory committee members:

Andrew Merryweather	, Chair	**12/31/14** Date Approved
Sanford Meek	, Member	**12/31/14** Date Approved
Donald Bloswick	, Member	**12/31/14** Date Approved

and by **Tim Ameel** , Chair/Dean of

the Department/College/School of **Mechanical Engineering**

and by David B. Kieda, Dean of The Graduate School.

ABSTRACT

Lateral epicondylalgia (LE), commonly known as tennis elbow, is an upper extremity musculoskeletal disorder that affects 1-3% of the general population. Despite the prevalence and persistence, specific diagnoses and a preferred treatment approach remain in question.

Eccentric wrist extension therapy has recently shown promise in rehabilitation of LE. A device has been developed to assist in future research of eccentric therapy protocols. This device is capable of simulating conventional eccentric loading methods while offering additional functionality and features. A motion capture and surface electromyography study has been conducted to evaluate the ability of the device to supply comparable stimuli to three conventional loading methods.

Study results indicate the developed device is capable of producing similar wrist kinematics and forearm extensor muscle potential to all three conventional methods. Wrist motion during wrist extensions shows some differences though not statistically significant. The similar wrist kinematics and forearm extensor muscle electromyography produced while using the device support the need for further studies and development of the device's relevance in rehabilitation of LE.

CONTENTS

LIST OF FIGURES

LIST OF TABLES

CHAPTER 1

INTRODUCTION AND BACKGROUND

Lateral epicondylalgia is a painful disorder with no current gold standard for treatment. A device was developed to characterize the effects of novel treatment methods that have recently shown promise, eccentric exercise therapy. This document will describe the initial development and testing of this device.

1.1 Lateral Epicondylalgia (Tennis Elbow)

Lateral epicondylalgia, referred to as LE through the remainder of this document, also commonly known as tennis elbow, is a common upper extremity disorder that affects 1-3% of the general population [1]. The majority of those affected are ages 35 to 54 [2]. Hamilton found that this is a recurring condition with over half of the cases followed for 18 months suffering a recurrence and over a third of the cases followed for six months suffering one or more recurrences [2]. LE involves pathological changes at the insertion of the extensor carpi radialis brevis and extensor digitorum tendon [3]. Despite the prevalence and persistence, specific diagnoses and a preferred treatment course remain in question [4–8].

At least 22 treatment methods have been investigated through randomized clinical trials (RTC) [9]. In addition to surgical interventions, there are many common conservative treatment methods. These conservative treatment methods include: NSAIDs, steroid injections, conic therapies, stretching, exercise, acupuncture, and wait-and-see approaches. Most treatments have little or weak supporting evidence [4, 5, 8, 10]. In addition to inconsistent results, some treatments result in negative side-effects [11].

More recently, studies related to loading the muscle-tendon unit via eccentric wrist contractions have shown promise in treatment of tendinopathies [12–23], though additional research is necessary [24]. A recent comprehensive review of tendinopathy treatment with eccentric loading conducted by Murtaugh indicates that eccentric exercise has shown promis-

ing benefits as an intervention to several tendinopathies but further research is necessary to determine optimal protocol characteristics [25].

1.2 Eccentric Treatment Methods

Researchers studying the effects of eccentric interventions most commonly follow the original frequency protocol developed by Alfredson [26]. Frohm compared Alfredson's original protocol to a lower repetition, higher weight alternative and was able to achieve similar results [15]. Frohm's results raise the question of how protocols might be modified to increase benefit while also decreasing patient therapy time and/or effort. A robotic device allows easy variability of frequency, speed, and load to assist future research in this field.

Along with frequency and intensity, the method of loading remains variable and unexplored. Current eccentric interventions utilize modified strength training equipment [13], free weights [17, 19, 22, 23], or elastic members [18, 21, 27]. These loading methods have differing load characteristics [28] including their torque-angle profiles during wrist extension. Three example torque-angle profiles of common conventional loading methods are shown in Figure 1.1. A literature review conducted related to LE eccentric loading interventions shows no existing comparisons of existing loading methods. It is unclear if one method is more beneficial than another. The developed device is designed to allow modification of the torque-angle profile to match any conventional and nonconventional load profile to further our understanding of this costly disorder.

1.3 Robots in Rehabilitation

A recent robotic therapy review conducted by Reinkensmeyer touted the potential of robotic therapies to reduce costs while offering more intensive and more engaging therapies [29]. With robotic assisted therapies, a therapist is not required to supervise as closely, reducing the provider and patient costs for rehabilitation. There have been a plethora of robotic devices developed to assist in patient rehabilitation [29–35]. Many of these devices are designed for rehabilitation from stroke, spinal cord injury, or other neurological maladies. This type of rehabilitation often requires multiple degrees of freedom as the machine moves through the complex motions of the human arm [32]. For the developed device, the focus was solely on flexion-extension of the wrist. This simpler system allows a reduced cost, a reduced overall weight, and a reduced control complexity.

1.4 Device Summary

A device was developed to assist in the research and treatment of LE. The objectives of this device include:

- Variable speed, frequency, and load of wrist extensions
- Simulate conventional loading methods
- Simulate loading methods not yet tested
- Assist motions when desired
- Track and save patient performance metrics for study and evaluation

Upon meeting these objectives, the device will be capable of assisting future research efforts in LE and similar tendinopathies as a whole.

The following manuscript is organized into sections.

- Chapter 2: Hardware and software development of the device.
- Chapter 3: Device performance evaluation- A study conducted to quantify the device's ability to simulate conventional loading methods
- Chapters 4 and 5: Summary of results and discussion of the device's relevance in a clinical setting.

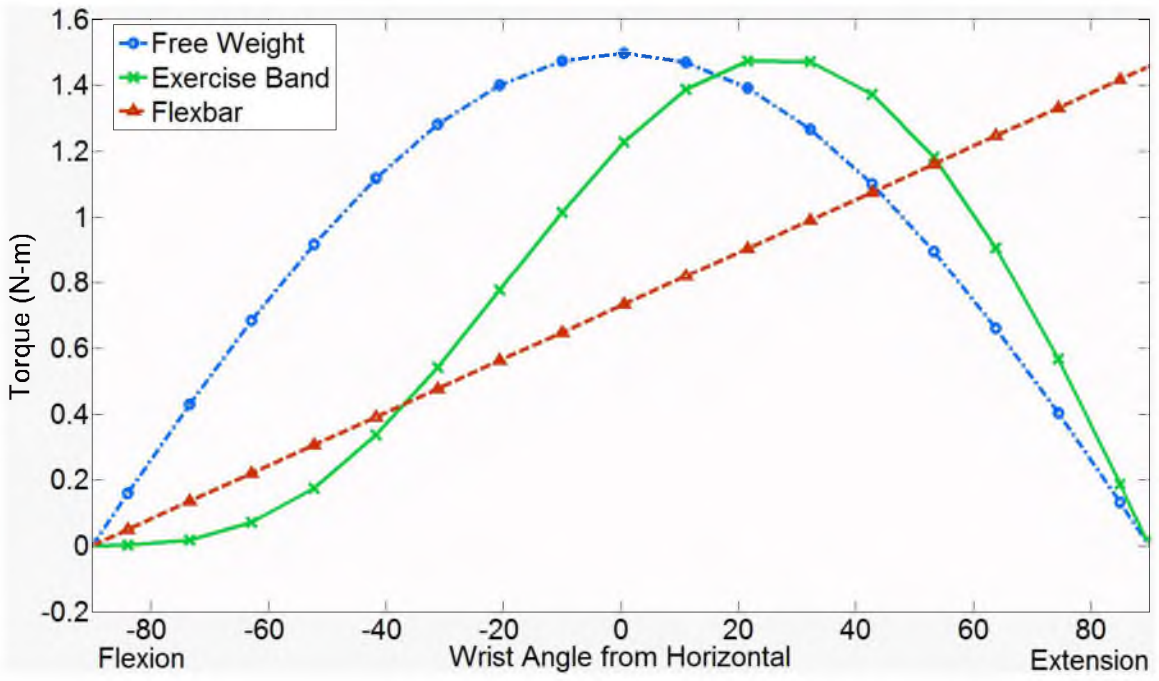

Figure 1.1. Example torque applied to the wrist through the range of motion for a Free Weight, Stretch Band, and Flexbar®

CHAPTER 2

DEVICE DEVELOPMENT

2.1 System Overview

The device performed two primary functions implemented through two subsystems: the computer and the resistance device. The computer provides a graphic user interface to input parameters, constructs a control scheme from those parameters, and controls the resistance device through an output command voltage. The resistance device converts the command voltage to a torque output applied to the participant through the device handle and armrest. A system diagram is shown in Figure 2.1

2.1.1 Physical Requirements

Benchmark speeds and expected torques were gathered from the existing lateral epicondylalgia eccentric intervention studies. These values included isometric [6,36,37], concentric extension [6, 13, 21, 36–39], and eccentric extension [13] strength. The average maximal isometric concentric torque across the literature was 10.6 N-m [6, 36, 37]. The average eccentric torque at 60 degrees per second found by Croisier et al. was 17.4 N-m [13]. A continuous torque of 20 N-m was chosen as the design specification to meet the testing and demands of a majority of the population. Few eccentric data were found. Eccentric strength is considered difficult to measure safely with conventional methods [40]. This may account for the meager data currently available. The maximum isokinetic test velocities found in the eccentric interventions were found to be 180 degrees per second [39].

A single axis design was chosen for this device iteration. Studies have shown there is translation accompanying rotation, particularly under load [41, 42]. However, these translations have been found to be small [43, 44]. The small magnitude of the translation would indicate that this simplification may be acceptable.

The required range of motion was defined from Brigstocke's research in wrist flexion-extension. Brigstocke et al. found mean flexion to be 84 degrees ± 8.6 SD and mean extension to be 48 degrees ± 10.6 SD [45]. A maximum wrist extension of 98 degrees and

maximum wrist flexion of 65.4 degrees were chosen to meet the anthropometry of the 95 percentile most flexible portion of the population. The device was designed to be adjustable to fit a 5 percentile female up to a 95 percentile male. The handle was designed to allow a grip to wrist-center length of 5.87 to 7.82 cm [46]. Restraints were designed to accommodate a forearm length, specifically radiale-stylion length, of 21.87 to 29.69 cm [46]. The wrist restraint was designed to accommodate wrist circumferences of 14.02 to 18.85 cm [46, 47]. The forearm restraint was designed to accommodate flexed forearm circumferences of 22.99 to 33.60 cm [46].

2.1.2 Torque Generation

A 150 Watt RE 40 graphite brushed DC motor (Maxon Motor, San Mateo, CA) was chosen to generate the device torque. The motor was capable of supplying a maximum continuous torque of 177 mN-m. The expectation of potentially near zero speeds during eccentric contractions indicated that the 20 N-m design specification should be within the maximum continuous torque opposed to the stall torque of the motor. A Maxon 1:230 planetary gearhead converted the 177 mN-m continuous torque to 40.7 N-m. The 64% maximum efficiency of the gearhead reported by Maxon reduced the maximum continuous torque down to 26 N-m.

The motor was capable of a no load speed of 7580 revolutions per minute. The 1:230 gear ratio converted this to 198 degrees per second. The 198 degree per second capability exceeded the design specification of 180 degrees per second described in Section 2.1.1. The system was capable of supplying 16 N-m at 186 degrees per second under worst case conditions and under normal conditions was capable of the 20 N-m at 180 degrees per second design specifications. A Maxon HEDL 5540 quadrature encoder was chosen to measure the axle orientation. The HEDL 5540 quadrature encoder supplied 1000 counts per motor turn for each of the two channels available. The 1:230 gear ratio converted this to 460 thousand counts per full revolution or 209 thousand counts within the 164 degree operating range.

2.1.2.1 Power Regeneration

Commanded deceleration of the handle generates power that then feeds back to the servo drive and the power supply. The current power supply has an overvoltage protection at 30.25 - 35.5V. Upon raising the voltage to these levels, the power supply shuts down until the excess energy is dissipated. This occurs in the range of tenths of a second. This is, however, a limitation of the system. In high-torque, high-speed conditions, the system motion is choppy and unpleasant. These high-torque, high-speed conditions were not the intended

use of the device or the conditions to be tested and thus did not affect the conducted study.

2.1.3 Data Acquisition

Initial iterations for motor control included use of Mathworks' Matlab (version 8.3.0.532), Simulink (version 8.3), and Data Acquisition Toolbox (version 3.5) (The Mathworks, Inc., Natick, MA), a National Instruments USB 6008 (National Instruments, Austin, TX), and a Arduino Uno or Due (Arduino, Torino, Italy). An Advanced Motion Control 30A8 analog servo drive (Advance Motion Control, Camarillo, CA) was used to amplify the command signal to the power the motor. The USB 6008 was used to send the command voltages to the servo drive. Initially, the Arduino Uno was used to read the encoder location. It quickly became apparent that the encoder counts were occurring much faster than the Uno could update the position. An Arduino Due with a hardware decoder was then attempted. This iteration was able to accurately measure the handle position, yet performance issues remained.

The next hurdle came with instability in the system after successive high-speed rotations. It became clear that the software and hardware were not able to sample and command the motor quickly enough, resulting in instability. For faster step iterations, the control software was changed from Mathworks' Data Acquisition Toolbox to Mathworks' Real-Time Windows Toolbox (version 4.4). The hardware was also upgraded. The data acquisition and command signal were now transmitted through a National Instruments PCIe-6323 data acquisition card and BNC-2110 break out board. The updated system was capable of analog sampling rates of 2.5 MHz and analog output rates of 100 kHz. A slower speed was used to control the device, 10 kHz, as at the higher speeds, the computer was much less stable.

2.1.4 General Control Scheme

Two main control schemes were used for control of this resistance device. Both schemes follow a closed loop structure. One control scheme was for torque-based explicit torque control with feedback from a torque transducer, shown in Figure 2.2. The torque control scheme was used to control the device during the study discussed later in this document. The second control scheme was angular velocity motion control with feedback from the encoder, shown in Figure 2.3. A torque transducer was chosen to be incorporated in the system to allow for accurate measurement of participant applied torque. A Futek TFF400 reaction torque transducer (Futek, Irvine, CA) was selected for this in-line torque measurement between the motor/gearhead and handle.

2.1.5 PID Tuning and System Characteristics

The Ziegler-Nichols PID tuning technique was used as a starting point for PID gain selection [48, 49]. This process included setting the derivative and integral gains to zero and sending step torque commands to the device with varying proportional gains. The proportional gain was increased if the system steady state quickly dampened out. Alternatively, the gain was decreased if the system steady state would go unstable after the step response. This was repeated until a near continuous steady-state oscillation would occur. The proportional gain at this point was deemed the ultimate gain, K_U. For the setup tested, the ultimate gain was found to be 75. The period of the steady-state oscillation, T_U, was measured as 0.028 seconds. The Ziegler-Nichols no overshoot guideline gains were tested. These values correspond to a proportional gain, K_P, of 0.2 K_U, a derivative gain, K_D, of $2K_P/T_U$, and an integral gain,K_I, of 0.33 T_U/K_P.

The system was tested under expected use conditions with the Ziegler-Nichols no overshoot gain estimates and the gains were varied to improve performance. With the designed control scheme, it became apparent that some conditions improve tracking of desired torques but would result in undesirable behaviors. One such behavior, increasing proportional gains, would increase a grainy feel while moving the handle under load. Another such behavior, increasing integral gains sufficiently, would cause instability after hitting the developed virtual walls at higher angular velocities, $\omega > 30$. The final gains used during the experiment were K_P=50, K_I=1, and K_D=4.

2.1.6 Gravity Compensation

The torque applied to the user is measured through the torque transducer. Any torque generated on the user end of the torque transducer is measured as user-generated torque. The handle and connecting arm each have weight that applies a gravity-induced torque on the torque transducer. These torques would either assist or hinder a user if not compensated for. The gravity-induced torques for this system, $\vec{\tau}_g$, can be calculated using the distance from component center of mass to the axis of rotation of the handle, $\vec{r}_i$, mass of each component, m_i, and the acceleration due to gravity, $\vec{g}$, utilizing Equation 2.1. The negative cosine term of this equation allowed for a zeroing of the measured torque at a zero handle orientation within the torque transducer. The mass of the connecting arm was 0.185 kg and the moment arm was 0.033 meters. The mass of the handle was 0.205 kg and the moment arm was 0.070 meters.

$$\vec{\tau}_g = (1 - \cos\theta) \sum \vec{r}_i \times m_i \vec{g} \tag{2.1}$$

The calculated torque applied to the load cell due to the handle and connecting arm through the range of motion is displayed in Figure 2.4. This torque was then compensated in the control scheme, as shown in Figure 2.5.

2.1.7 Safeguards

The foremost requirement of the device is to be safe for users. Several safeguards were developed to restrict the device from inducing unsafe conditions. These safeguards include:

- unexpected input confirmation,
- parameter monitoring,
- virtual walls,
- and adjustable mechanical stops, shown in Figure 2.6 .

The virtual walls were designed as a stiff spring system. The virtual spring was designed to exhibit a minimum spring coefficient of 20 N/m. This value translated into the rotational motion with a maximum 3.08 inch moment arm was 0.21 N-m/degree. A value of 0.21 N-m/degree was implemented for this system and was effective at stopping motion upon crossing the set boundary. The control scheme with virtual walls implemented are shown in Figure 2.7.

2.1.8 User Interface

The user interface of the device was developed for use in a clinical setting for rehabilitation or research. The user interface encompasses a graphic user interface suite, a user pain input, an armrest, a handle, and additional attributes of the user experience, specifically sound and feel. The remainder of this document discusses a study to evaluate the devices ability to simulate conventional loading methods. For more information on the user interface and its development, please see Appendix A.

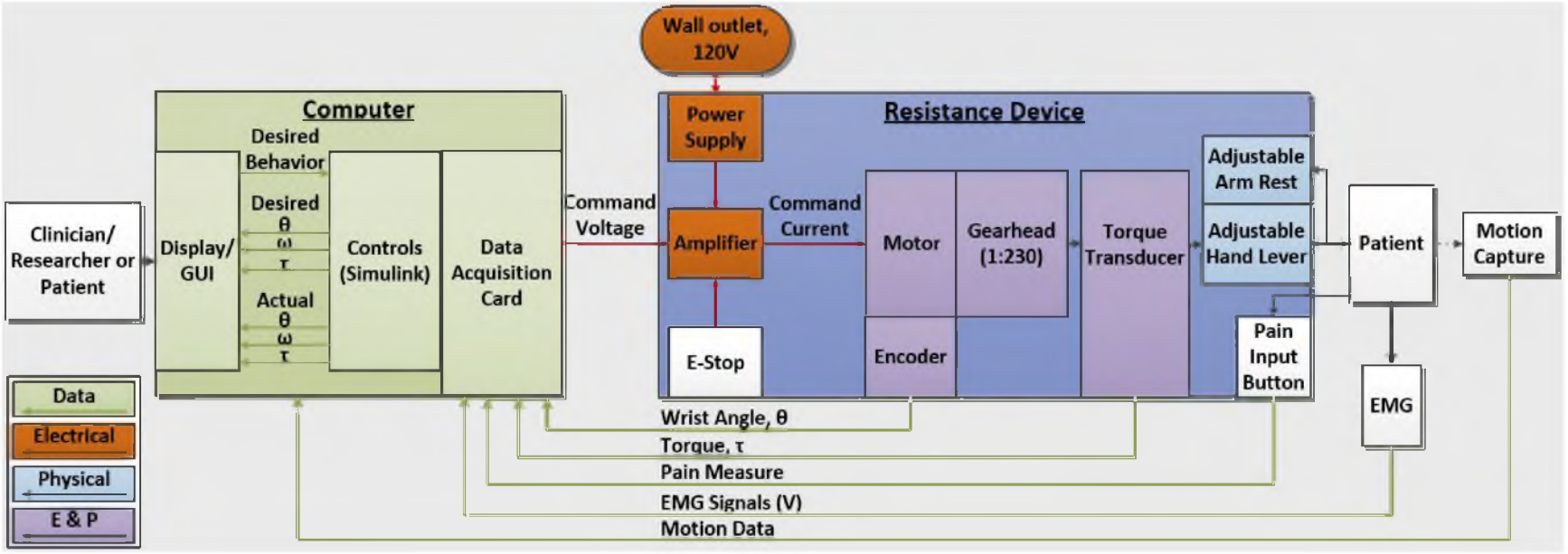

Figure 2.1. System diagram

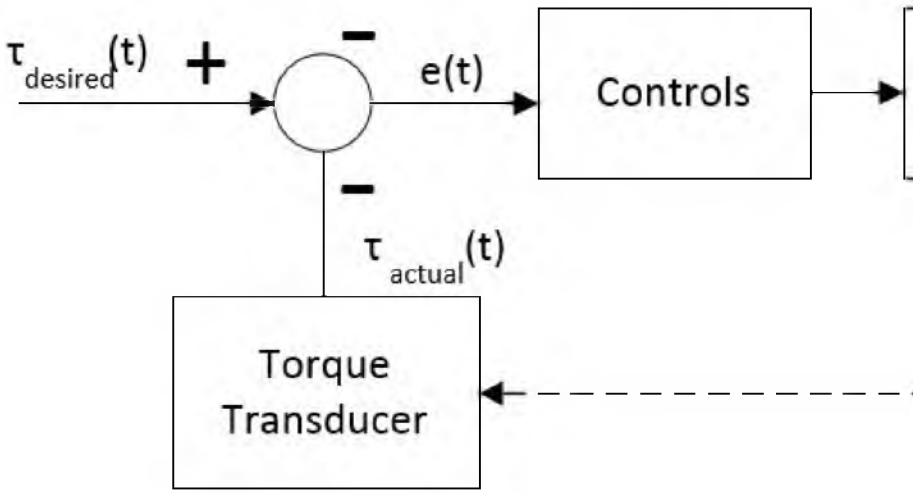

Figure 2.2. Torque control feedback scheme

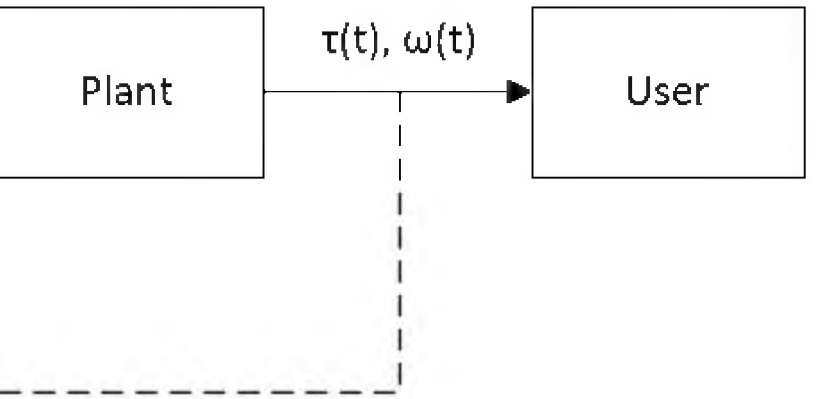
Plant
τ(t), ω(t)
User

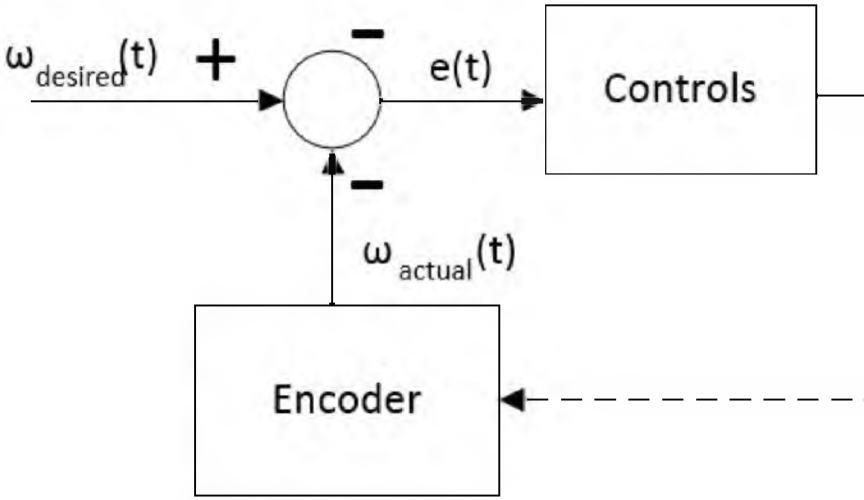

Figure 2.3. Angular velocity control feedback scheme

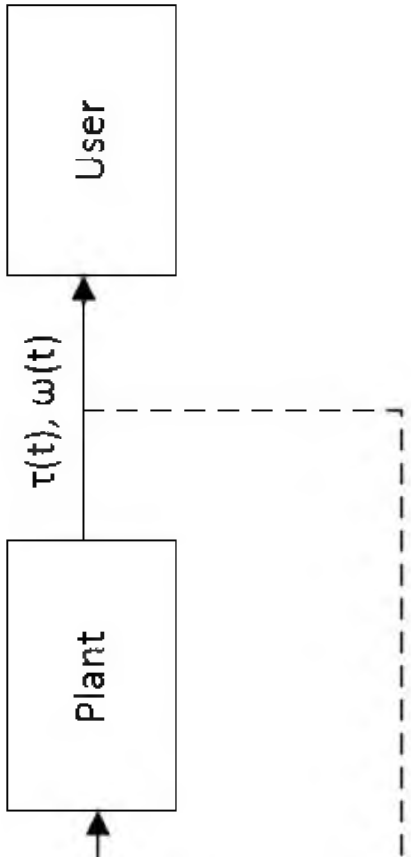
User
τ(t), ω(t)
Plant

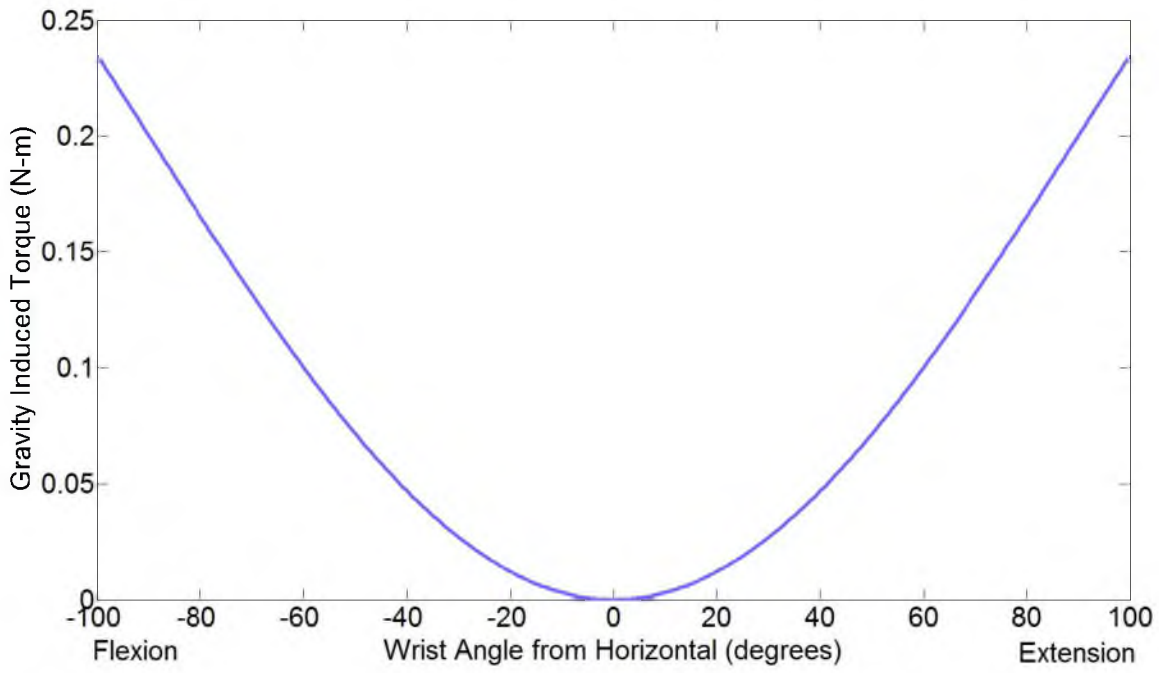

Figure 2.4. Gravity-induced torque through range of motion

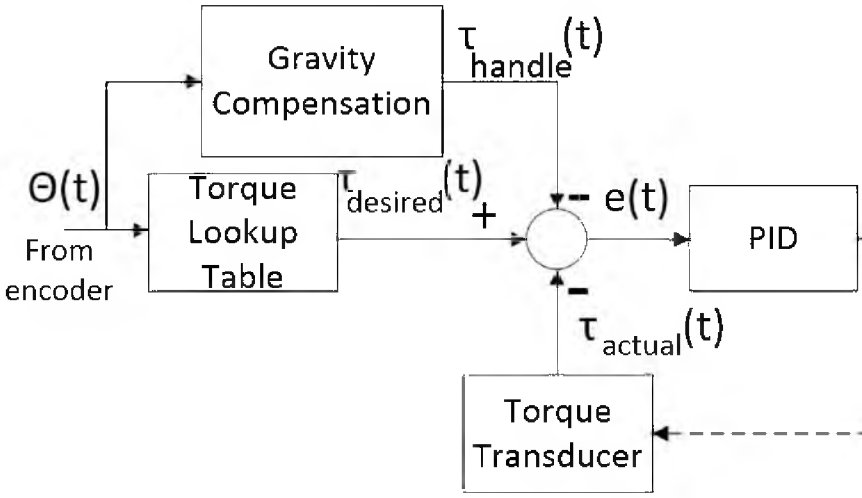

Figure 2.5. Torque control loop with gravity compensation

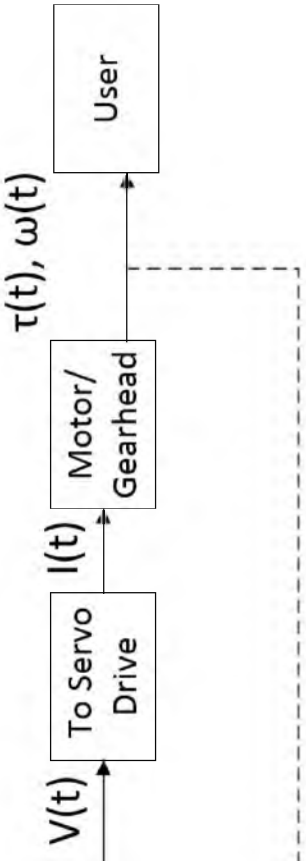
User
τ(t), ω(t)
Motor/
Gearhead
I(t)
To Servo
Drive
V(t)

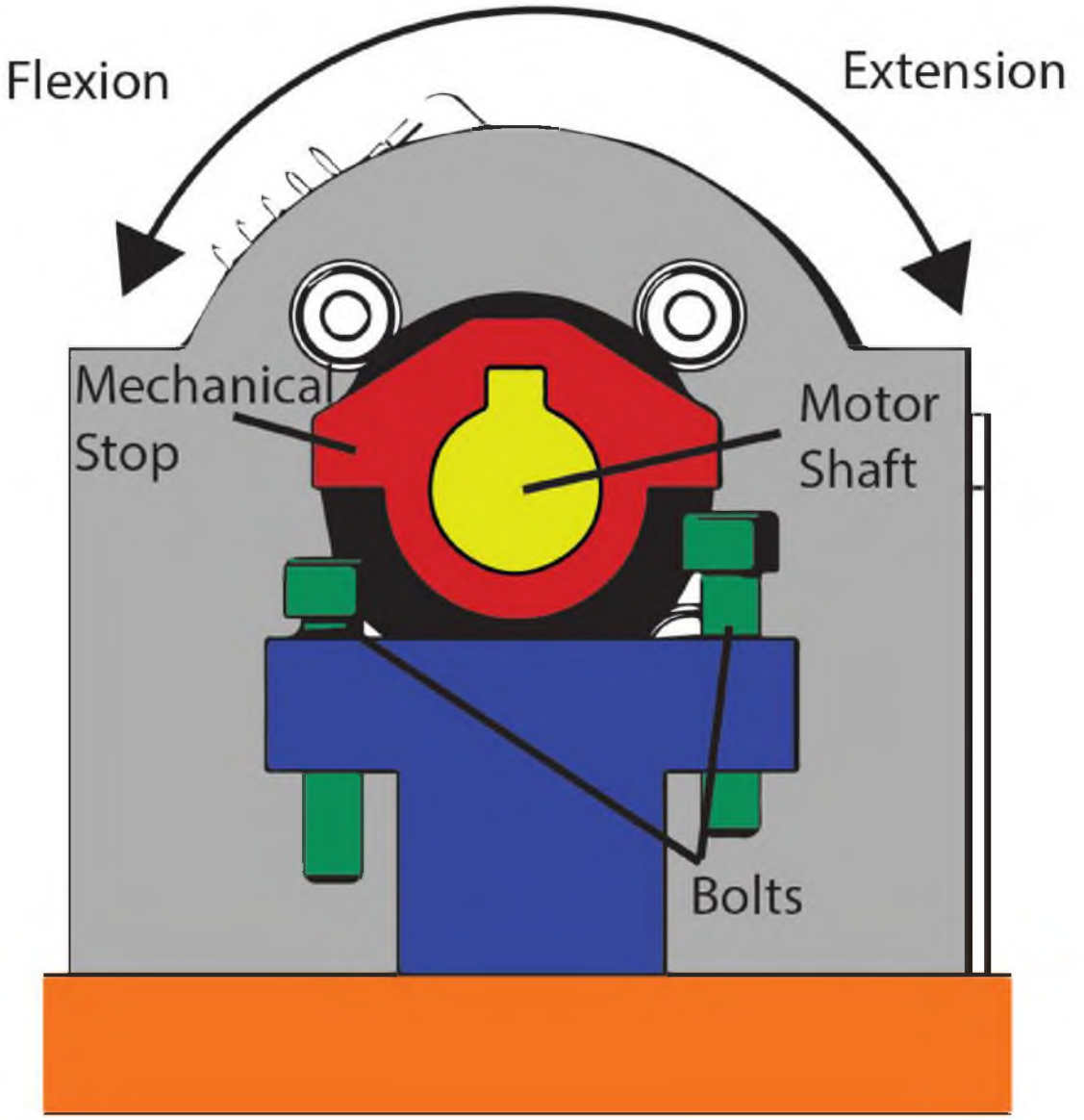

Figure 2.6. Adjustable mechanical hard stops. Orange: Baseplate, Purple: Hard stop platform, Yellow: Motor shaft, Red: Mechanical stop, Green: Screw heads to adjust the surface the mechanical stop comes in contact with to stop motion.

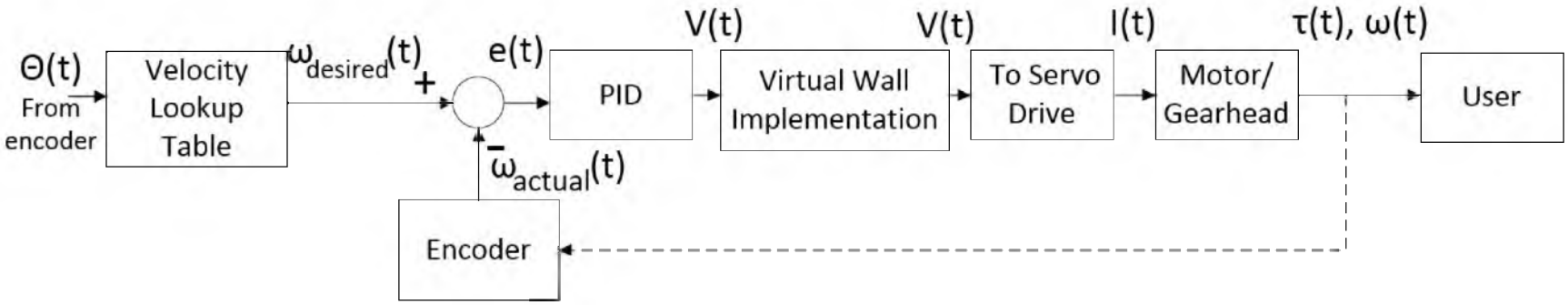

Figure 2.7. Torque control loop with virtual walls added

CHAPTER 3

METHODS

This research protocol was approved for conduct by the University of Utah Institutional Review Board under approval #00067952. The purpose of this study was to compare the muscle activation and wrist kinematics during use of conventional resistance tools and during use of the developed device. This study focused specifically on the eccentric portion of wrist extensions.

3.1 Recruitment

Twenty subjects were recruited through word of mouth (9 men, 11 women). All subjects gave written informed consent. The age, height, and weight for the participants averaged 27.6 $\pm$ 6.04 SD years, 172.09 $\pm$ 11.84 SD cm, and 73.64 $\pm$ 19.33 SD kg, respectively. Participants were free of significant upper limb disorders: history of elbow or wrist surgery or current infection, carpal tunnel, fracture, deformity, elbow or wrist osteoarthritis, rheumatoid arthritis, or other inflammatory arthritis affecting the wrist or elbow. The maximal voluntary isometric contractions were found to have a mean of 8.22 N-m and standard deviation of 3.3. This range and distribution are similar to literature values, Vanswearingen: 6.14 $\pm$ 2.00 N-m, and Delp: range of 3.4 to 9.4 N-m [36, 37].

3.2 Experimental Procedure

Subjects were informed of the study purpose and procedure. Subjects were then fit with surface electromyography (sEMG) electrodes and nineteen reflective surface markers. The device was also fit with five reflective markers. Each subject performed a maximal voluntary isometric wrist extension contraction at a self-defined neutral wrist posture. The maximum force and sEMG readings were recorded for this contraction.

Subjects were asked to perform wrist extensions for seven different conditions. These conditions included: (1) a green difficulty level TheraBand FlexBar® (TheraBand, Akron, Ohio), (2) a 2.27 kg dumbbell, (3) a blue difficulty level TheraBand resistance band, (4-

6) three torque profiles supplied by the developed device informed by the previous three methods, and (7) a constant torque of 1.0 N-m supplied by the developed device. The derivation of the conventional loading models is described in Section 3.3.4. Subjects were introduced to each condition before beginning data collection.

Subjects were asked to perform wrist extensions at a four second descent and four second ascent speed through their accessible range of motion for each condition. A visual aid was provided to help subjects keep a consistent pace across repetitions. A one second pause at top and bottom of the extension was added to aid in maintaining a consistent pace. Figure 3.1 shows a participant performing wrist extensions during data collection. A close-up of the device and the participant's forearm are shown in Figure 3.2.

Subjects were secured to the armrest identically under all conditions. Subjects were asked to practice one to two wrist extensions with the visual aid to match the requested speed. Once a subject became in sync with the visual aid, data collection was started and the subject was asked to complete five extensions. Subjects were then given five minutes of rest before beginning the next condition to help avoid fatigue. This process was repeated for each condition.

3.3 Experimental Setup

3.3.1 Surface Electromyography

Muscle potential was chosen as a measure to compare the torque applied through the wrist during wrist extensions. Surface electromyography was used to measure muscle potential near the electrode placements. A Delsys Bagnoli 8-channel amplifier (Delsys, Natick, MA) with single differential silver contact electrodes and preamplifier were used for EMG collection. This system has a band pass of 20-450 Hz $\pm$ 10%.

Electrodes were placed near the extensor carpi radialis longus (ECRL), extensor carpi radialis brevis (ECRB), extensor digitorum (ED), extensor carpi ulnaris (ECU), flexor carpi ulnaris (FCU), and flexor carpi radialis (FCR). These muscles were chosen due to the emphasis on extensor activation and the extensor communis tendon. Two of the wrist flexor muscles were added to allow for modeling in future work.

Electrode placement was adapted from the guidelines indicated by Perotto [50]. Example electrode placements are shown in Figure 3.3. An electrode was placed on the ECRL muscle belly by palpation near the lateral epicondyle while the participant performed slow repeated wrist extensions. The electrode on the ECRB muscle belly was found similarly but more distally along the length of the radialis bone. The electrode for the ED muscle belly was placed by palpation of the volar forearm while the participant performed slow repeated

finger extensions of their second and third fingers. The electrode for the ECU muscle belly was placed by palpation approximately half way along the length of the ulnaris bone slightly dorsal to the ulna edge while the participant alternated between ulnar deviations and wrist extensions. The electrode for the FCU was placed similar to the ECU but slightly volar to the ulna bone. The participant was then asked to flex their right bicep with an elbow near 90 degrees. The common bicep tendon and medial epicondyle were palpated and a midpoint between them was determined. The midpoint was extended approximately four finger widths distal along the forearm and participants were then asked to perform wrist flexions. Palpations were used near the identified region to determine the location of the FCR and the electrode was placed. Last, a reference electrode was placed on the ulnar olecranon process.

After electrodes were placed, the EMG signals were observed while the participant performed the same motions performed during placement. If an electrode's readings did not align with the expected excitation, that electrode placement was revisited. EMG readings were sampled at 1 kHz. The same National Instruments data acquisition card and break out box used for device control were used for EMG reading collection.

3.3.2 Maximal Voluntary Contraction Test

An Interface SM-250 S-Type load cell (Scottsdale, AZ) was used to measure a maximal voluntary isometric wrist extension contraction, referred to as MVIC for the remainder of this document. The S-Beam was affixed to a stationary object with a handle attached. The MVIC testing was conducted with the participant seated in a chair with forearm resting on an armrest and palm down. The participant was able to self-select a comfortable elbow posture. Elbow angles were between 75 and 135 degrees. The wrist was positioned to support the forearm as much as possible while also allowing full wrist flexion. The test setup was adjusted to test extension at the participant's self-selected straight wrist posture and then secured with a wrist strap. Participants were asked to perform a five second maximal exertion wrist extension. The force recorded was then converted to torque using a measurement of the distance from their radial head to the axis of a pen held along the breadth of their hand. Participants were instructed to hold the pen in a dumbbell grip.

3.3.3 Motion Capture

Ten Natural Point Flex13 cameras were arranged to capture an approximately 1 cubic meter capture space (Natural Point, Corvallis, OR). C-Motion's Acquire 3D capture software (C-Motion, Germantown, MD) (version 1.0.0.98) was used for point-ray data collection.

C-Motion's AMASS software (version 2.0.0) was used to convert the two-dimensional data to three-dimensional coordinates. The motion was captured at a sample rate greater than or equal to 100Hz. Prior to each trial, a calibration was conducted using a C-Motion calibration wand. Point residuals were consistently below 0.2 mm, 1.59 mm mean. Cameras were placed to allow a marker to be visible to a minimum of three cameras in all postures. Ten cameras were chosen to accommodate redundancy with the back-of-hand orientations in full flexion and full extension.

C-Motion's Visual3D (version 5.01.25) was used to then assign markers to a model of the participant and calculate joint angles and marker locations relative to the lab coordinate system. Initial angle tracking attempts had excessive crosstalk between the flexion-extension and ulnar-radial deviation. This was improved significantly by adopting the marker set used by Li and later Brigstocke [45,51]. This marker set was the basis for the set used for tracking of wrist flexion-extension and ulnar-radial deviation. Li's methods used midpoints measured on the back of the wrist and forearm while the participant rested their forearm on a table with the ulna surface of the wrist touching the table. A plastic isosceles triangle was used for the reflective markers applied to the forearm. The triangle was 4 cm along the base with the third marker a height of 2 cm from the center of the base. The base of the triangle was then placed along a line drawn between the two midpoints with the third marker on the radial side of the forearm.

With the palm-down orientation desired in this study the marker set described in Li caused excessive crosstalk between the axes as it did not properly take into account the pronation of the forearm. The marker set was thus adapted to placing the base of the triangle along an approximate centerline from the wrist to elbow along the top of the forearm. From Li's research, four markers were placed on the hand. One on the heads of the second, third, and fourth metacarpals and one half way along the third metacarpal. A figure of this marker set is displayed in Figure 3.4. A lab coordinate system was used for marker motion descriptors. For this lab coordinate system the positive x-direction was directed towards the device, the positive y-direction was directed forward out of the chair in which the participant was seated, and the positive z-direction was directed vertically upward. All marker motion descriptors discussed later in this document were measured in reference to the lab coordinate system.

3.3.4 Modeling of Conventional Systems

Kinetic models of existing resistance tools were developed to perform a comparison of muscle activation and wrist kinematics between conventional loading methods and the

developed device. Kinetic models were developed for a 2.27 kg dumbbell free weight, a blue level difficulty TheraBand exercise band, and a green level difficulty TheraBand FlexBar®. These models were used to develop the torque profile of the developed device to mimic the kinetics of the conventional therapies. The models were derived assuming a slow velocity in line with the expected eccentric training protocol. This assumption removed the inertial effects on the system. The derivation of these models from free body diagrams follow.

3.3.4.1 Free Weight

Figure 3.5 shows the diagram of the force on the wrist due to a free weight through flexion-extension. Through inspection of Figure 3.5, the relationship between wrist angle from horizontal, θ, and torque applied to the wrist, $\vec{\tau}$, given a dumbbell of weight, $m\vec{g}$, and distance from the wrist axis to center of mass of the weight, $\vec{r}$, is shown Equation 3.1.

$$\vec{\tau} = \vec{r} \times m\vec{g} \tag{3.1}$$

3.3.4.2 TheraBand Latex Exercise Bands

Figure 3.6 shows a side diagram of the force of a TheraBand latex exercise band through the range of motion. Figure 3.7 shows a front diagram of the force of a TheraBand latex exercise band through the range of motion. The exercise band was found to behave very similarly to a linear spring. The model was developed based on this simplification. The experiment was designed to have zero elongation at the participant's full flexion posture, thus only the weight of the setup would be felt at that time.

The relationship between wrist angle and torque applied to the wrist is not as self-evident compared to the free weight. The torque is similarly dependent on the wrist axis to weight moment arm, $\vec{r}$, the stretch band force applied, $\vec{F}_{Band}$, as well as the weight of the setup, $m\vec{g}$; however, the applied force is dependent of slightly more complex geometry, as is seen from Figure 3.6 and Figure 3.7.

The combined length from anchor to hand, L_{Total}, can be found using the law of cosines and the fixed length portion of the setup, L_{Set}, the wrist angle from parallel, θ, and the height of the wrist from the anchor, H, shown in Equation 3.2.

$$L_{Total} = \left(\|\vec{r}\|^2 + H^2 - 2\|\vec{r}\|H\cos\theta\right)^{1/2} \tag{3.2}$$

The effective length of the band, L_{Eff}, is then the difference between the total length and the fixed length portion, as shown in Equation 3.3.

$$L_{Eff} = L_{Total} - L_{Set} \tag{3.3}$$

The length of each side of the loop, L_{Side}, can be found using the using Equation 3.4 with the breadth of the hand, b, and effective length of the band.

$$L_{Side} = \left(\left(\frac{b}{2} \right)^2 + {L_{Eff}}^2 \right)^{1/2} \tag{3.4}$$

The hand breadth, b, and effective length of the band, L_{Eff}, can be used to find the angle of each side of the stretch band loop from vertical, α, using Equation 3.5.

$$\alpha = \tan^{-1} \left(\frac{b/2}{L_{Eff}} \right) \tag{3.5}$$

From the law of sines, the angle from the anchor to the hand, ϕ, can be found through Equation 3.6.

$$\phi = \sin^{-1} \left(\frac{\|\vec{r}\| \sin\theta}{L_{Eff} - L_{Set}} \right) \tag{3.6}$$

The assumption was made that the two sides of the stretch band loop were of equal length and generated equal force and the horizontal forces balance out to result in a single force coincident to the length of the exercise band axis. This is believed to be a reasonable assumption given that through the range of motion, a person will typically adjust to balance the forces on their hand. With this assumption, the known spring constant of the material, k, and the angle α, Equation 3.7 can be used to determine the combined force generated, $\vec{F}_{Band}$.

$$\vec{F}_{Band} = 2\Big((L_{Side} - L_{Rest}) k \cos\alpha \Big) (\sin\phi \hat{i} + \cos\phi \hat{j}) \tag{3.7}$$

The torque required at the wrist, $\vec{\tau}$, can then be found using the combined force and wrist axis to weight moment arm, $\vec{r}$, as shown in Equation 3.8.

$$\vec{\tau} = \vec{r} \times \vec{F}_{Band} \tag{3.8}$$

For the experiment setup, the set variables were as follows: H was 73.66 cm and L_{Set} was 54.86 cm. Hand breadth, b, was estimated by using a relation derived from anthropometry data [46] between the wrist length measured and hand breadth being a ratio of approximately 1:1.248.

To determine the force-percent elongation relationship, a 15.24 cm section of exercise band was elongated to 200% elongation for 50 cycles using an Instron Tensile Machine (Instron, Norwood, Massachusetts). The force versus percent elongation for the tested stretch band is shown in Figure 3.8(A). Over the 50 cycles the force-percent elongation trend converged, as can be seen in Figure 3.8(B).

As can be seen in Figure 3.8(A), the testing indicated that force-percent elongation was not linear. The last 25 cycles were averaged to approximate the expected force versus percent elongation during the study. This averaged force versus percent elongation curve was used as a lookup table substitute for the spring constant in Equation 3.8. This combination of the empirical and derived terms was used to compute the desired torque through the range of motion.

The weight of the exercise band setup was included in the model. The weight of the setup was 0.282 kg. This weight was assumed to be distributed evenly across the length of the setup. The weight of the setup was added to the torque applied to the wrist using Equation 3.1.

3.3.4.3 TheraBand FlexBar®

Figure 3.9 shows the diagram of the forces and moment for a TheraBand FlexBar® through the range of motion with a fixed wrist. The FlexBar® was found to behave similar to a torsional spring. The experiment was designed to have zero twisting at full flexion of the participant, thus only the weight of the setup would be felt at that time.

Varignon's second moment theorem, Equation 3.9, indicates that given a couple generated by a summation of forces, the moment generated is independent of distance from axis of rotation, $\vec{r}$.

$$\begin{aligned} \vec{M} &= \sum_{i=1}^{\infty} \vec{r_i} \times \vec{F_i} \\ &\textit{and} \\ \vec{M'} &= \sum_{i=1}^{\infty} (\vec{r_i} + \vec{r}) \times \vec{F_i} \\ &\rightarrow \vec{M'} \equiv \vec{M} \end{aligned} \tag{3.9}$$

Assuming the torque applied by the FlexBar® to the user's hands can be represented as a summation of couples around the circumference of the FlexBar®, the torque required at the wrist, $\vec{\tau}$, can be simplified to the linear relationship shown in Equation 3.10 with the torsional spring constant, κ, and the wrist angle from neutral, θ.

$$\vec{\tau} = \kappa\theta \tag{3.10}$$

The torsional spring constant, κ, for a green difficulty level FlexBar® was calculated by measuring generated torques for a 6 inch segment through a 120 degree range at 20 degree intervals and fit to a linear model. The κ for a green difficulty level FlexBar® was calculated to be 0.0226 Nm/degree.

The weight of the FlexBar® was not included in the model. The mass of the Flexbar® was 421 kg. This weight was distributed between the two hands and the percentage of the weight in the right hand was uncertain with the loading of the member.

3.4 Data Processing

3.4.1 Processing for EMG Comparison Between Conventional and Developed Device

Mathworks' Matlab was used for data processing. The EMG measurements were measured with the Delsys Bagnoli EMG Amplifier. The Delsys Bagnoli EMG Amplifier had a 20-450 bandwidth. The EMG signals were then full-wave rectified and filtered with a dual pass second order Butterworth filter with 1 Hz cut-off frequency (τ= 159ms). Joint angles from the motion capture data were used to identify beginning and ending of eccentric descent. The filtered EMG signal was then segmented according to these events for the descent portion of the repetition. Figure 3.10 shows an example of the EMG segments prior to low-pass filtering.

These descent segments were then binned according to angle. A bin range of one degree was used. The bins were then averaged and descriptive statistics were then calculated for these averaged bins across participants. This process is displayed in Figure 3.11. The average descent segments for each muscle were then compared across conditions through Pearson product-moment correlations to evaluate how closely the EMG trends compared across the conditions.

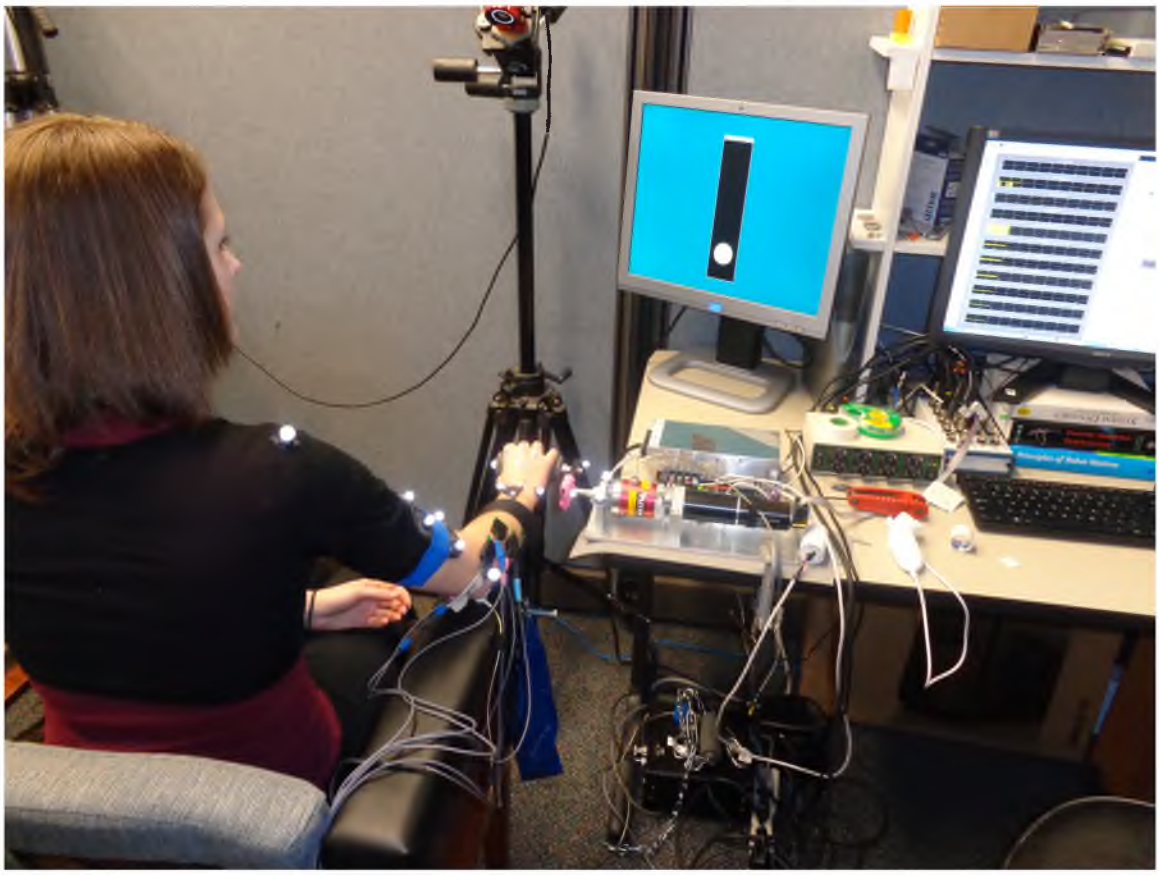

Figure 3.1. Participant performing wrist extensions during data collection. Visual aid is shown in left-most screen.

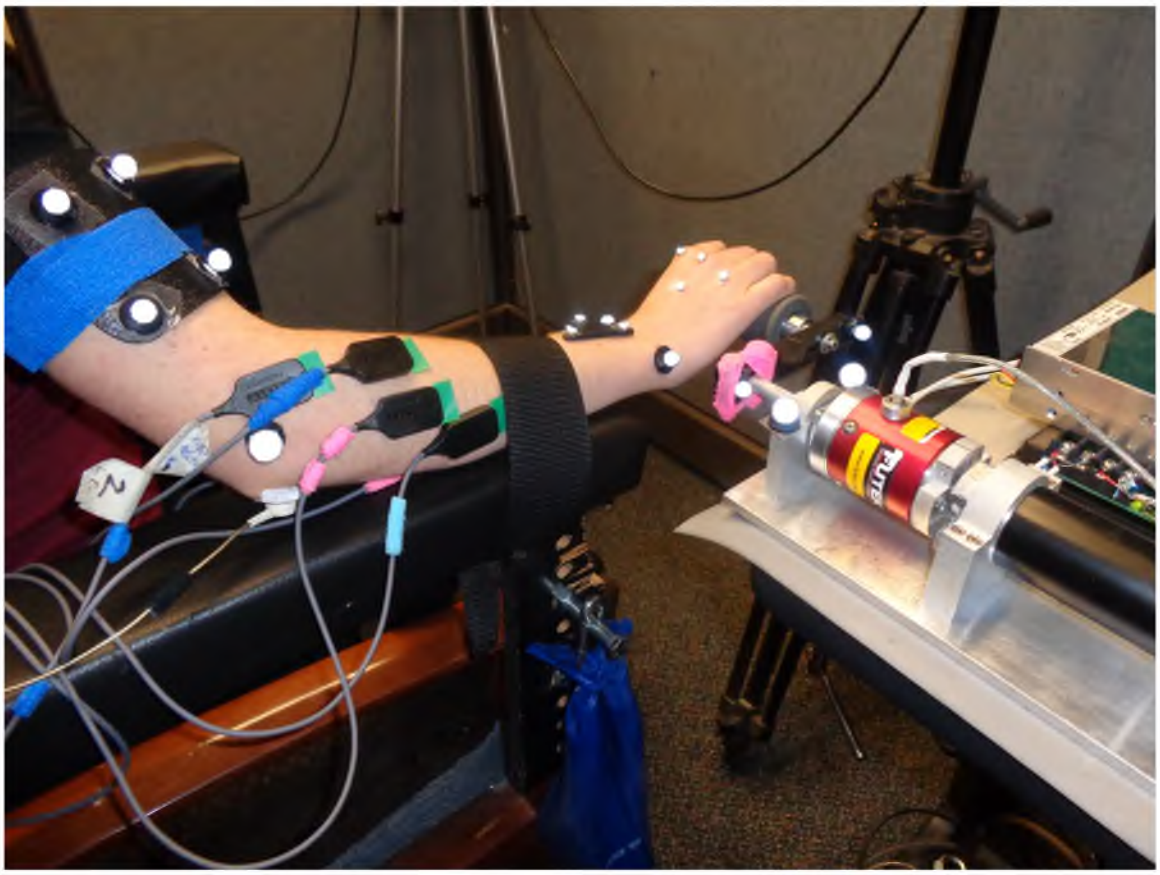

Figure 3.2. Close-up of device and participant's forearm after electrode and marker attachment.

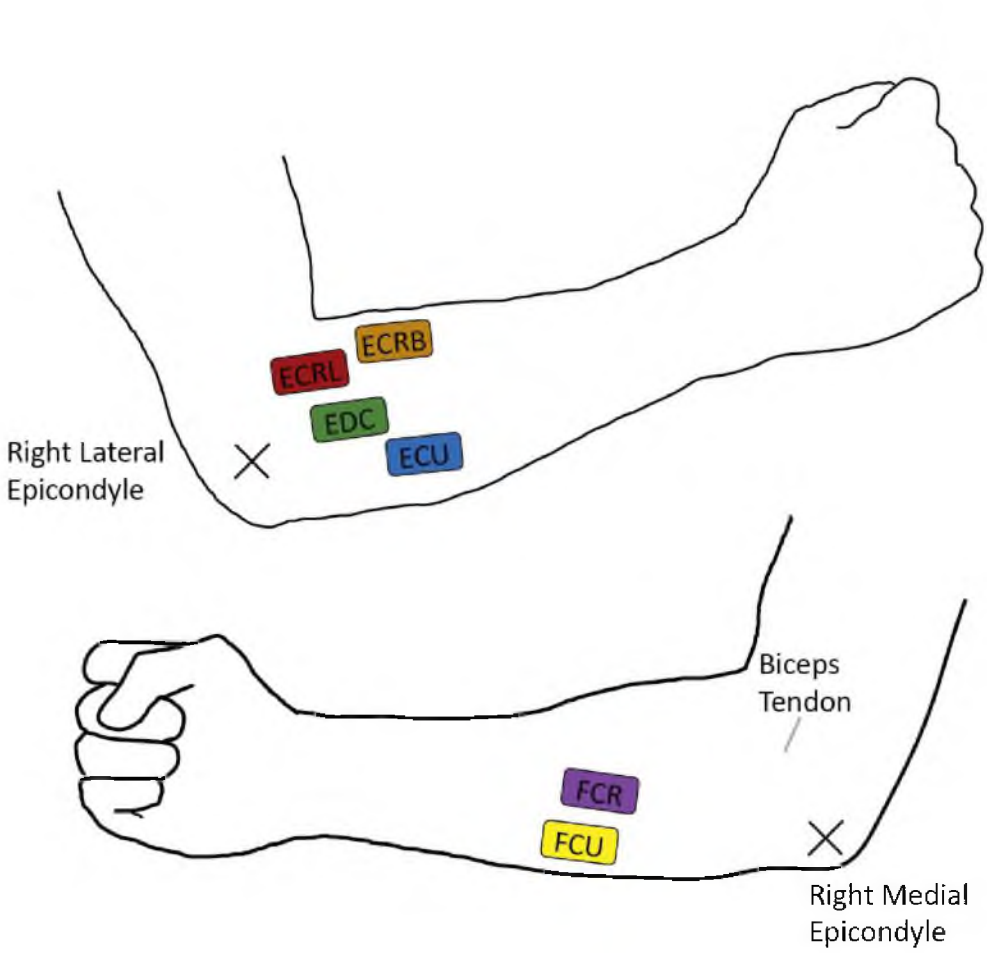

Figure 3.3. Electrode placement on the right arm, top to bottom: extensor carpi radialis brevis (ECRB) in orange, extensor carpi radialis longus (ECRL) in red, extensor digitorum communis (ECU) in green, extensor carpi ulnaris (ECU) in blue, flexor carpi radialis (FCR) in purple, and flexor carpi ulnaris (FCU) in yellow.

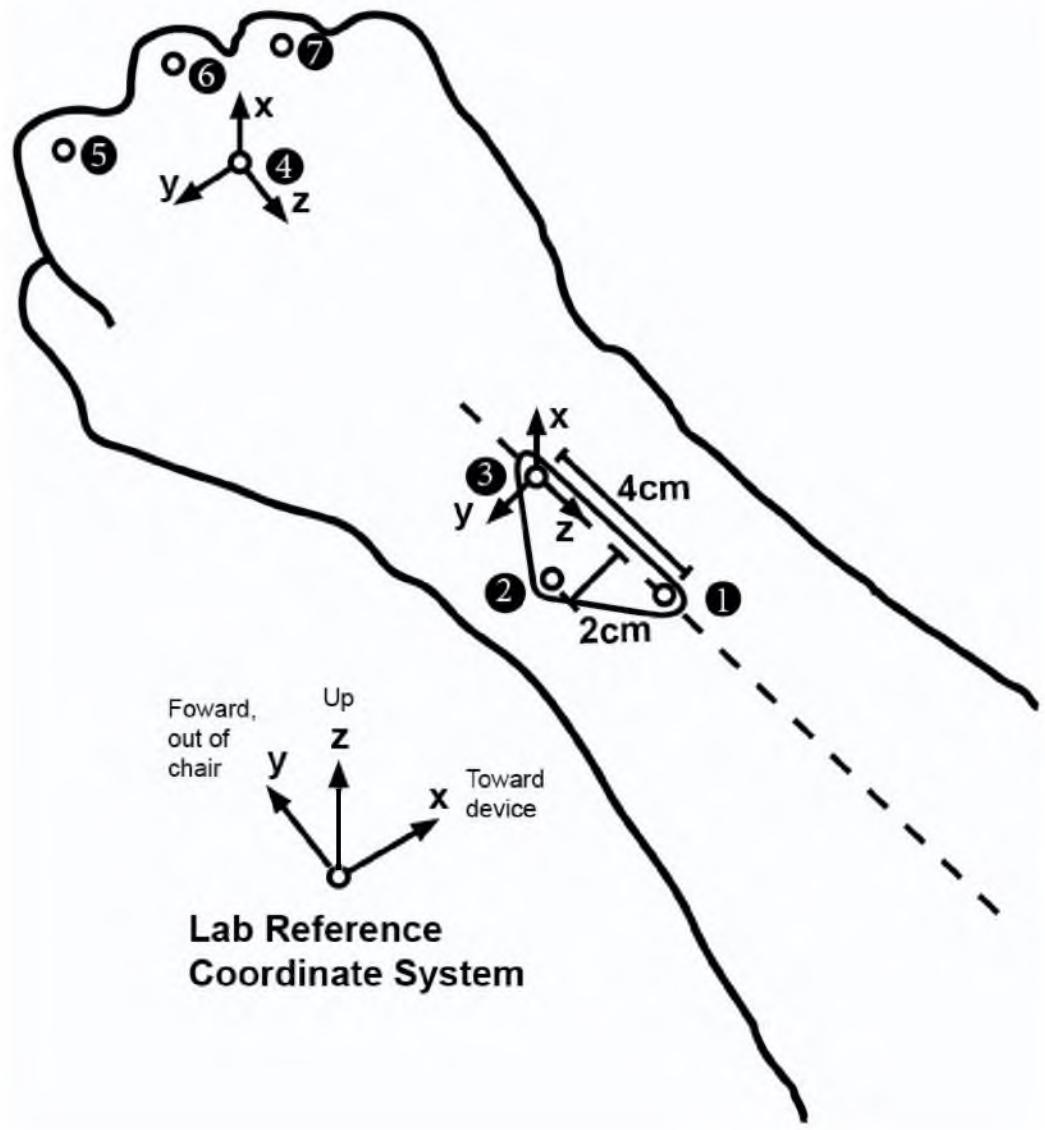

Figure 3.4. Motion capture marker set. Markers #1-3 define the forearm coordinate system, coordinate system centered on marker #3. Markers #4-7 define the hand coordinate system with redundancy, coordinate system centered on marker #4. The centerline of the forearm as viewed from the top is denoted with the dashed line. A lab coordinate system was used for marker motion descriptors. For this lab coordinate system, the positive x-direction was directed towards the device, the positive y-direction was directed forward out of the chair in which the participant was seated, and the positive z-direction was directed vertically upward. All marker motion descriptors discussed later in this document were measured from the lab reference.

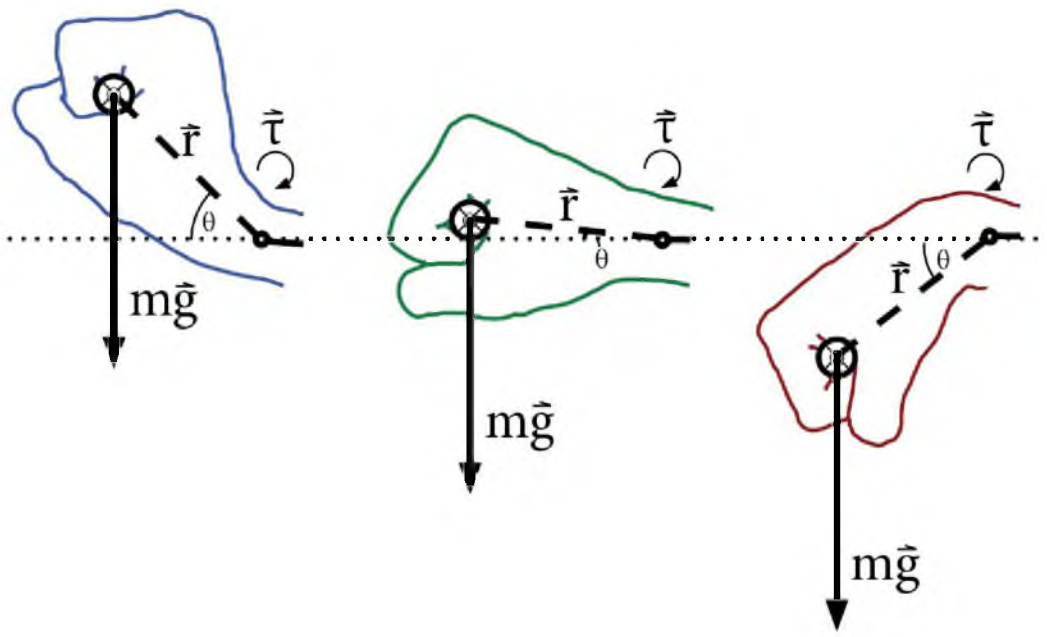

Figure 3.5. Diagram of force of free weight through range of motion

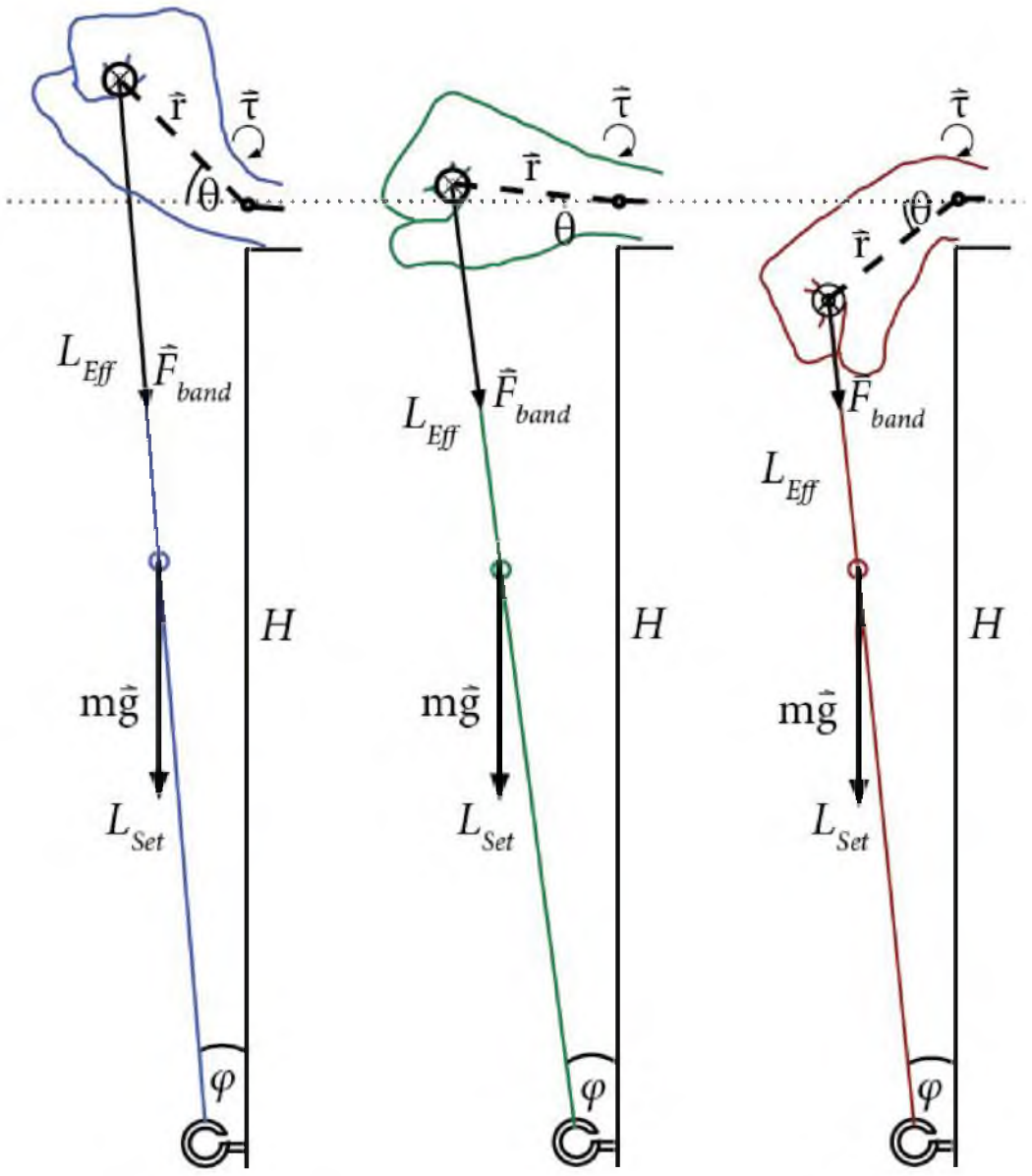

Figure 3.6. Side diagram of the force of exercise band through range of motion

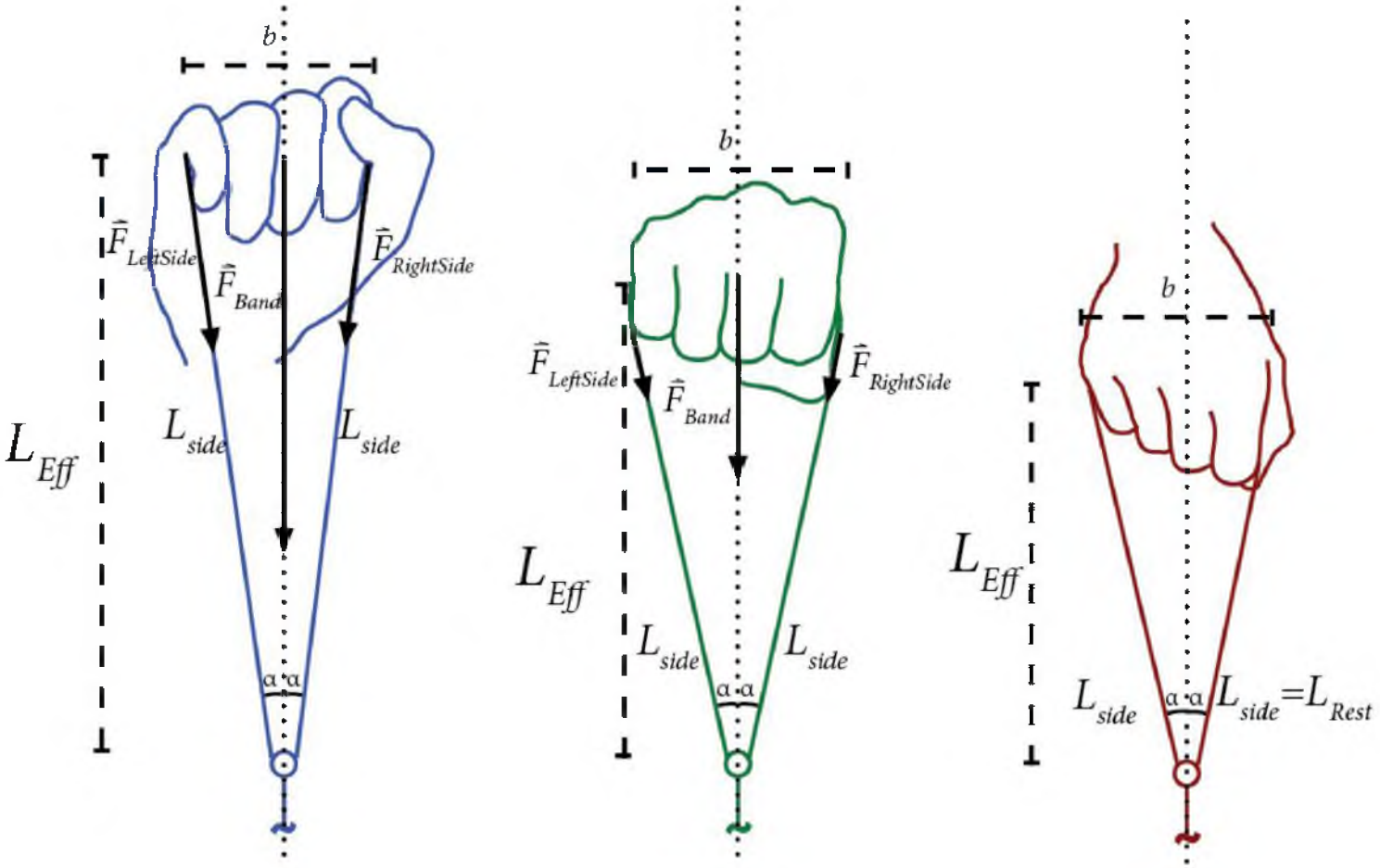

Figure 3.7. Front diagram of the force of exercise band through range of motion

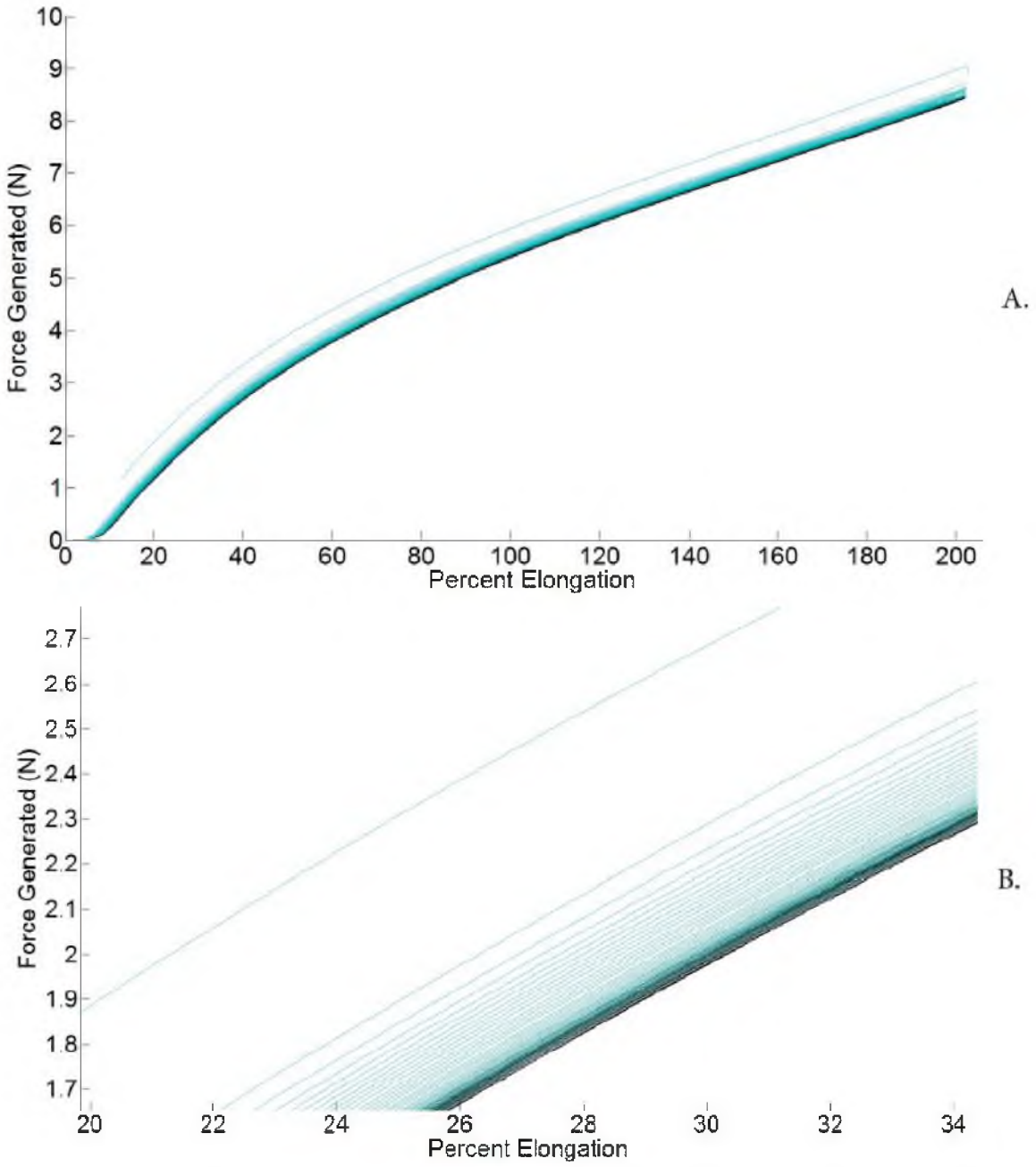

Figure 3.8. Force versus percent elongation for blue level difficulty TheraBand exercise band over 50 cycles. Lighter segments indicate earlier cycles, darker segments refer to later cycles. A: full range of force versus percent elongation. B: close-up of collected data showing convergence of properties over the 50 cycles.

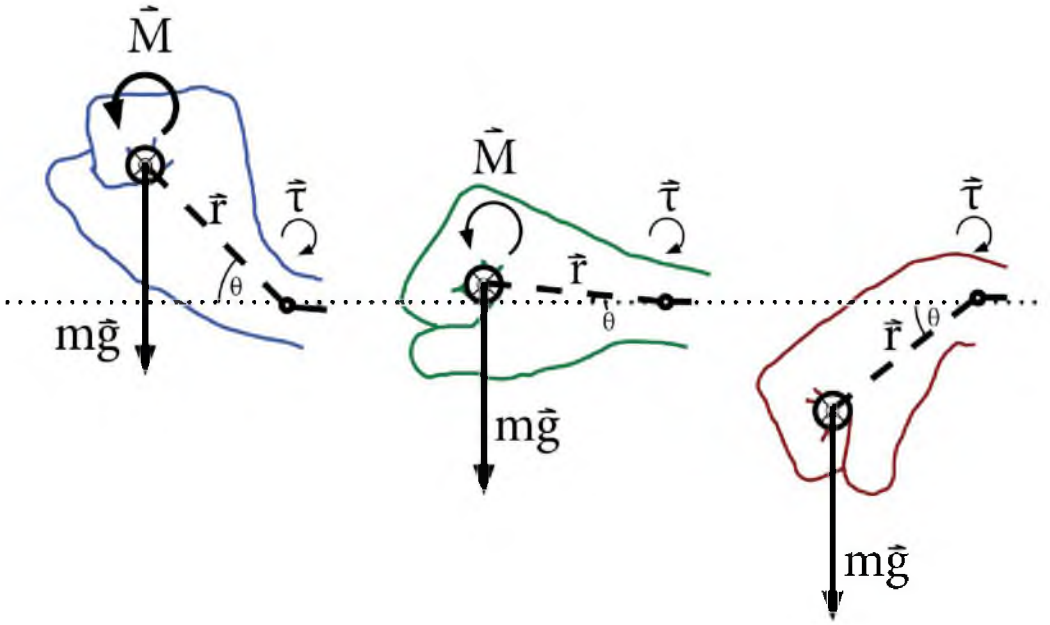

Figure 3.9. Diagram of force and moments due to FlexBar® through range of motion

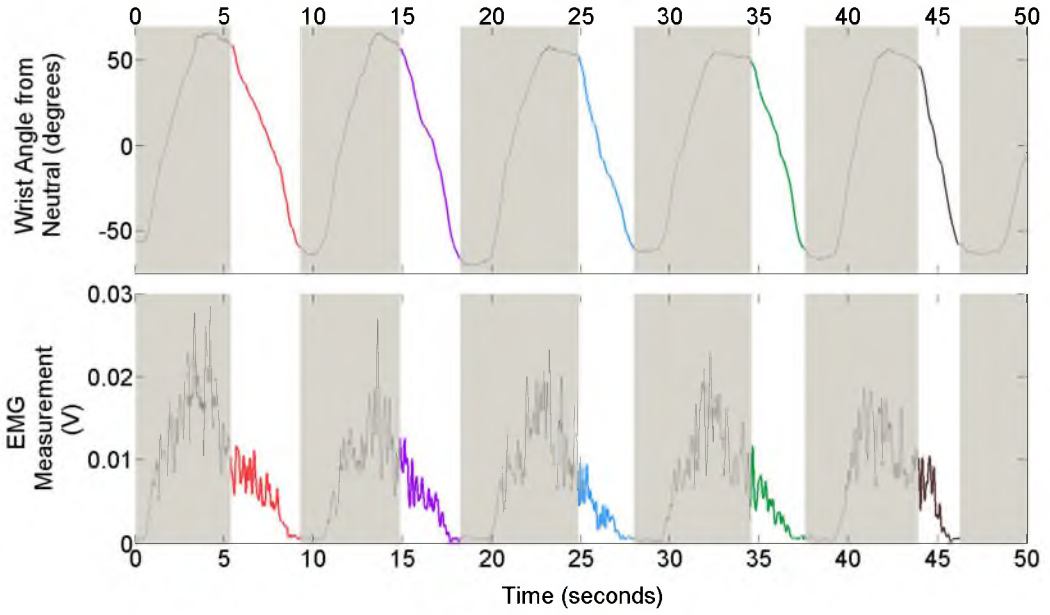

Figure 3.10. Example trial for free weight with motion capture angles and extensor digitorum communis EMG prior to low-pass filtering segmented for each repetition. Colors indicate differing repetition, further shown in Figure 3.11. Top: wrist angle from neutral from motion capture. Bottom: EMG signal prior to low-pass filtering through a single example trial.

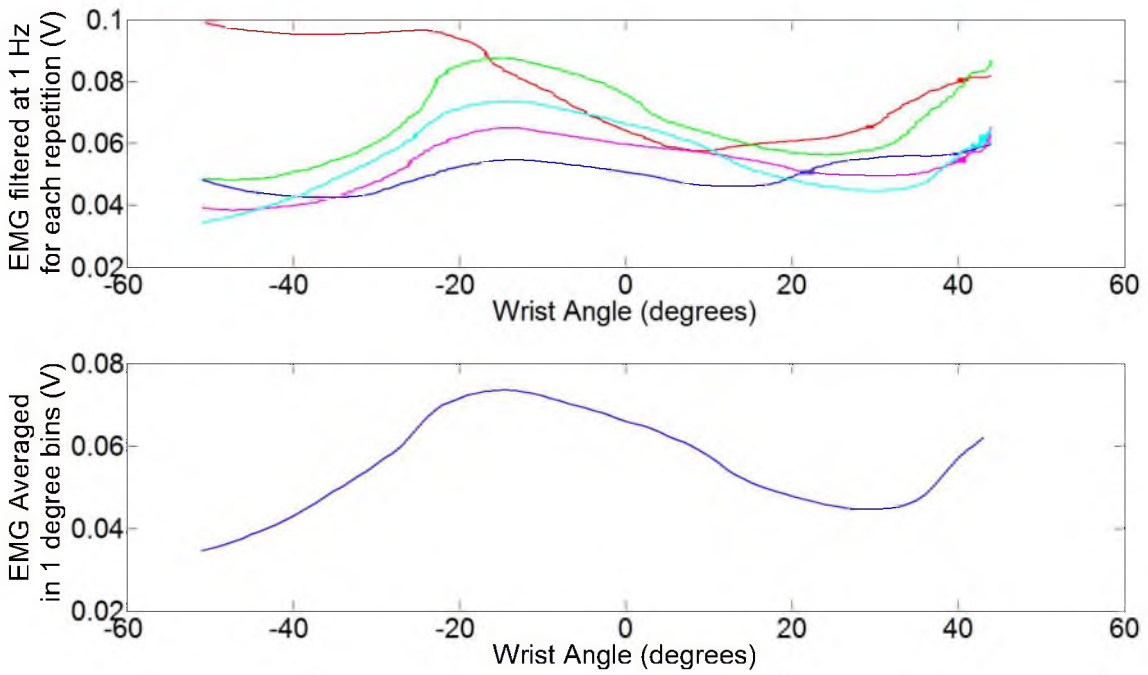

Figure 3.11. Example filtered EMG binning for the extensor digitorum data shown in Figure 3.10. Top: EMG readings for five repetitions filtered at 1 Hz. Bottom: Binned and averaged EMG readings.

CHAPTER 4

RESULTS

The metrics used to evaluate the developed device are based on four categories:

- performance error from desired,
- wrist position kinematics,
- wrist angle range of motion,
- and sEMG readings.

The performance error from desired metrics describes how well this device can provide a desired stimulus. The other three categories then compare how the stimulus from the device compares to the stimuli it has been programmed to simulate.

4.1 Torque Measured to Desired Torque

As discussed in Section 2.1.5, a compromise was necessary in selecting the PID gains to accommodate both feel, behavior, and acceptable torque tracking while a participant moved through a range of motion. An example of the desired torque and the measured torque are shown in Figure 4.1. The error between the measured descent torques and the desired torque for the example trials shown in Figure 4.1 are displayed in Figure 4.2. An ANOVA across participants and loading conditions was conducted for the mean torque error, the standard deviation of the torque error, maximum positive error, and maximum negative error across the range of motion. Tukey range tests were then conducted with the ANOVA results. No significance was found between the four conditions. The root mean square errors for each model are displayed in Figure 4.3. Additional descriptive statistics are displayed in Table 4.1. The average RMS error is relatively small, approx. 0.1 N-m, for the up to 3 N-m torque applied, as seen in Table 4.1 There were some larger dissimilarities as seen from the mean maximum overshoot and mean maximum undershoot also shown in Table 4.1. Further iterations with the control scheme may allow for an improved tracking and feel solution.

4.2 Joint Kinematics

The location and motion of a marker located posterior to the wrist, marker #3 in Figure 3.4, was analyzed as a surrogate for wrist location and motion. An example of the motion of the wrist marker throughout a trial is displayed in Figure 4.4. As a reminder, all marker motion descriptors were referenced from the lab coordinate system shown in Figure 3.4. The marker coordinates for the same trial versus time are displayed in Figure 4.5 and displayed versus wrist angle in Figure 4.6. Some interesting movement/posture patterns, as seen in Figure 4.7, were visible between trials and participants; however, that analysis is not within the scope of this evaluation and will not be discussed in this document.

An ANOVA across participants and loading conditions was conducted for (1) the range traveled by the wrist marker in the X-, Y-, and Z-directions, (2) the standard deviation of the wrist marker coordinate relative to a mean wrist marker coordinate in the X-, Y-, and Z-directions, (3) the maximum positive coordinate relative to a mean wrist marker coordinate in the X-, Y-, and Z-directions, and the (4) maximum negative coordinate relative to a mean wrist marker coordinate in the X-, Y-, and Z-directions. The ranges, standard deviations, maximum positive coordinates, and maximum negative coordinates showed very similar trends. The ranges of the wrist marker coordinates are displayed in Figure 4.8. In Figure 4.8 (A) and (C), a small division between the grouping of the conventional loading values and a grouping of the device values is visible. Figure 4.8 is representative of the trends found in the other metrics. A trend for increased movement in the X-direction and decreased movement in the Z-direction for the conventional loading conditions in comparison to the device loading conditions was present throughout the considered metrics listed above. The FlexBar® differed most greatly through the range of motion. This is not unexpected given the nonsymmetric loading applied by the torsional member.

The trend for increased movement in the X-direction and decreased movement in the Y-direction for the conventional loading conditions corresponds with the differing motion patterns shown in Figure 4.7. Further analysis is necessary to distinguish the cause of these differences. Possible causes for this motion pattern difference may be explained by the horizontal handle of the device opposed to a more natural dart throwing motion [45] or the constant handle length that is not apparent with the conventional methods.

4.3 Wrist Angles

An example of flexion-extension and ulnar-radial deviation wrist angles during a trial is shown in Figure 4.9. The mean flexion-extension ranges, maximum flexions, flexion percentages of overall range, extension percentages of overall range, and ulnar-radial deviation

ranges are displayed in Table 4.2. The average flexion-extension range of 109 degrees and ulnar-radial deviation range of 31 degrees fall well within the previously reported values, as shown in Table 4.3. It is worth noting that these ranges were measured during the repetitions and not during a separate active range of motion test and thus, a smaller overall range for ulnar-radial deviation is very reasonable.

The large range of ulnar-radial deviation was initially unexpected, as mentioned in Section 3.3.3. However, upon further review, Li found similar coupling between flexion-extension and ulnar-radial deviation of the wrist [51]. Li's results showed a nonlinear relationship between flexion-extension and ulnar-radial deviation of the wrist, an average 21.2 degrees of ulnar-radial deviation for an average 108.3 degree flexion extension. Within the current study, an average of 31 degrees of ulnar-radial deviation was measured during an average 109 degrees of extension and flexion. The differences between the current values and Li's may be due to a less robust setup during this study or the loading may have had an effect of the ulnar-radial deviation elicited.

Interesting patterns are apparent in the flexion-extension (FE) and ulnar-radial deviation (URD) coupling: linear, nonlinear monotonic, parabolic, and cubic patterns are apparent within the FE-URD relationships, as seen in Figure 4.10. This is another aspect that is beyond the scope of this thesis work and will be analyzed in the future.

With the ability to measure both the wrist flexion-extension and the orientation of the device handle, a comparison between the values from these two sources was possible. An example of these two signals and the difference between them is displayed in Figure 4.11. The maximum measured angle differences are displayed in Table 4.4. The differences as seen in the bottom plot of Figure 4.11 show an offset between the device and the motion capture measurements as expected. The device reference was a horizontal position. The motion capture reference was a neutral wrist posture taken during the static capture. In addition to the offset, an oscillation of the differences is evident in the signal. This pattern would indicate that the motion of the handle is not achieved solely through wrist flexion-extension. Alternative sources to account for this additional motion of the device handle could be ulnar-radial deviation, finger flexion-extension, or a combination of these two.

4.4 Comparison of EMG Between Conventional Methods and Developed Device

The final category for comparison relies on the sEMG readings taken during the trials. An example of the binned average values for each muscle can be seen in Figure 4.12. The

synergies between the muscles can more easily be seen in Figure 4.13. ANOVAs were run across binned values at -10 degrees, 0 degrees, and 10 degrees. The -10, 0, 10 degree angles were chosen to allow comparison across participants, loading conditions, and repetitions with varying range of motion. This was the extent of the range available for comparison across all trials. The trends between these three angles were very similar. This similarity is likely due to the proximity of these readings. The ANOVA for average bin readings at 0 degrees, shown in Figure 4.14 and Figure 4.15, is representative of the -10 and 10 degree results as well.

ANOVAs were run for means and sums of the averages of binned EMG readings across loading conditions. The means and sums showed very similar trends. The results of the means ANOVA are shown in Figure 4.16 and Figure 4.17. These values are less controlled for as some participants would not have moved through the full range of motion for some more difficult conditions.

No significant difference was found between the above-mentioned muscle potential metrics using the conventional method and the corresponding device ($p>0.05$). For comparison, the conventional loading methods were also compared. There were some significant differences found between the measurements for the conventional methods. The variables that showed significant difference ($p<0.05$) are displayed in Table 4.5. As can be seen in Table 4.5, the ECRB and ED measurements with the free weight and the other two conventional methods were often different. There were additional differences visible, as shown in Figure 4.14 and Figure 4.15; however, the effect size was not large enough with the number of participants recruited to show statistical significance.

4.4.1 Pearson Product-Moment Correlations of the EMG Trends

The mean Pearson product-moment correlations of the EMG trends between the loading methods discussed in Section 3.4.1 for the free weight, exercise band, and FlexBar® are displayed in Figure 4.18, Figure 4.19, and Figure 4.20, respectively. Pearson product-moment correlations measure the linear correlation between two sets of values. In this analysis, a 1.0 would indicate a perfect match between the two data sets, excellent simulation of the conventional method, while a -1.0 would indicate an opposite linear correlation and a 0 would indicate no linear correlation, very poor simulation of the conventional method. Within Figure 4.18 through 4.20, it can be seen that the trends for the processed EMG readings are very dissimilar for the FCR and FCU, mean Pearson coefficients as low as 0.1337 and 0.1104, respectively. This can be attributed to differences in form and technique

as participants may grip the handle with varying strengths through the range of motion. However, the EMG trends appear relatively similar for the extensor muscles that were the intended muscles of interest for this device, mean Pearson coefficients >0.64. The mean Pearson coefficients are particularly high for the ED, mean Pearson coefficient >0.85. However, comparison between the conventional loading methods found similarly high mean Pearson coefficients for ED, mean Pearson coefficients >0.88.

4.4.2 Root Mean Square (RMS) Difference Between the Loading Methods

The binned averages across the range of motion were compared using a root mean square (RMS) difference between the loading methods. This was a method to effectively quantify the differences in muscle potential at each angle across the range of motion between two loading methods. While the Pearson product-moment correlations compare the EMG reading trends, the root mean square difference between the loading methods allowed comparison of the magnitude of the values across the range of motion. While high values were indicative of strong correlation for the Pearson product-moment correlations, low RMS values indicate a smaller difference between the two data sets. ANOVAs were run for the resulting RMS values. No significance was found between the conventional methods or between the conventional loading method and corresponding device. The means of the RMS values for the free weight, exercise band, and FlexBar are displayed in Figure 4.19, Figure 4.20, and Figure 4.21, respectively.

Though no statistical significance was found, the RMS values appear to be comparable or better for most muscles and loading method. It is worth noting that in Figure 4.21, exercise band-FlexBar® comparison has consistently lower values compared to the device and the free weight for the extensor muslces.

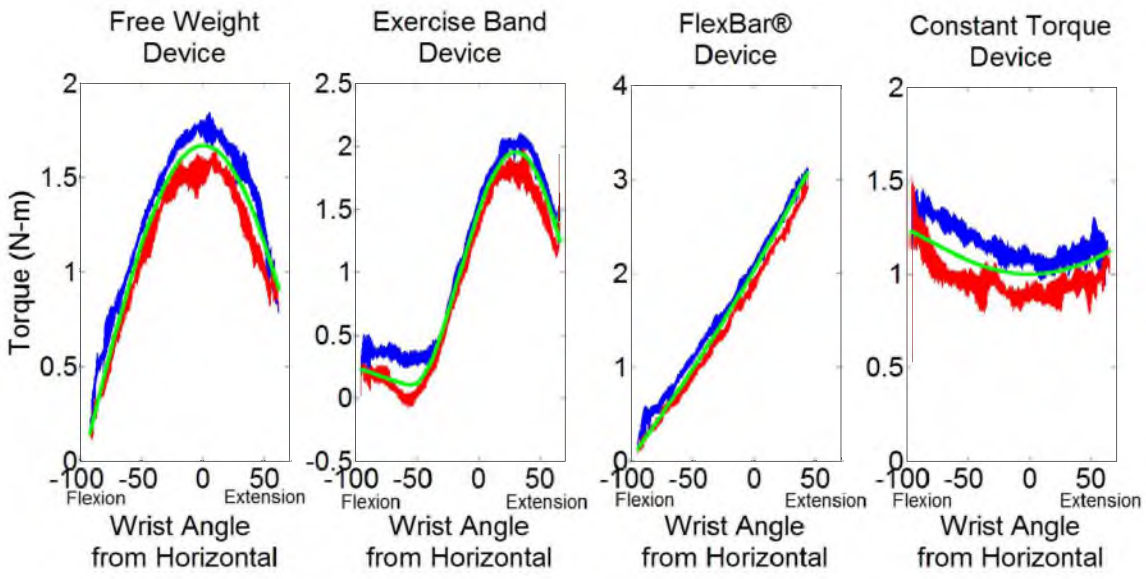

Figure 4.1. Example desired and measured torques across the range of motion. Green: Modeled torque plus gravity compensation, Blue: Torque measured during the concentric portion of the wrist extension. Red: Torque measured during the eccentric portion of the wrist extension

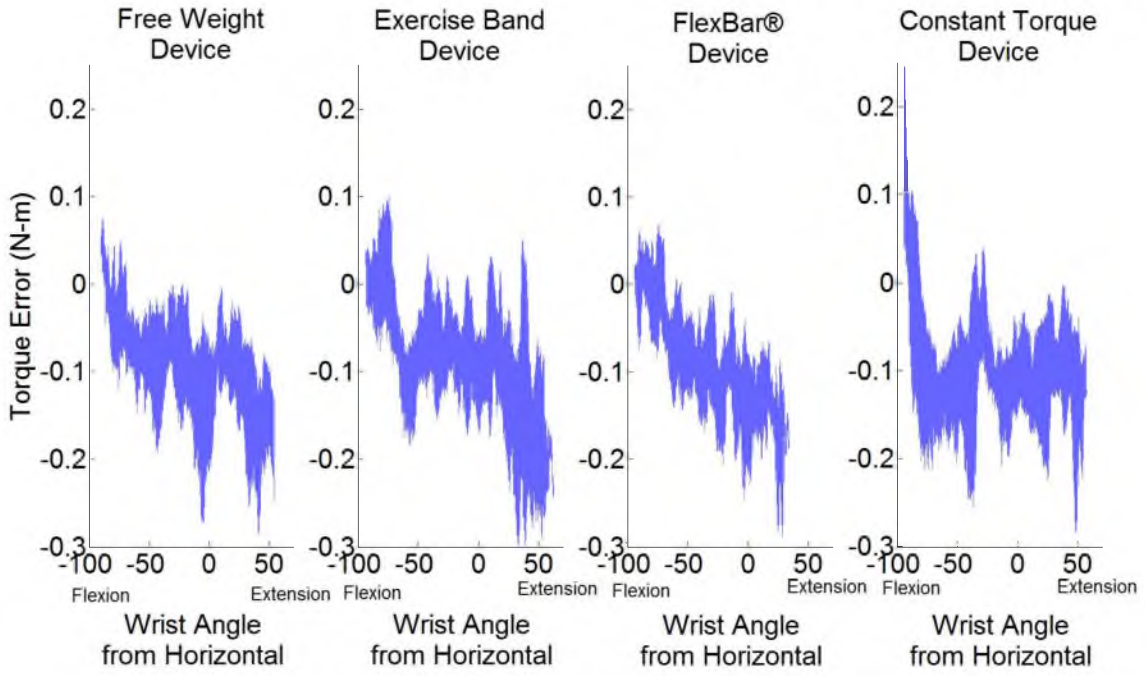

Figure 4.2. Example error between desired and measured torque during descent corresponding to torques represented in Figure 4.1.

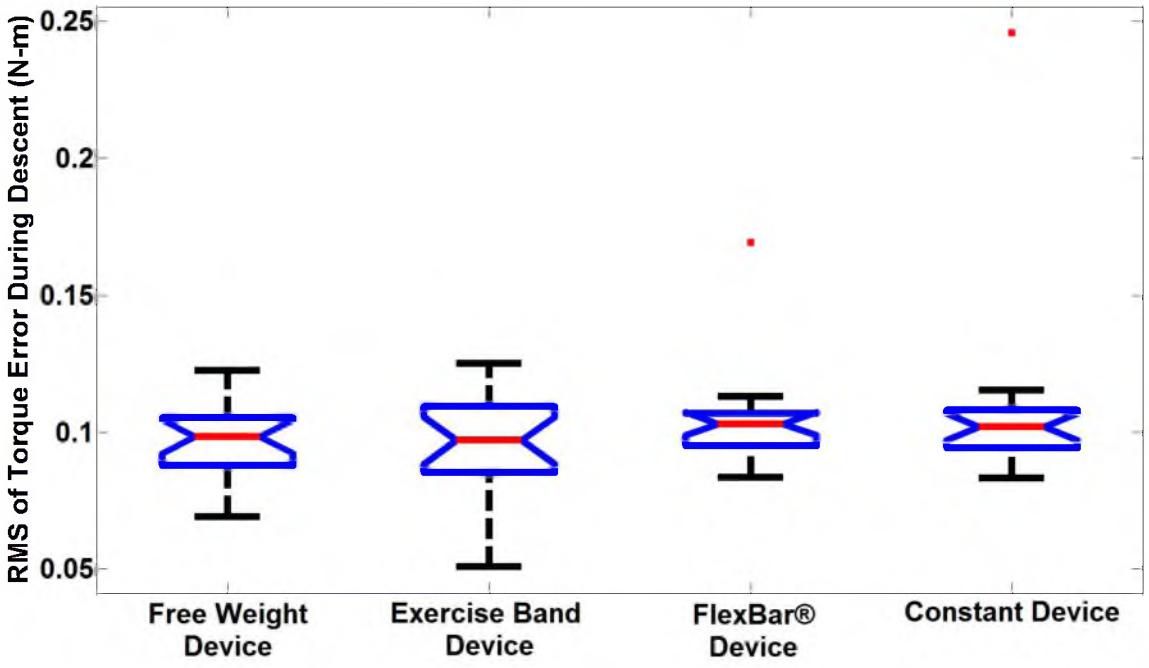

Figure 4.3. RMS of torque error during descent.

Table 4.1. Torque error descriptive statistics.

	Free Weight Device	Exercise Band Device	FlexBar® Device	Constant Device	Average
Mean RMS of Error (N-m)	0.978	0.0980	0.1041	0.1081	0.1020
Mean STD of Error	0.0586	0.0629	0.0639	0.0635	0.0622
Mean Max Overshoot Error (N-m)	0.1108	0.1348	0.1086	0.1187	0.1182
Mean Max Undershoot Error (N-m)	0.3152	0.3406	0.3021	0.3291	0.3218

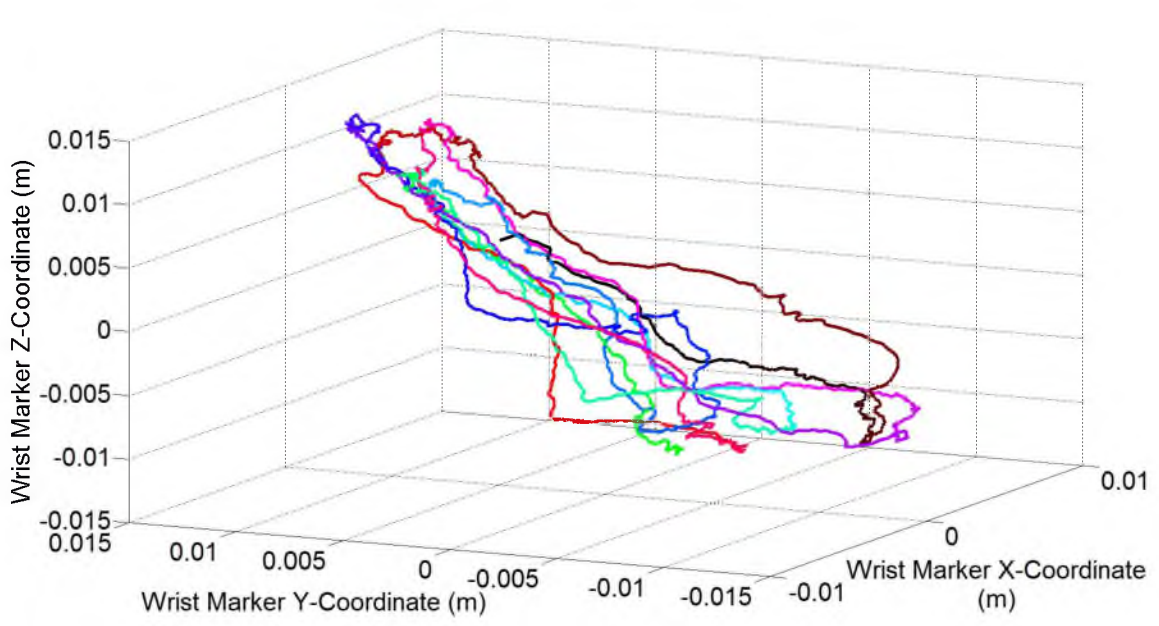

Figure 4.4. Example wrist motion over the duration of free weight trial. Trial time is represented with the color progression green, blue, purple, pink, red, brown, and ending in black.

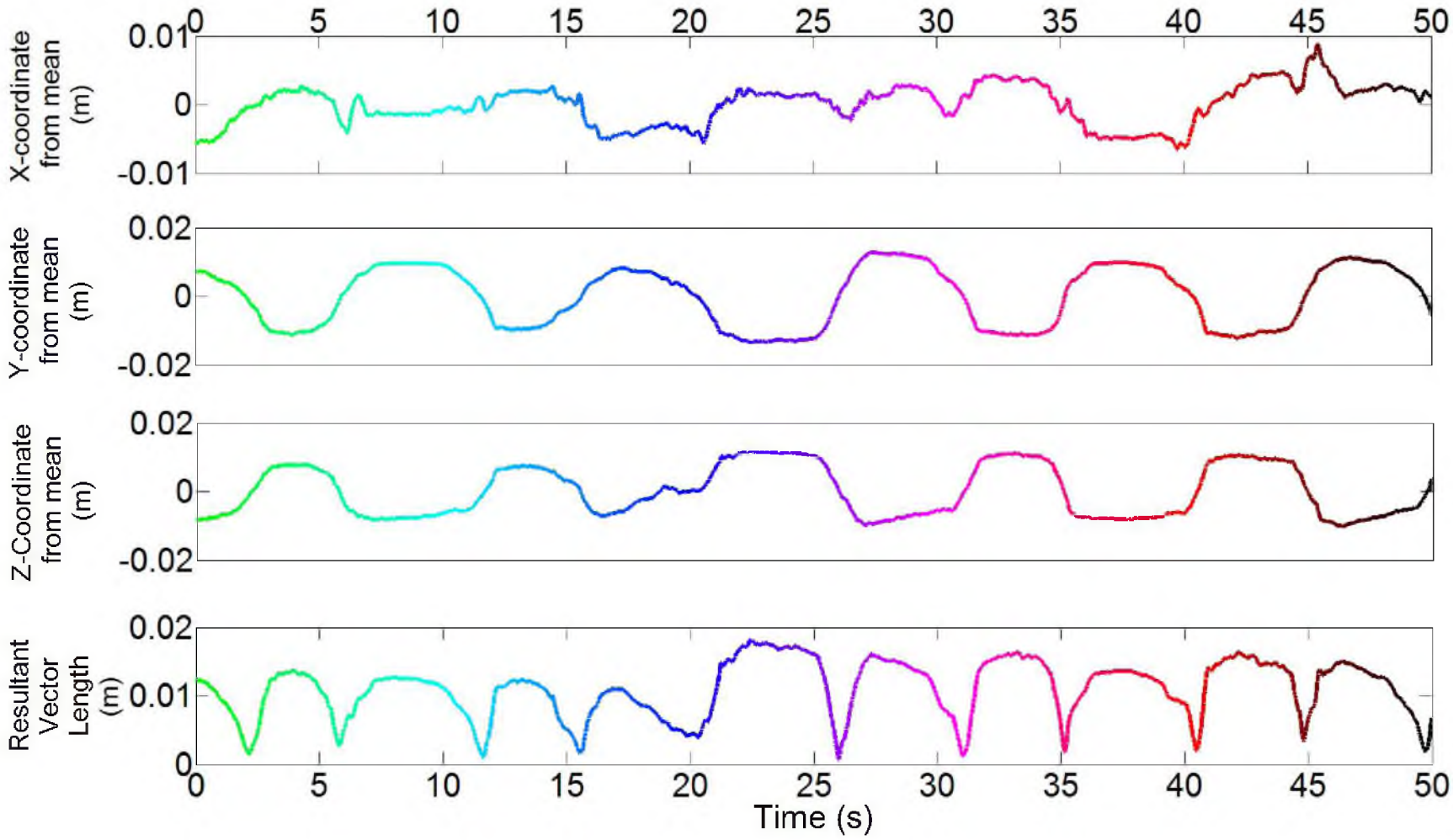

Figure 4.5. Example wrist coordinates over the duration of free weight trial represented in Figure 4.4.

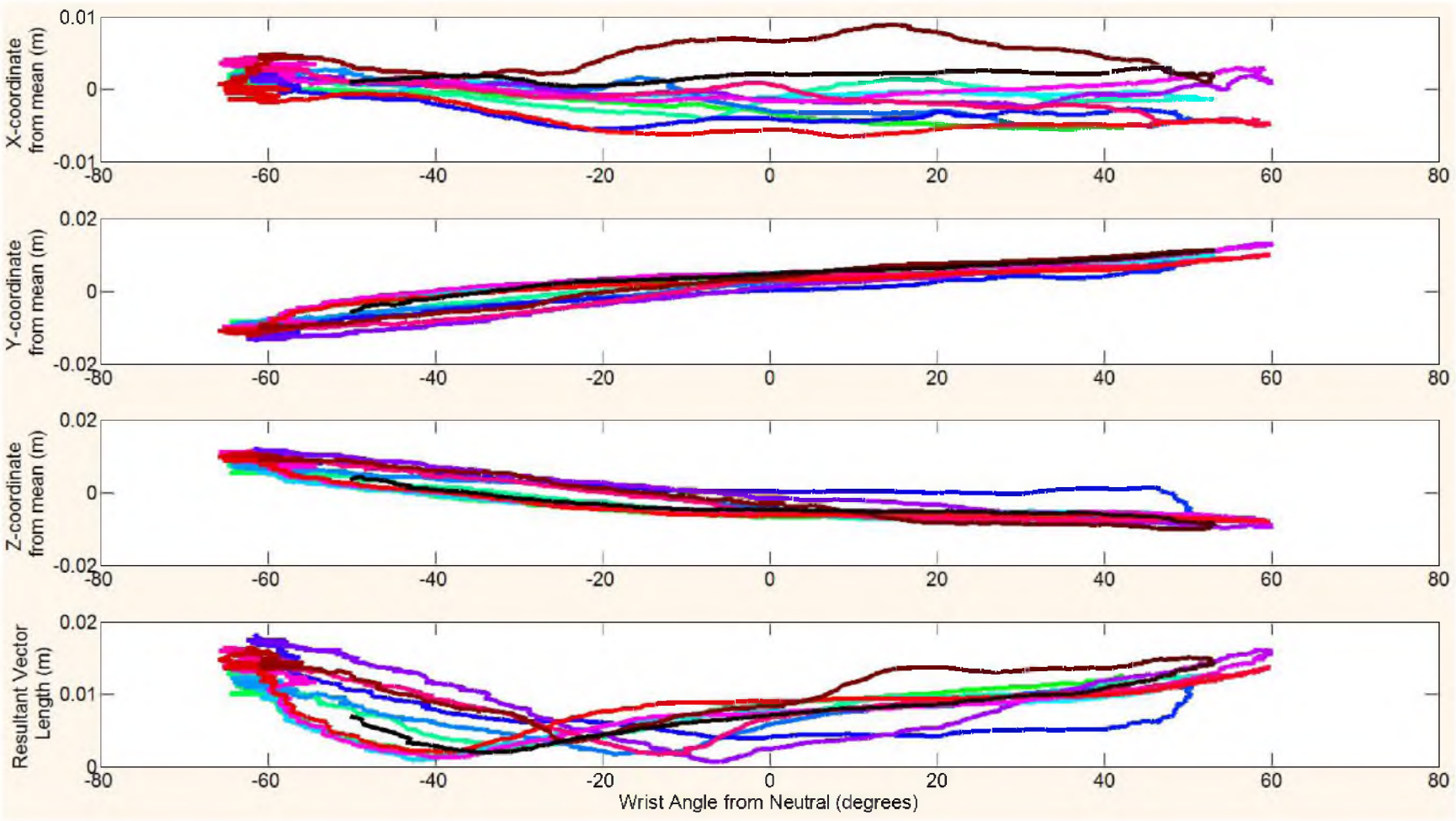

Figure 4.6. Example wrist coordinates over the duration of the free weight trial shown in Figure 4.5 versus wrist angle from neutral posture.

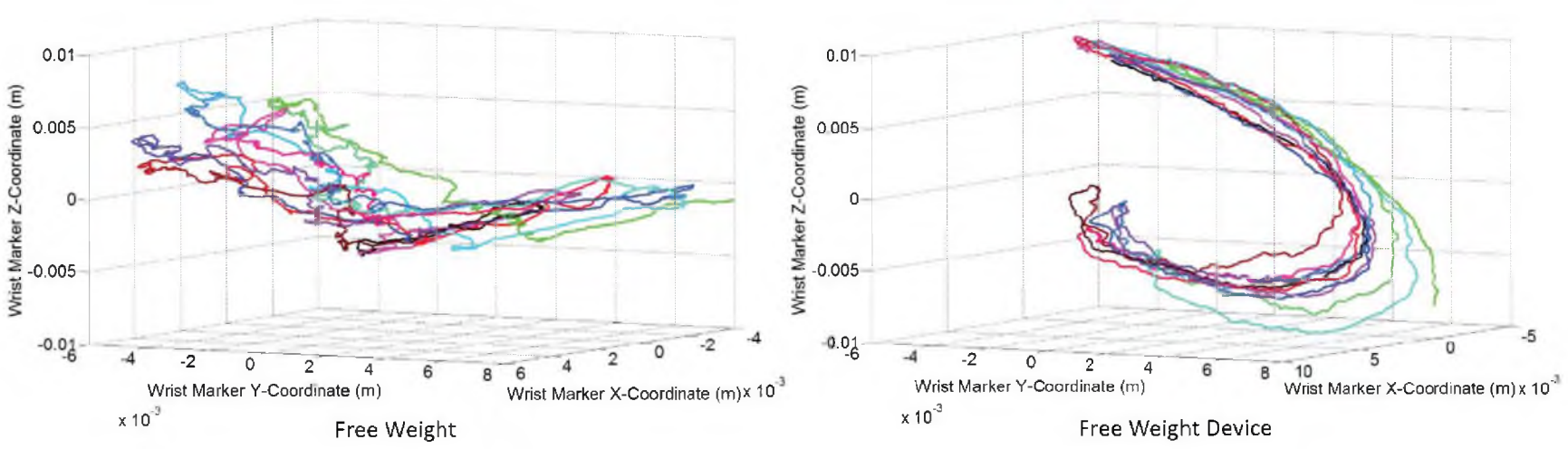

Figure 4.7. Wrist coordinates during a conventional loading trial and wrist coordinates during the corresponding device trial. Left: Free weight. Right: Free weight device.

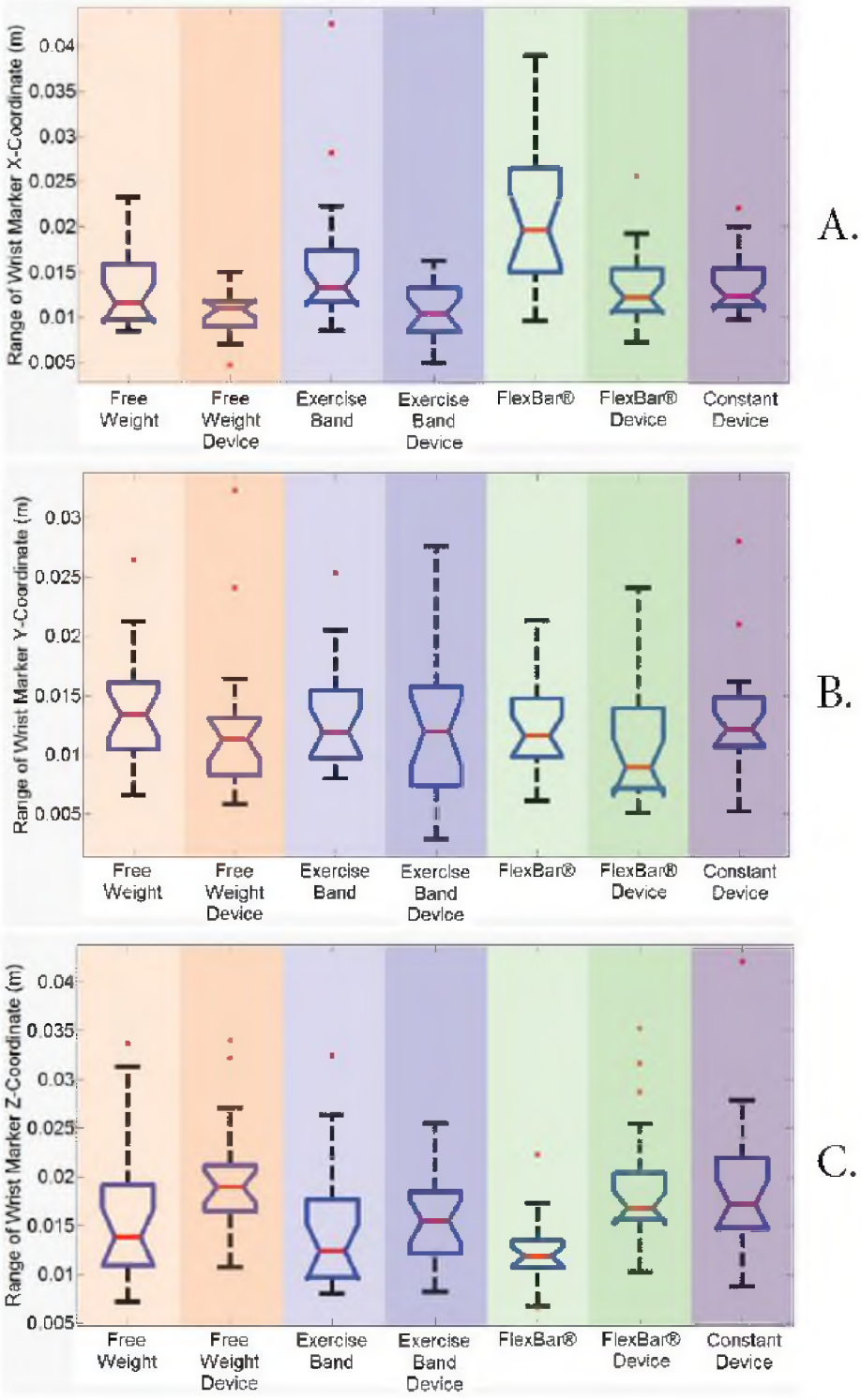

Figure 4.8. Range of wrist marker coordinate in X-direction (A), Y-direction (B), and Z-direction (C). FW device: Free weight device, EBand device: Exercise band device.

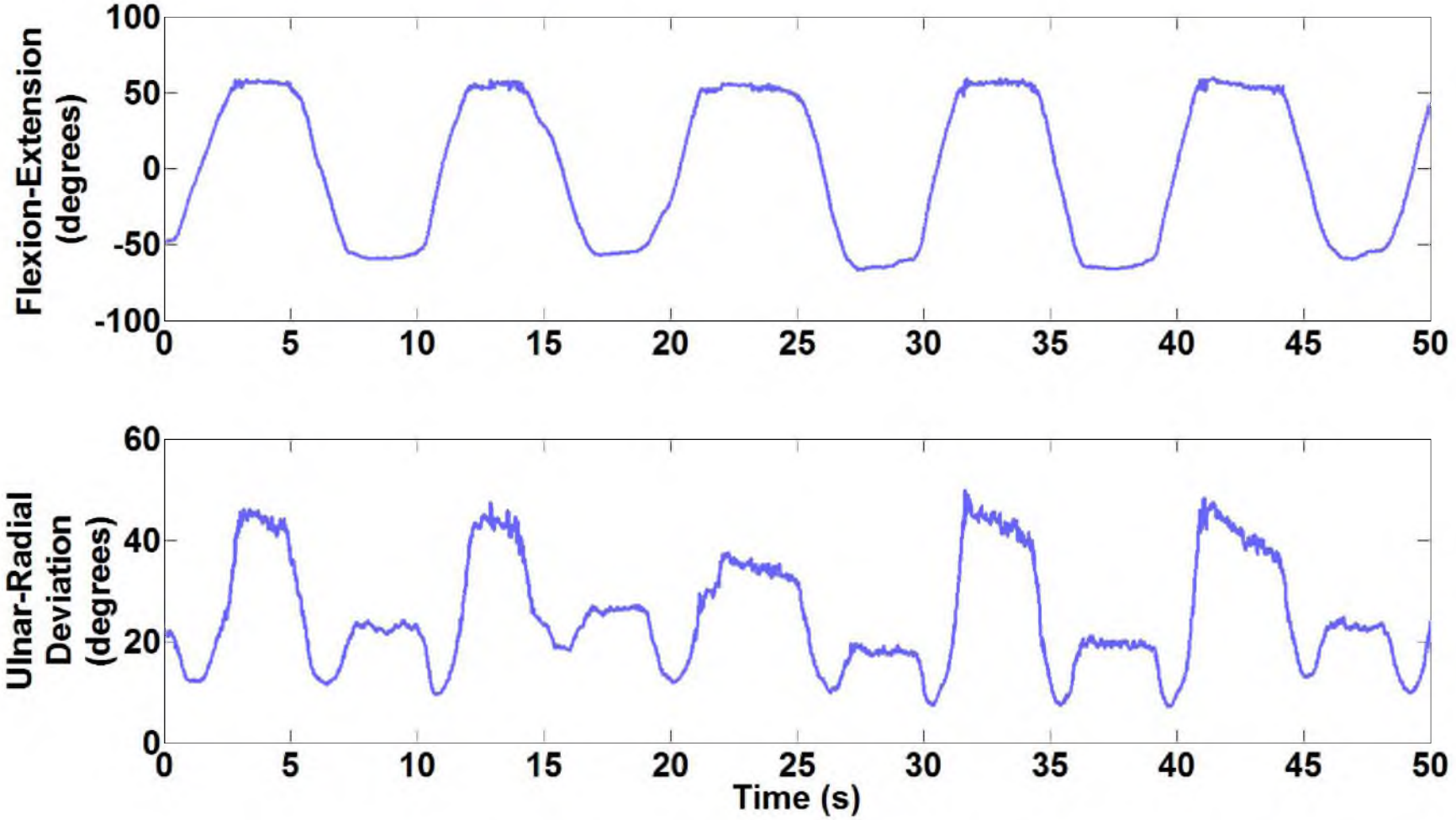

Figure 4.9. Example wrist extension-flexion (top) and wrist ulnar radial deviation angles from neutral (bottom) during a trial

Table 4.2. Flexion, extension, and ulnar-radial deviation range of motions across conditions.

	Free Weight	Free Weight Device	Exercise Band	Exercise Band Device	FlexBar®	FlexBar® Device	Constant Device	Average
Flexion-Extension Range	109	108	108	111	107	106	113	109
Extension	52	49	47	51	50	47	52	50
Extension %	48%	46%	43%	46%	47%	45%	46%	46%
Flexion	57	59	61	60	57	59	61	59
Flexion %	52%	54%	57%	54%	53%	55%	54%	54%
URD Range	34	31	35	29	29	30	32	31

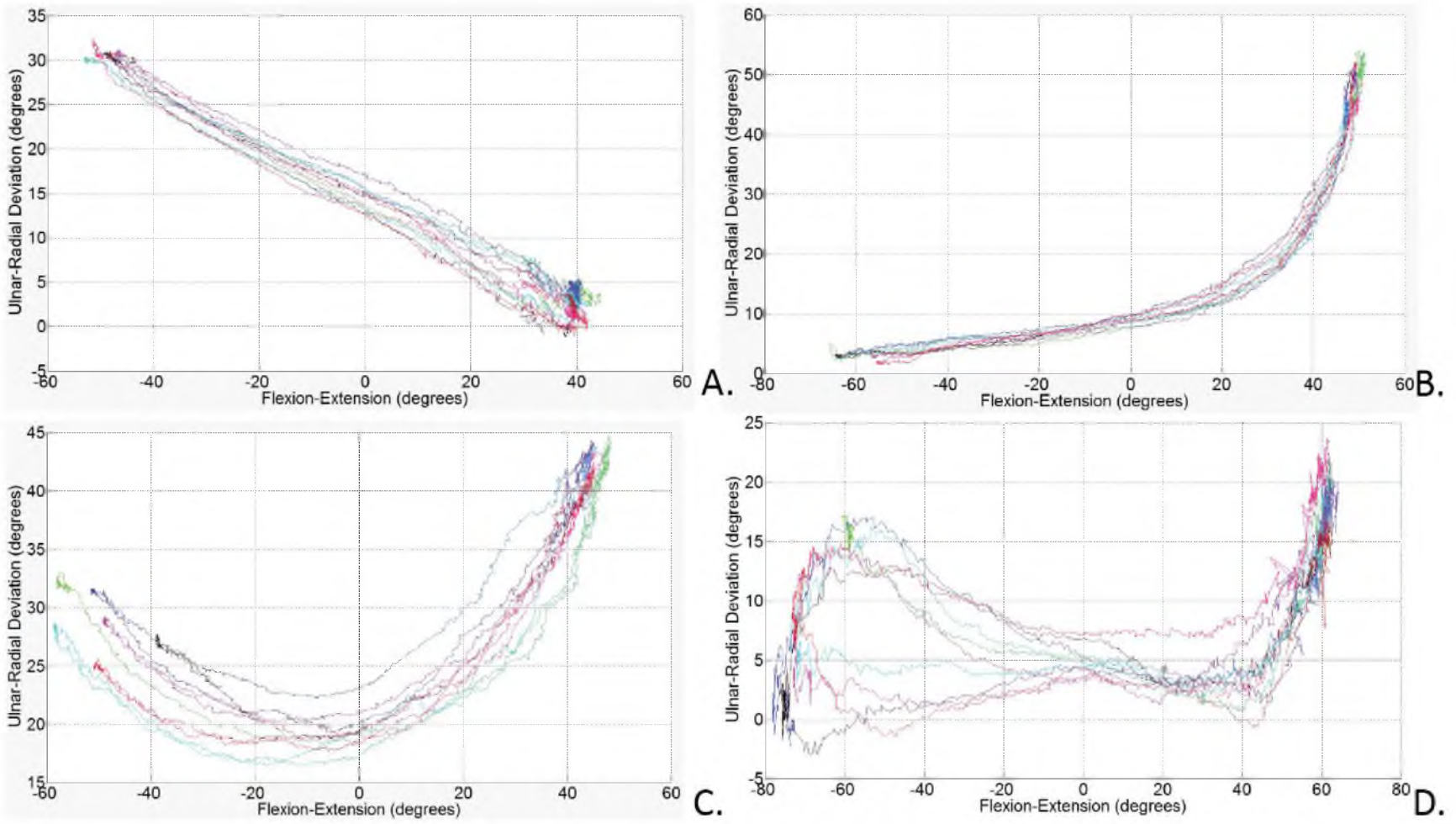

Figure 4.10. Example trends apparent in flexion-extension to ulnar-radial deviation coupling. All examples are taken from free weight device trials. A. Linear, B. Nonlinear monotonic, C. Parabolic, D. Cubic.

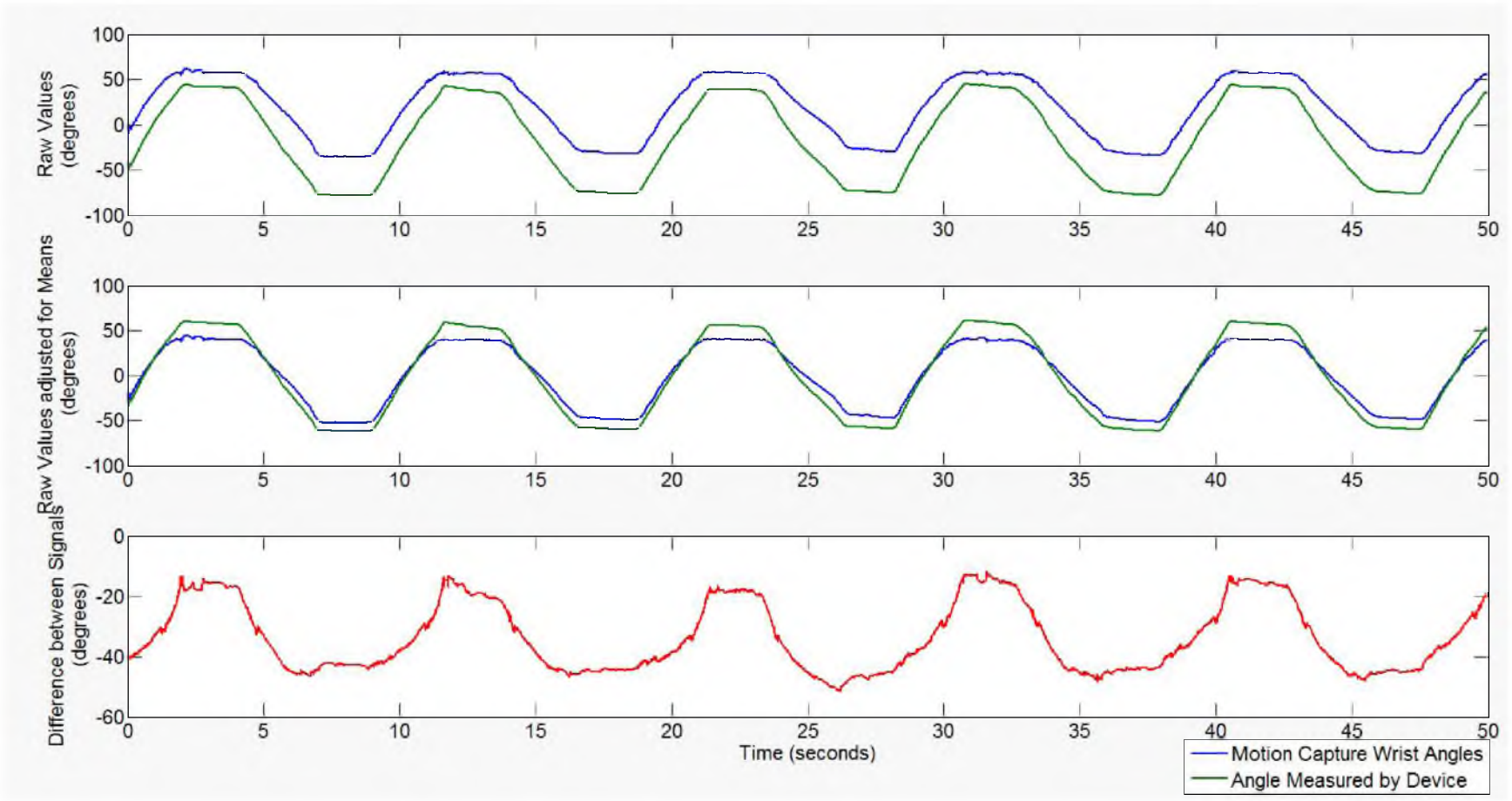

Figure 4.11. Example raw extension-flexion angles (Top), the angles offset by their respective means (Middle), and difference between the two signals (Bottom). Motion capture (blue), device encoder (green), and the difference between them (red).

Table 4.3. Comparison of previously determined wrist range of motions and measured ranges for flexion-extension (FE), and ulnar-radial (URD) [51–57]

	FE Range	**Flexion**	**Flexion%**	**Extension**	**Extension%**	**URD range**	**UD**	**UD%**	**RD**	**RD%**
Current	109	59	5%	49	46%	31				
Brigstocke (2013)	132	84	64%	48	36%	65	49	75%	16	25%
Li (2005)	108	41	38%	67	62%	55	35	64%	20	36%
Li (2002)	144	75	52%	69	48%	75	51	68%	24	32%
Salvia et al. (2000)	104	56	54%	48	46%	54	35	65%	19	35%
Marshall et al. (1999)	140	67	48%	73	52%	68	47	69%	21	31%
Ryu et al. (1991)	138	79	57%	59	43%	59	38	64%	21	36%
Boone and Azen (1979)	149	75	50%	74	50%	56	35	63%	21	38%
Heck et al. (1965)	144	73	51%	71	49%	52	33	63%	19	37%
Mean	132	67	50%	66	50%	57	39	65%	21	35%

Table 4.4. Differences between wrist angles extracted from motion capture and device encoder

	Free Weight Device	**Exercise Band Device**	**FlexBar® Device**	**Constant Device**
Mean Max Positive Angle Difference	21.6	18.2	16.7	22.2
Mean Max Negative Angle Difference	18.5	15.6	18.0	21.5
Mean Range Difference	40.2	33.8	34.7	43.4

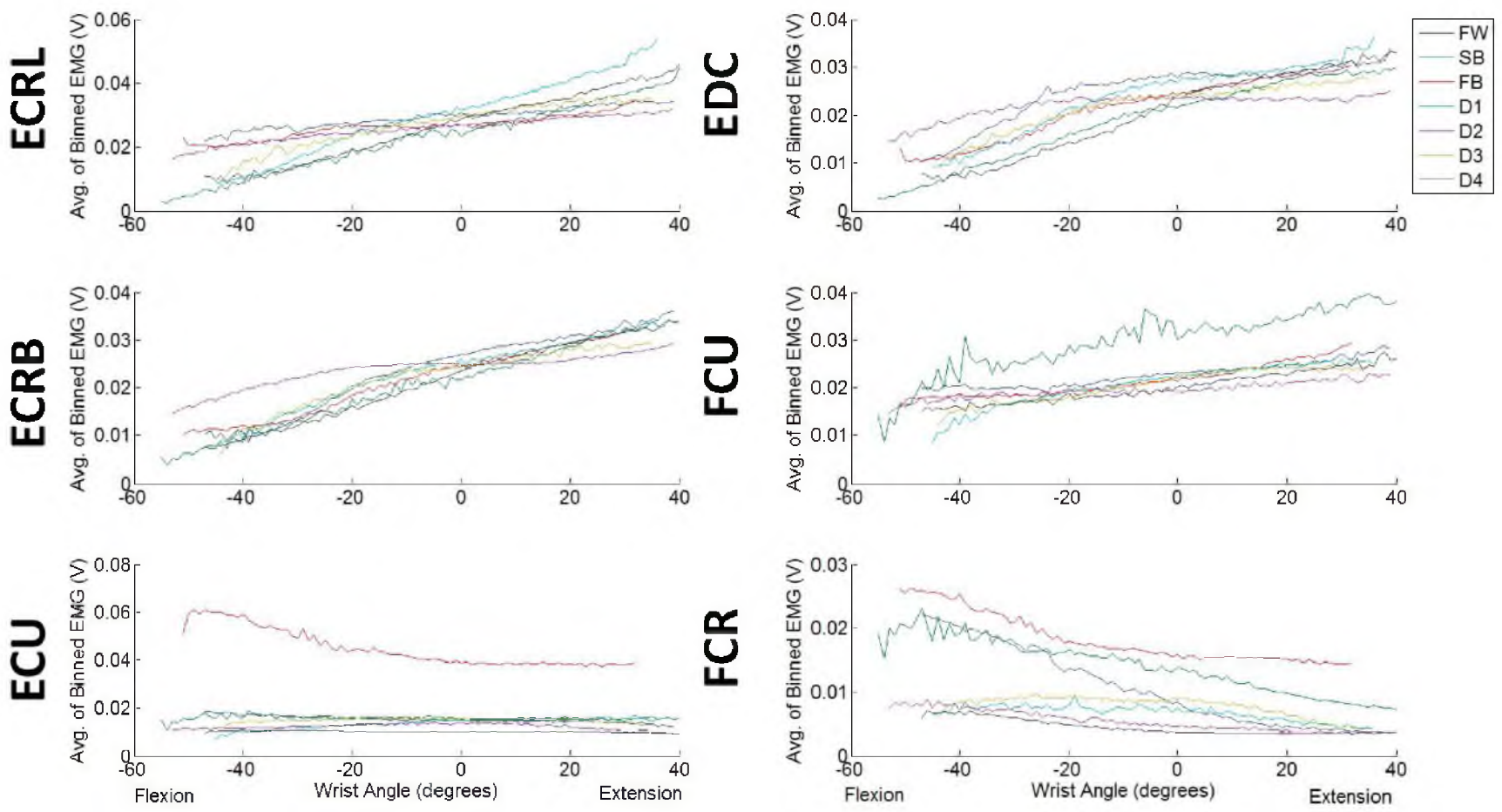

Figure 4.12. Example averages of binned EMG readings across range of motion. FW: Free weight, SB: Exercise band, FB: FlexBar®, D1: FlexBar® device, D2: Constant device, D3: Free weight device, D4: Exercise band device.

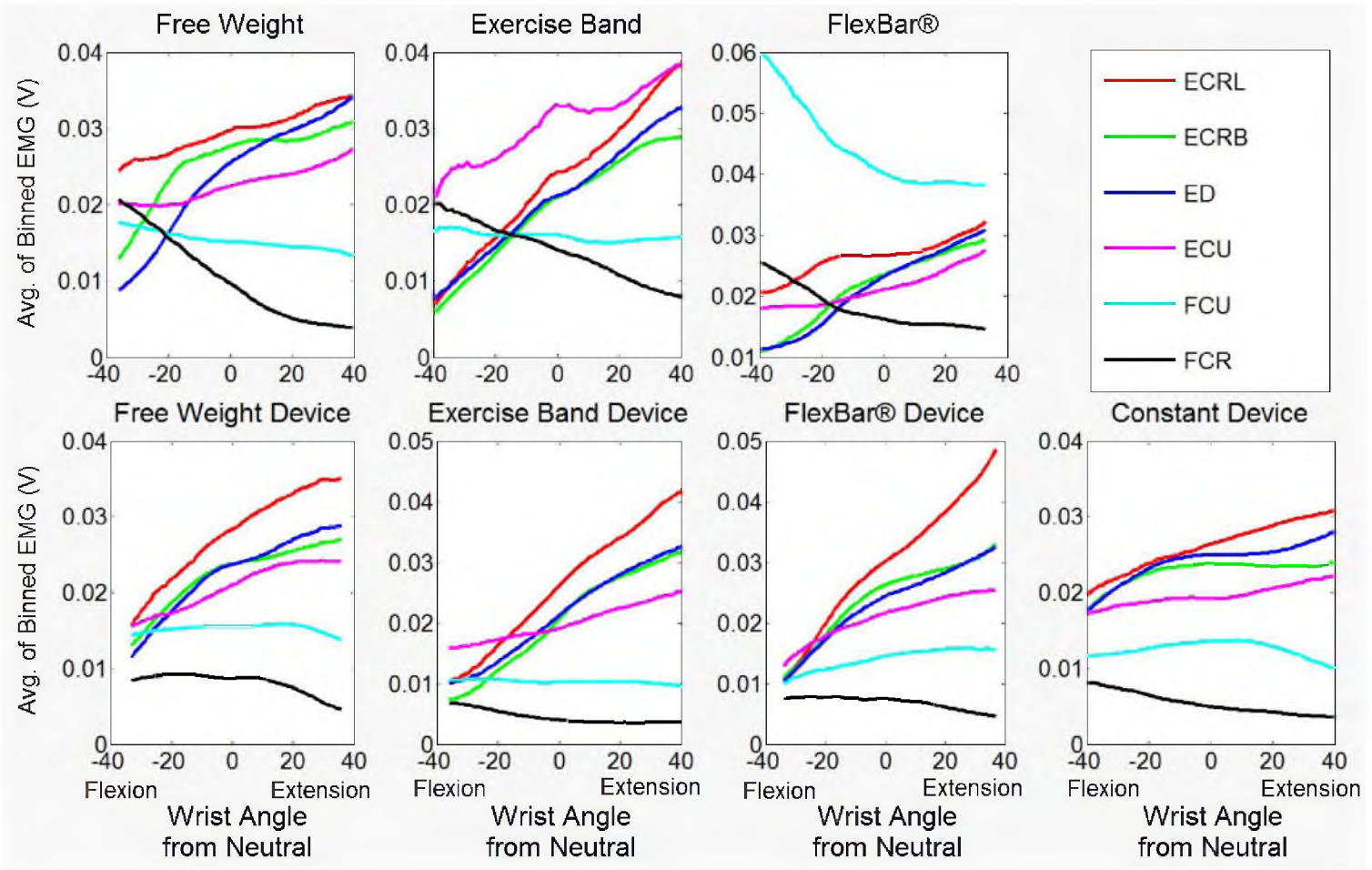

Figure 4.13. Example averages of binned EMG readings across range of motion with each loading condition.

Table 4.5. EMG readings found to have significant difference ($p<0.05$) between conventional methods

Muscle	**Variable**	**Conventional Method 1**	**Conventional Method 2**	**P-Value**
ECRB	EMG at -10 degrees	Free Weight	Exercise Band	0.0044
ECRB	EMG at -10 degrees	Free Weight	FlexBar®	0.0040
ED	EMG at -10 degrees	Free Weight	Exercise Band	0.0273
ED	EMG at -10 degrees	Free Weight	FlexBar®	0.0232
ED	EMG at 10 degrees	Free Weight	FlexBar®	0.0397
ECRB	EMG at -10 degrees	Free Weight	Exercise Band	0.0131
ECRB	EMG at -10 degrees	Free Weight	FlexBar®	0.0199
ED	EMG at 0 degrees	Free Weight	Exercise Band	0.0408
ED	EMG at 0 degrees	Free Weight	FlexBar®	0.0163
ECRB	EMG mean	Free Weight	Exercise Band	0.0332
ED	EMG mean	Free Weight	Exercise Band	0.0364

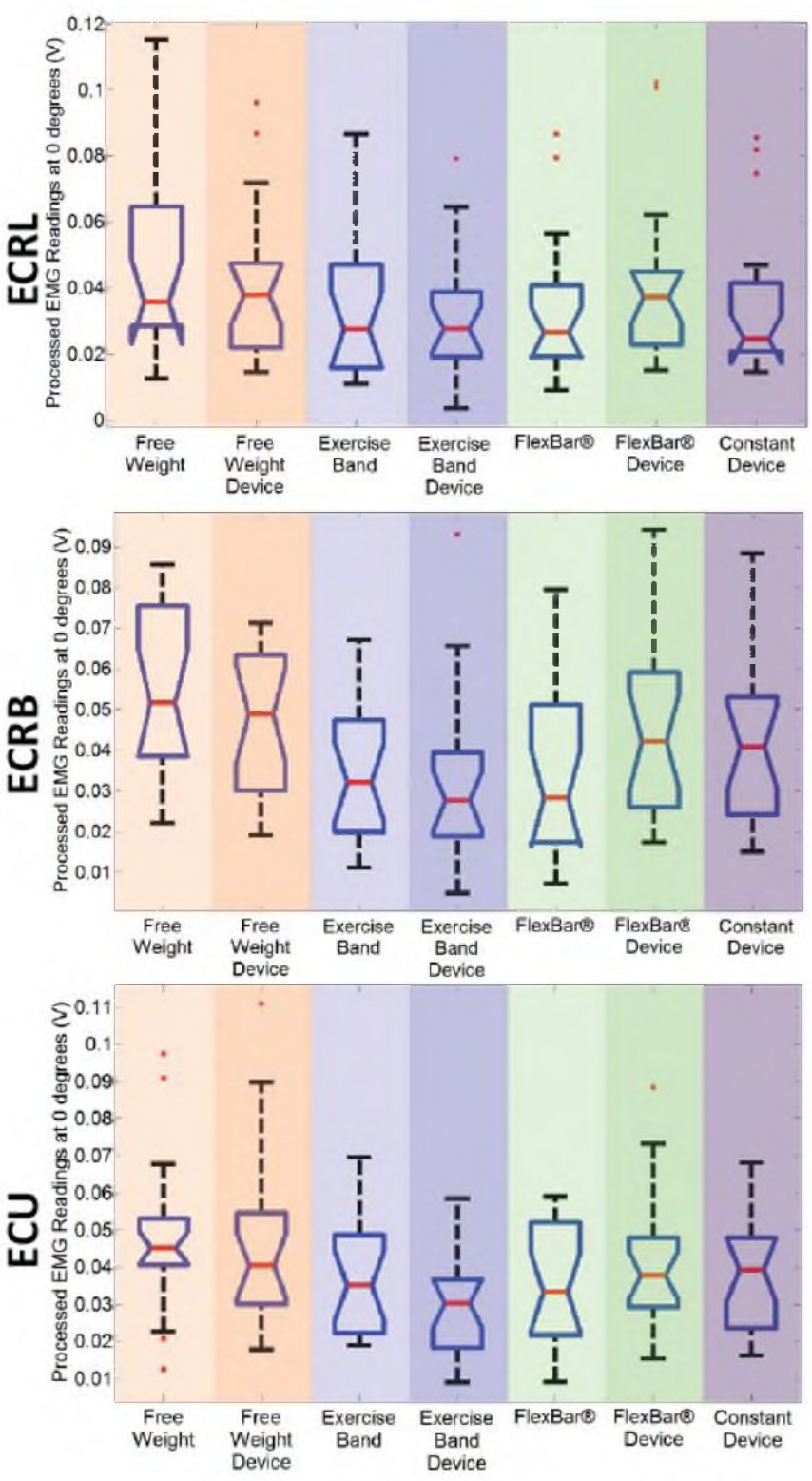

Figure 4.14. ANOVAs for filtered bin readings at 0 degrees across muscles for ECRL, ECRB, and ECU. FW device: Free weight device, EB device: Exercise band device, FB device: FlexBar device

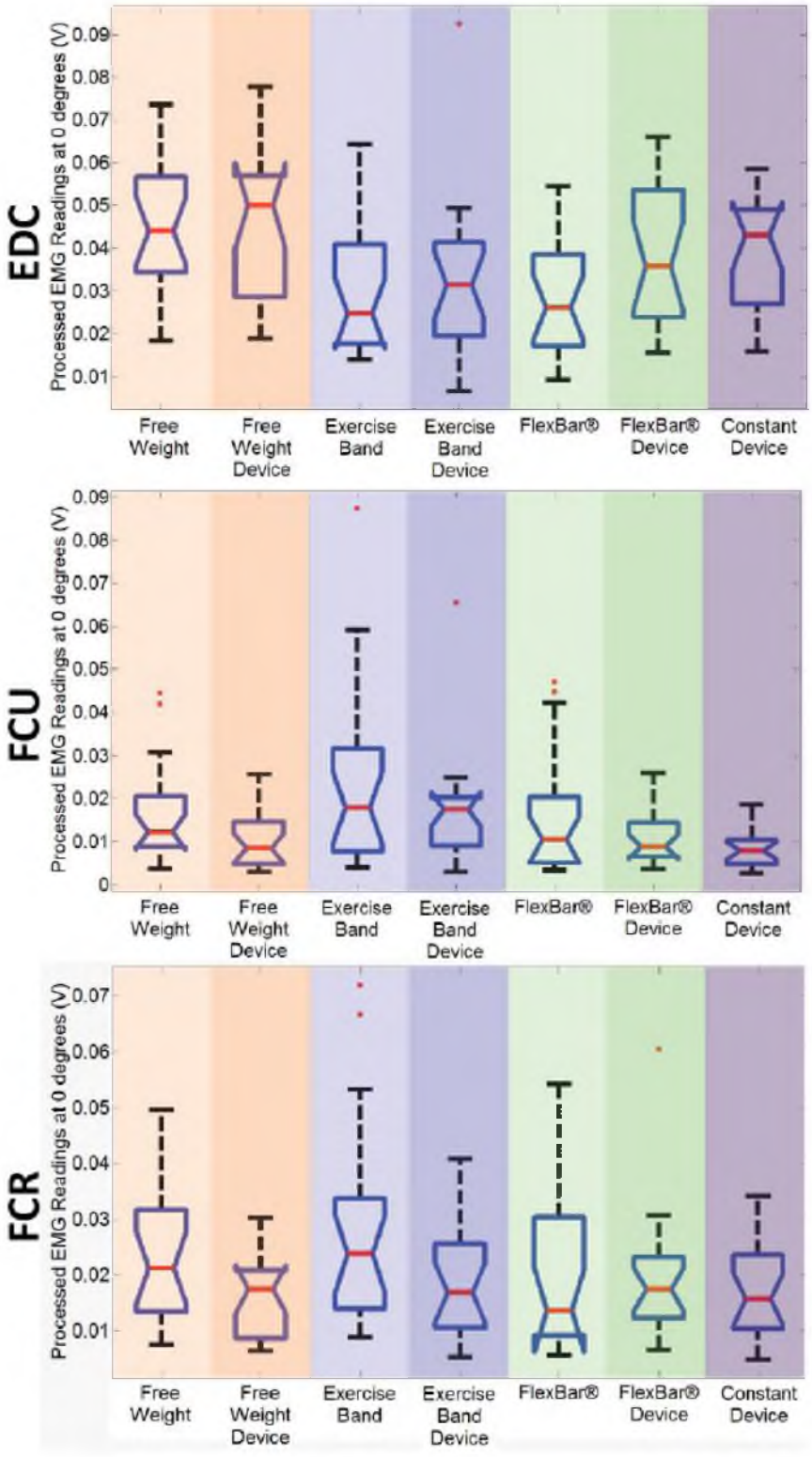

Figure 4.15. ANOVAs for filtered bin readings at 0 degrees across muscles for EDC, FCU, and FCR. FW device: Free weight device, EB device: Exercise band device, FB device: FlexBar device

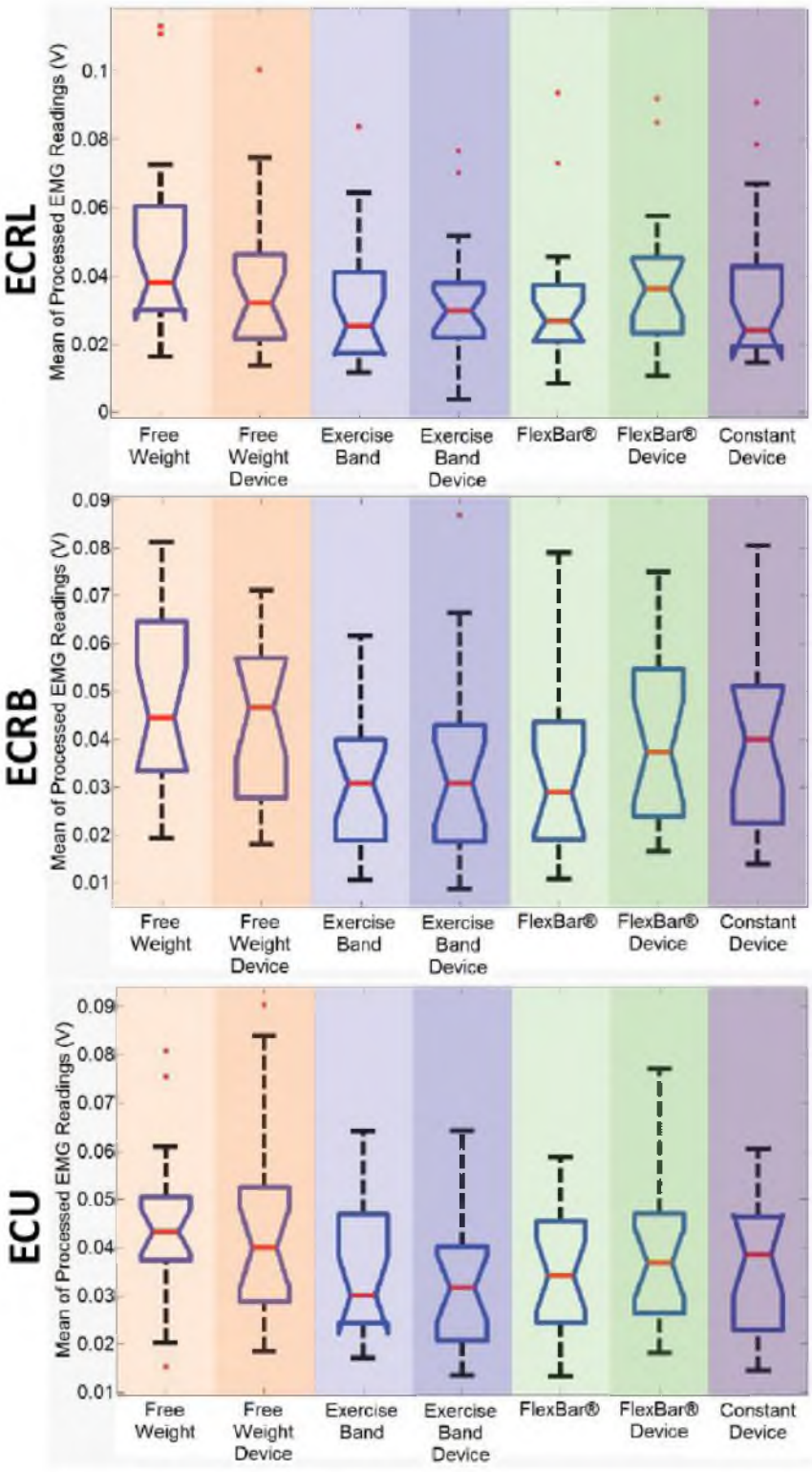

Figure 4.16. Means of averaged binned EMG reading ANOVAs across muscles for ECRL, ECRB, and ECU. FW device: Free weight device, EB device: Exercise band device, FB device: FlexBar device

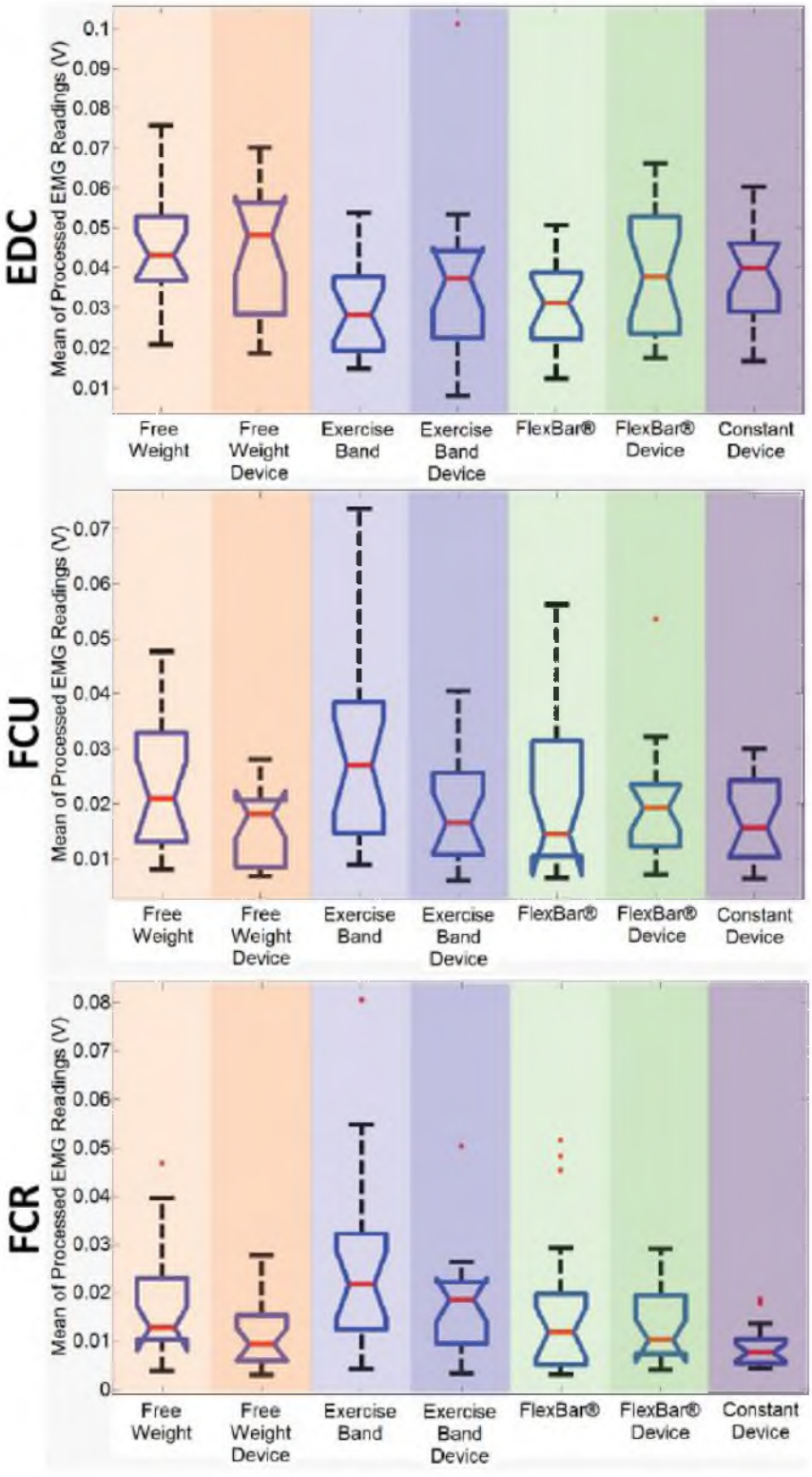

Figure 4.17. Means of averaged binned EMG reading ANOVAs across muscles for EDC, FCU, and FCR. FW device: Free weight device, EB device: Exercise band device, FB device: FlexBar device

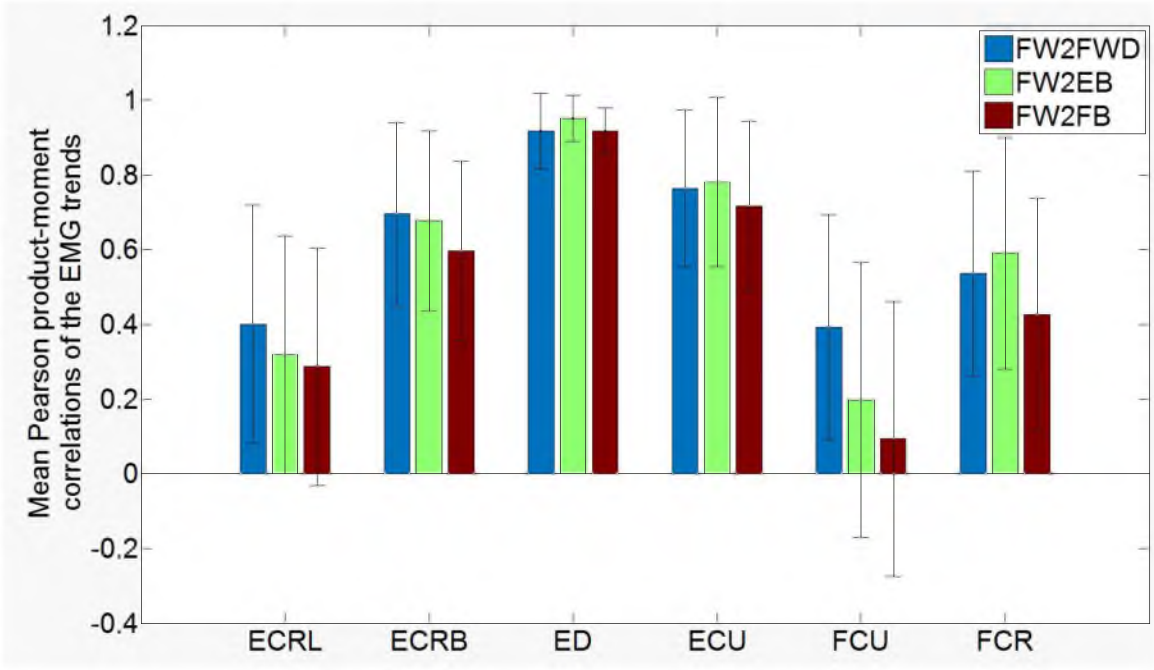

Figure 4.18. Mean Pearson product-moment correlations of the filtered binned EMG readings for the free weight. FW2FWD: Free weight compared to the corresponding device, FW2EB: Free weight compared to the exercise band, FB2EB: Free weight compared to the FlexBar.

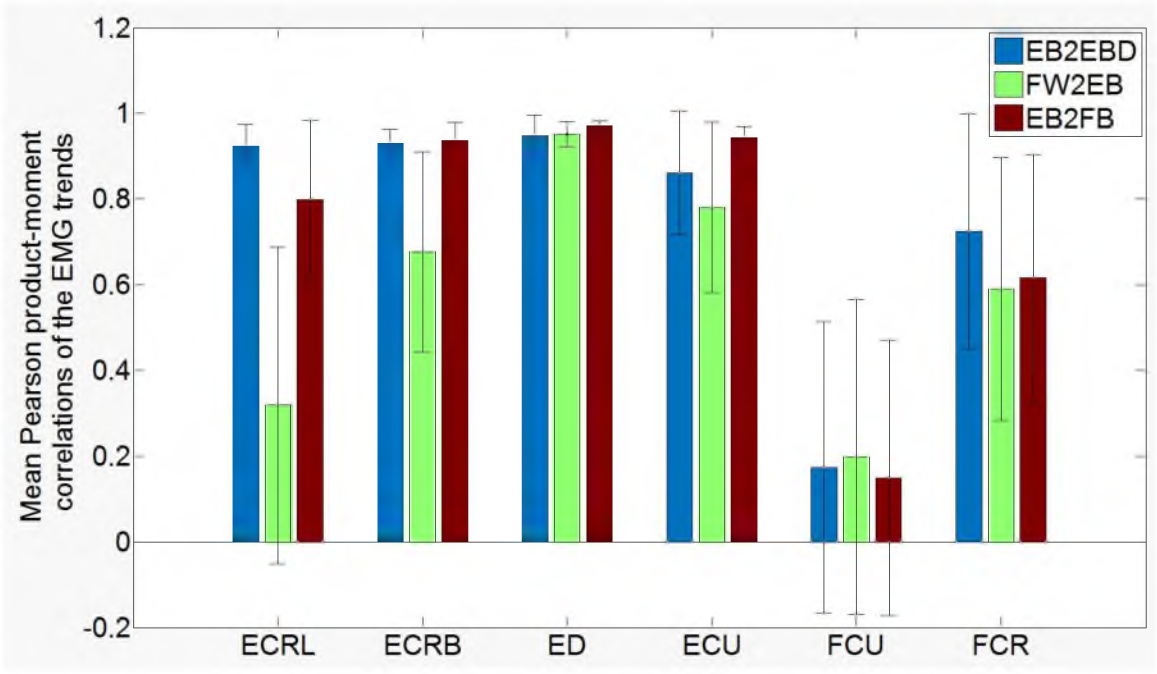

Figure 4.19. Mean Pearson product-moment correlations of the filtered binned EMG readings for the exercise band. EB2EBD: Exercise band compared to the corresponding device, FW2EB: Exercise band compared to the free weight, FB2EB: Exercise band compared to the FlexBar®.

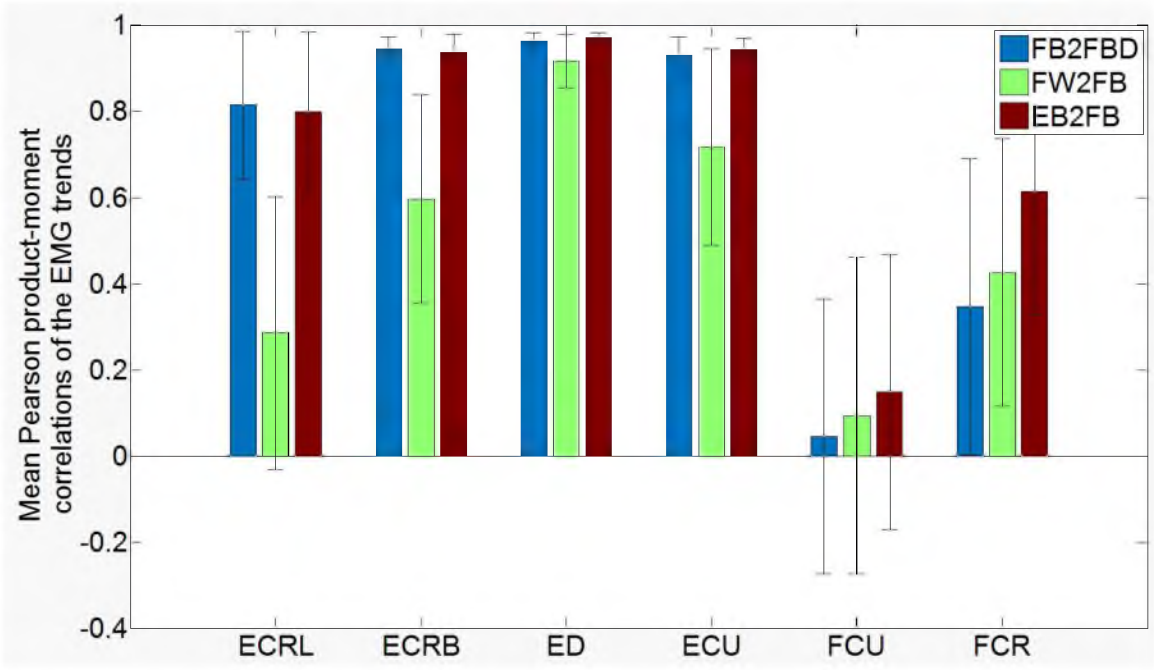

Figure 4.20. Mean Pearson product-moment correlations of the filtered binned EMG readings for the FlexBar®. FB2FBD: FlexBar® compared to the corresponding device, FW2FB: FlexBar compared to the free weight, EB2FB: FlexBar compared to the exercise band.

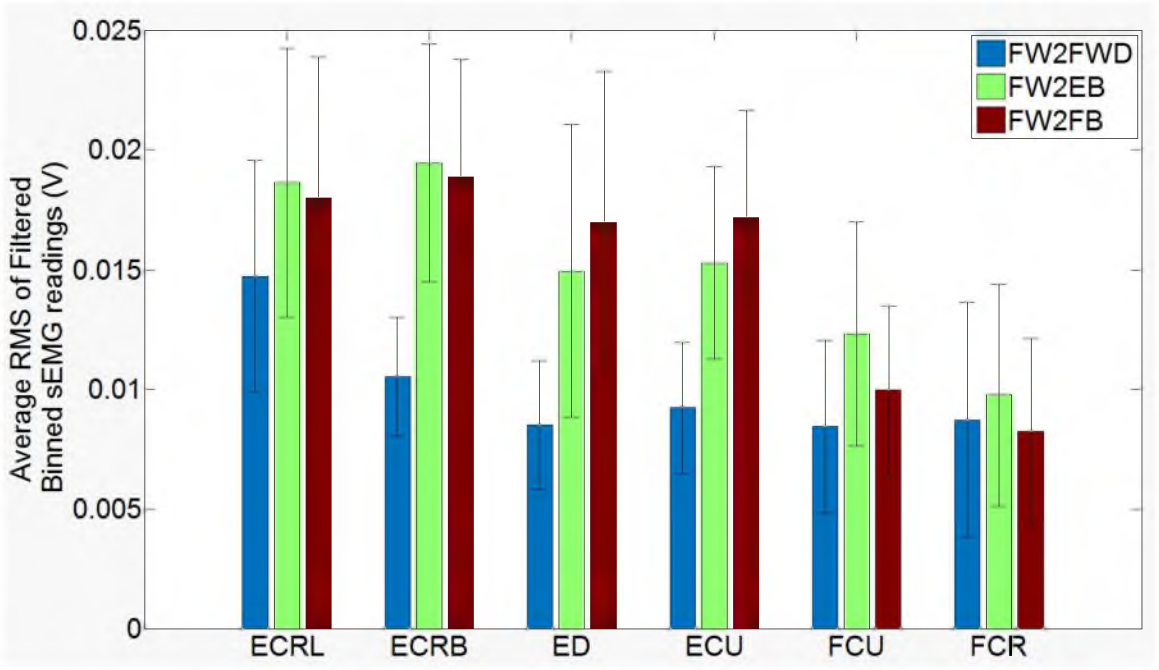

Figure 4.21. Mean RMS of the filtered binned EMG readings for the free weight. FW2FWD: Free weight compared to the corresponding device, FW2EB: Free weight compared to the exercise band, FB2EB: Free weight compared to the FlexBar®.

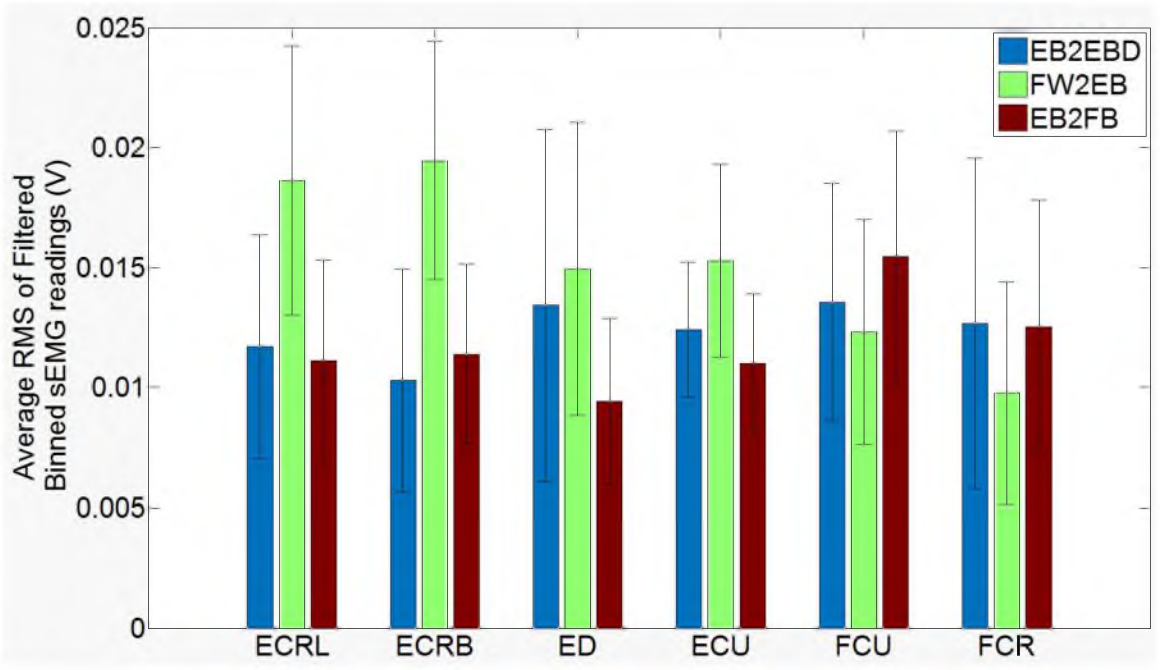

Figure 4.22. Mean RMS of the filtered binned EMG readings for the exercise band. EB2EBD: Exercise band compared to the corresponding device, FW2EB: Exercise band compared to the free weight, FB2EB: Exercise band compared to the FlexBar®.

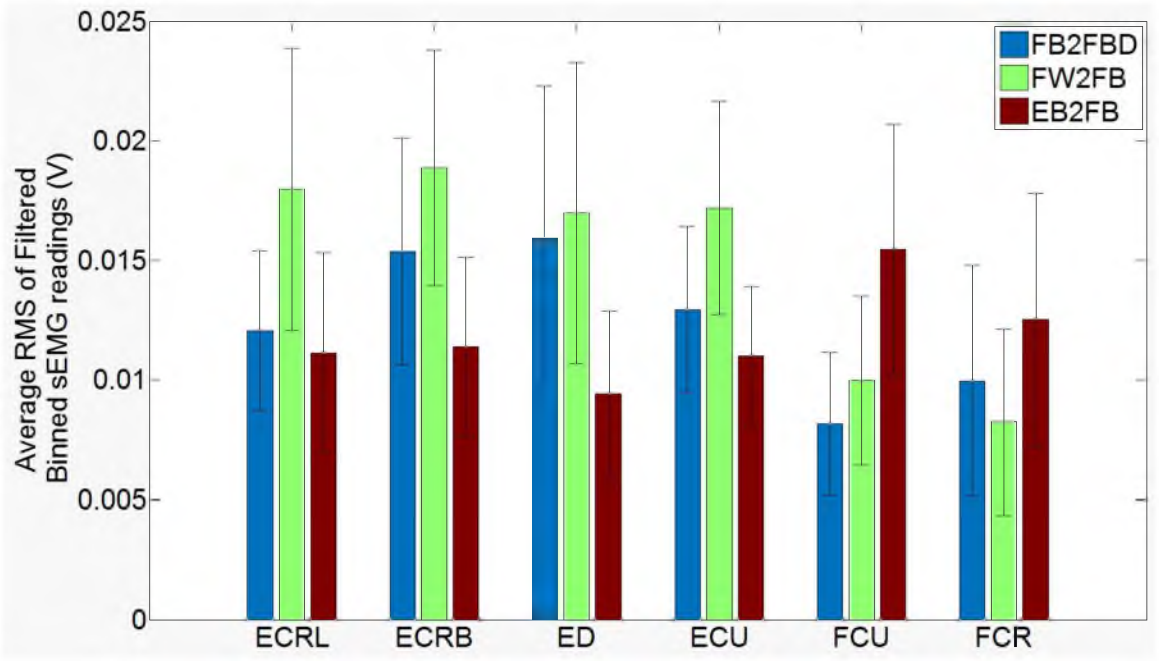

Figure 4.23. Mean RMS of the filtered binned EMG readings for the FlexBar®. FB2FBD: FlexBar® compared to the corresponding device, FW2FB: FlexBar compared to the free weight, EB2FB: FlexBar® compared to the exercise band.

CHAPTER 5

DISCUSSION

A goal for device development was to achieve reasonable simulation of the conventional loading methods. There were few significant differences found between the conventional methods and corresponding device model. However, there were also few significant differences found between the conventional methods. The Pearson coefficients and RMS values indicate that the device and conventional methods are comparable in simulating the three conventional loading methods. The differing torque profiles discussed in Section 1.2 and further explained in Section 3.3.4 would indicate greater differences may be appropriate. It is suggested that alternative metrics be considered to further differentiate the physiological effects of these varying loading profiles. The results from the motion analysis showed some statistical significance between wrist marker motion across the loading methods. However, the wrist marker motion range differences between the loading methods were small, mean difference in range ¡ 1 cm. It remains unclear if this is an artifact of the handle orientation, ulnar-radial contribution, or due to another feature of the setup. It also remains unclear if this would have a detrimental effect on rehabilitation patients if left unaddressed. A literature review of the effects of similar joint restrictions in existing weight machines has returned no results. Caution would be warranted while testing rehabilitation protocols in the future if this wrist motion discrepancy is not addressed in future revisions.

There remains additional functionality and versatility in the device that was not tested under these criteria. The results indicate that the device is reasonably capable of simulating the loading profiles of conventional therapies. Additionally, the device has the added benefit of quantifying and recording key performance metrics for remote review as well as the ability to assist a participant in concentric extension. The combination of this load generation efficacy and functional versatility supports further development and testing.

CHAPTER 6

CONCLUSION

6.1 Summary

This document has presented a new device to help facilitate research related to a common musculoskeletal condition, lateral epicondylalgia, that affects 1-3% of the population [1]. The objectives for this device, as described in Section 1.4, were as follows:

- Variable speed, frequency, and load of wrist extensions
- Simulate conventional loading methods
- Simulate loading methods not yet tested
- Assist motions when desired
- Track and save patient performance metrics for study and evaluation

The development of the device to meet these objectives has been described as well as the testing to quantify the proficiency of the device at simulating conventional loading methods. The development and testing included development of kinetic models of three conventional eccentric therapy loading methods, safeguards to protect participants, and novel surface electromyography analysis methods.

The results of the motion capture and surface electromyography study found little difference between the conventional loading methods and the corresponding device model for all three conventional methods. This seems to indicate the device is effective at providing stimuli similar to the conventional methods with the added benefits. These benefits include quantification of multiple performance metrics and additional functionality available with robotic devices such as motion assistance and potential tele-therapy supervision. Little difference was also found within the results between the conventional loading methods. This similarity indicates further development of more representative comparison metrics may be necessary.

6.2 Future Work

Multiple motions patterns were apparent in the wrist marker coordinates through the range of motion under differing conditions and within the flexion-extension and ulnar-radial deviation angle relationship. Further analysis of these results may provide insight in how to improve the device for simulating conventional methods as well as more general knowledge on wrist flexion-extension under various conditions. Further studies analyzing these variables may lead to improvements in repetitive stress injury prevention.

In the scope of rehabilitation opposed to prevention, future clinical trials with the device will allow a true test of the efficacy of the device. Facilitating randomized control trials comparing protocols of varying loading intensity, loading torque-angle profile, frequency, and/or pain level is the primary design function of this device. These studies may reap invaluable insights in treatment of LE and potentially other similar tendinopathies. If randomized control trials deem therapy with the device beneficial, a plethora of features can be developed to expand the device effectiveness including:

- real time performance updates and analysis to patients,
- tracking and modification of assessment and training sessions through internet connectivity,
- and incentivizing therapy compliance through gaming.

In conclusion, the device presented in this document has proven to be effective at simulating conventional methods and has added functionality over conventional methods. Further studies are necessary to assess the device's clinical benefit but the potential for this device and its capabilities are substantial.

APPENDIX

USER INTERFACE

The user interface encompasses the graphic user interface, the user pain input, the armrest, the handle, and additional attributes of the user experience, specifically sound and feel.

A.1 Graphic User Interface

A graphic user interface was created to allow the user to have high-level control of the training parameters. This graphic user interface consisted of assessment modules (range of motion tests, isometric tests, etc.), training modules (a torque-defined training module and angular velocity-defined training module), and support modules. The support modules facilitate transitions between modules, record management, and review. The Research-Based Web Design and Usability Guidelines supplied by U.S. Department of Health and Human Services Usability.gov were used to guide design choices [58]. These guidelines provided research-based conventions used for user interfaces. The interface features affected by this guidance include items such as the following: use of radio buttons for mutually exclusive selections and use of checkboxes for multiple selections [59], use of common fonts and a minimum of 12-point font [60], and save and display data so a user does not have to recall previous inputs or recorded values [61].

A.1.1 Interface Modules and Corresponding Control Schemes

There are some features that were implemented across the modules. These include the following: pain input is recorded and displayed across the range of motion, a transition function to smoothly switch between behaviors, display of current handle location, as well as recording and editing of comments. The general layout of the modules is displayed in Figure A.1.

A.1.2 Active Range of Motion

The active range of motion module, displayed in Figure A.2, utilizes a zero desired torque control allowing the training user to move to the extent of their active range of motion in flexion and extension through their own volition and capability. Neutral posture is recorded from training user input. The control flow for the active range of motion assessment is displayed in Figure A.3.

A.1.3 Passive Range of Motion

The passive range of motion module, displayed in Figure A.4, was conducted similar to the active range of motion but the device rotated the handle into flexion and extension at an adjustable speed. The motion stops upon a measured torque exceeding the adjustable torque cut-off or the pain input exceeding the adjustable pain cut-off. Neutral posture is recorded similar to the active range of motion module. The control flow for passive range of motion assessment is displayed in Figure A.5.

A.1.4 Isometric Assessments

The isometric module, displayed in Figure A.6, includes both isometric fatigue test and isometric break test capability. The fatigue test supplies a stationary handle to which the training user is able to apply maximal flexion and extension to record the torque at selected wrist postures. Torque applied is recorded and presented as the maximum torque and displayable presented over the time period of the exertion test. The control flow for isometric fatigue assessment is displayed in Figure A.7.

The isometric break test starts as a zero torque and increases according to an adjustable rate in the direction selected by the driving user. The training user is meant to keep the handle stationary as long as possible. Upon deviating from the set angle by more than five degrees, the test ends and the maximum torque is presented for the tested angle. The control flow for isometric break assessment is displayed in Figure A.8.

A.1.5 Torque-Controlled Training

The force controlled training, displayed in Figure A.9, supplies an adjustable torque for extensor eccentric contraction and assists the training user back to a maximal extension position when maximal flexion is reached. The training user is to resist the extensor elongation according to the effort prescribed by the driving user. If the training user inputs a pain higher than the selected cut-off pain, the system will shut down to have the torque value modified. More advanced torque-defined stimuli customization is available

to advanced training users. The control flow for torque-controlled training is displayed in Figure A.10.

A.1.6 Velocity-Controlled Training

The velocity-controlled training, displayed in Figure A.11, supplies an adjustable velocity for extensor eccentric contraction and assists the training user back to a maximal extension position when maximal flexion is reached. The training user is to resist the extensor elongation according to the effort prescribed by the driving user. Similar to the torque control module, if the training user inputs a pain higher than the selected value, the system will shut down to have the torque value modified. More advanced velocity-defined stimuli customization is available to advanced training users. The control flow for velocity-controlled training is displayed in Figure A.12.

A.1.7 Additional Testing and Training Modules

Consultation with Dr. Paul LaStayo indicated that a simplification of features for the majority of users would be beneficial. Customization of torque-angle profiles was transitioned to Advanced Settings, shown in Figure A.13. Driving users researching more specific torque-defined stimuli are able to access these advanced settings.

A.2 Pain Measurement

Several pain input methods were tested to improve ease of use and intuition. The main design goals included measurement throughout the range of motion and allow analog measurement of pain opposed to a binary pain-no pain approach. Three designs were tested and preliminary findings are presented in Table A.1.

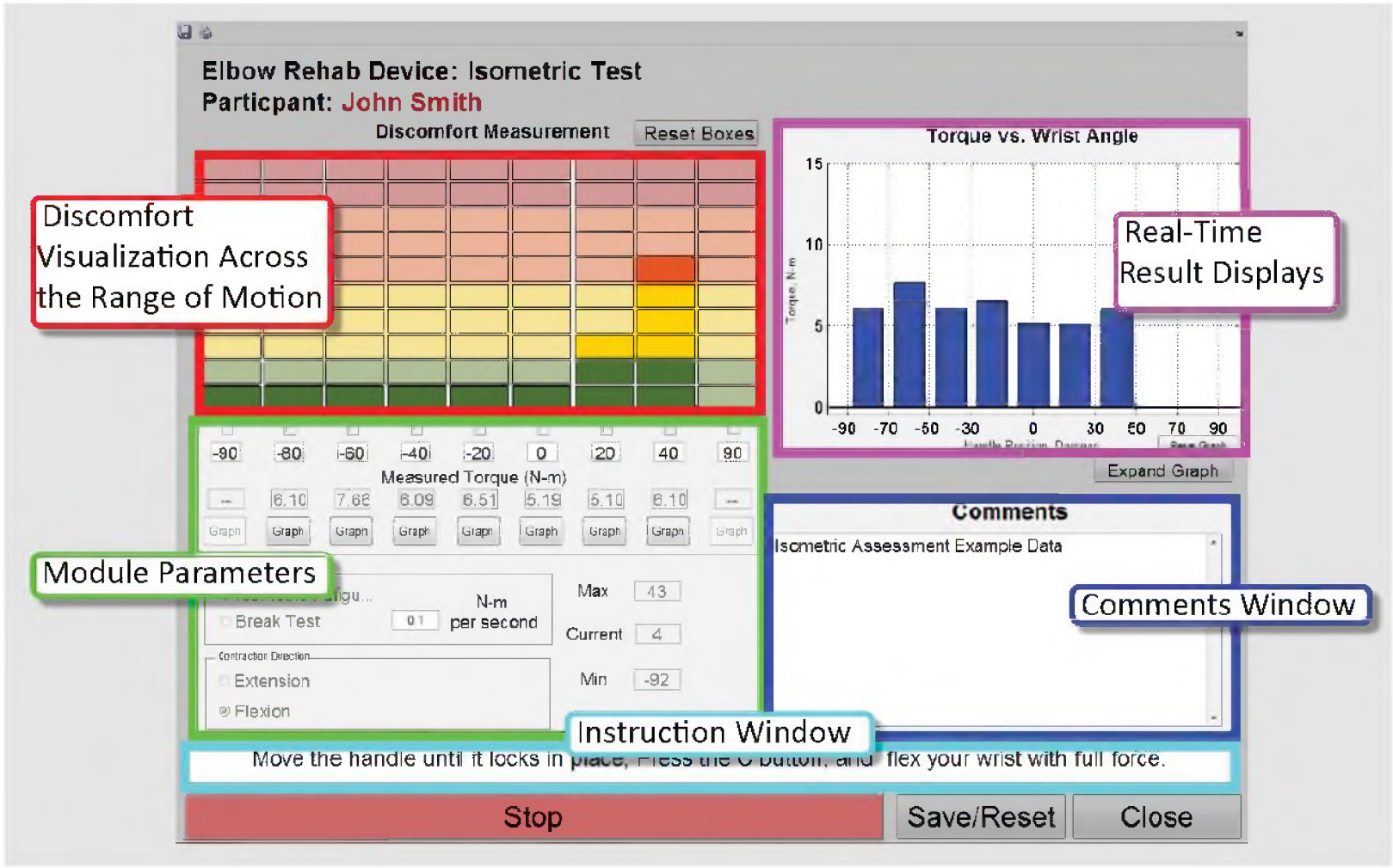

Figure A.1. General module components

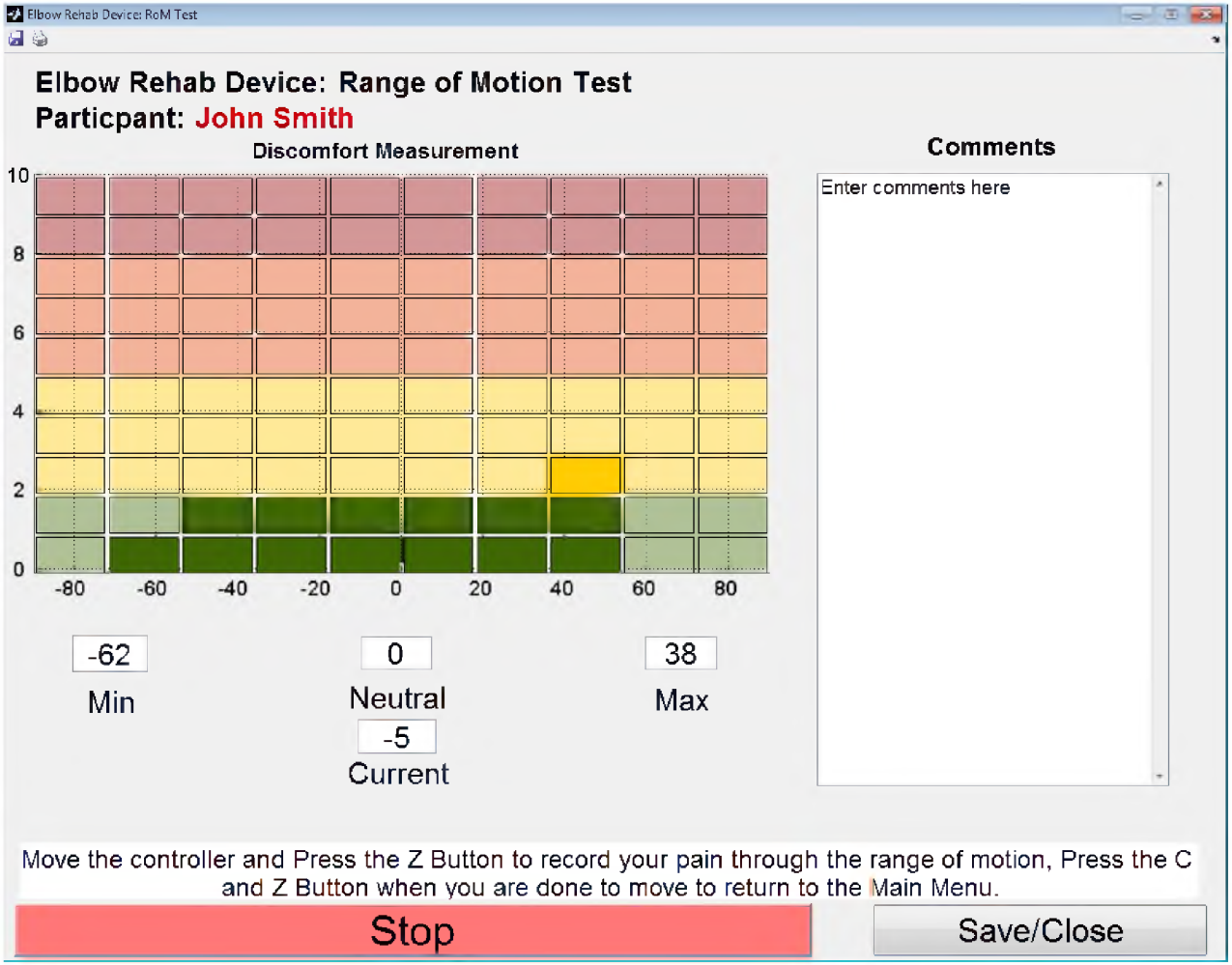

Figure A.2. Example active range of motion assessment module

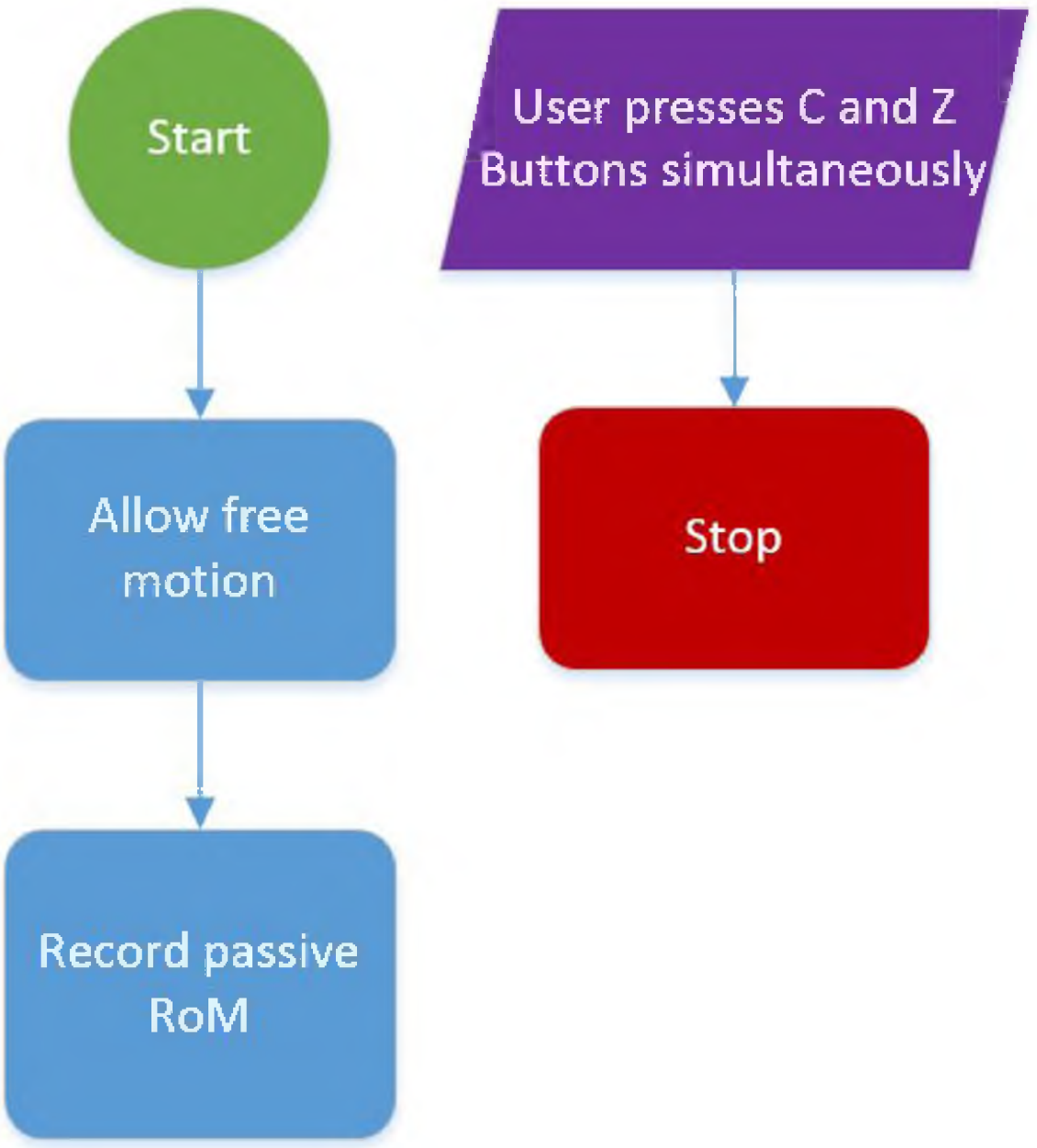

Figure A.3. Active range of motion control flow diagram

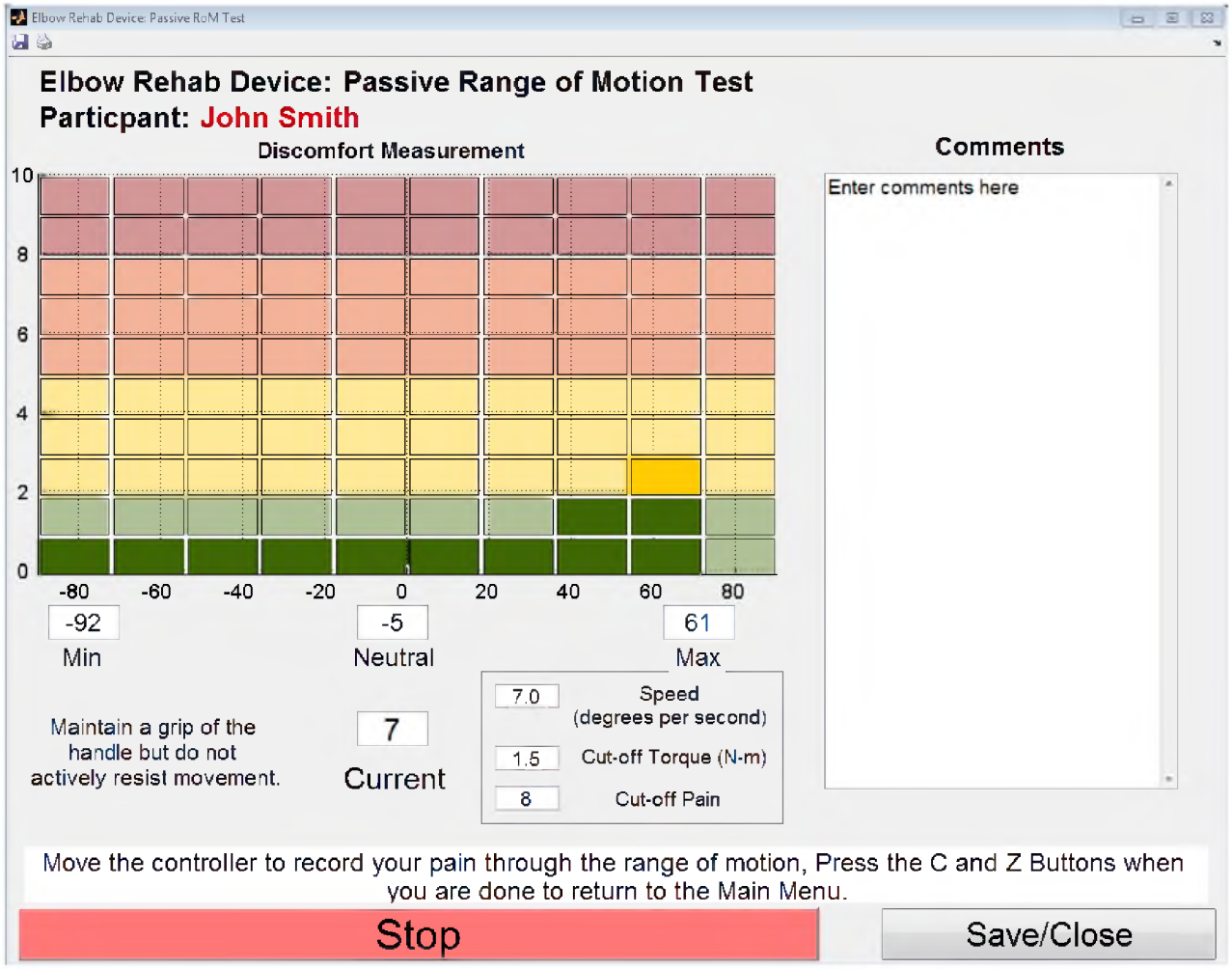

Figure A.4. Example passive range of motion assessment module

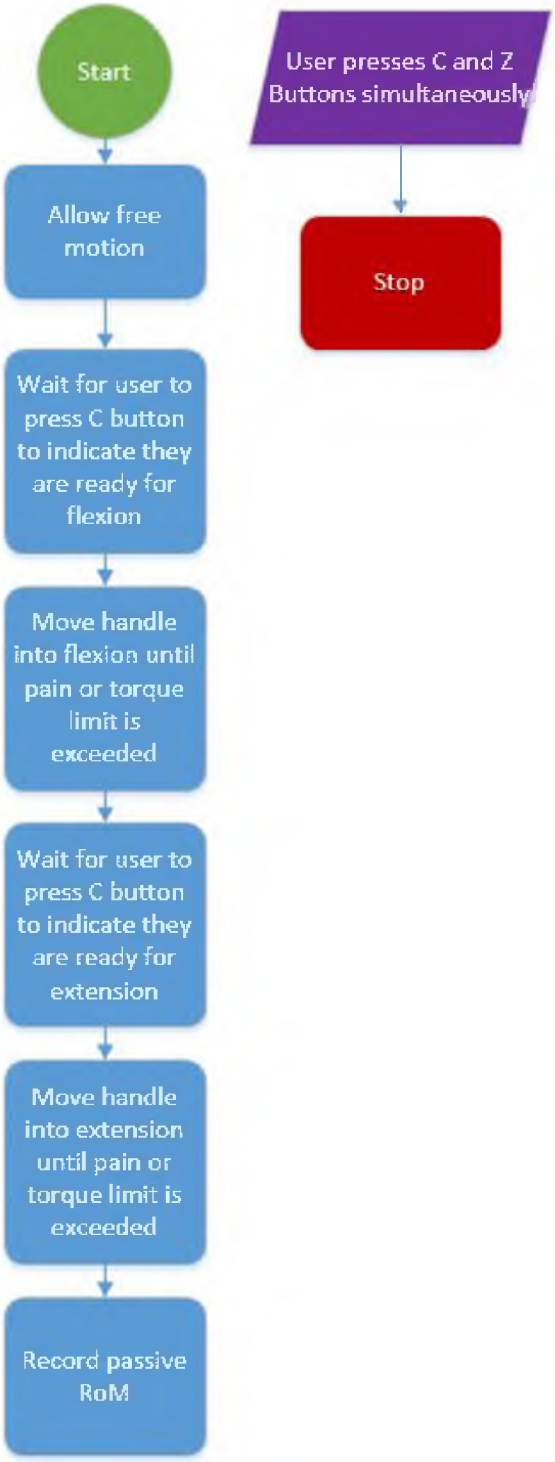

Figure A.5. Passive range of motion control flow diagram

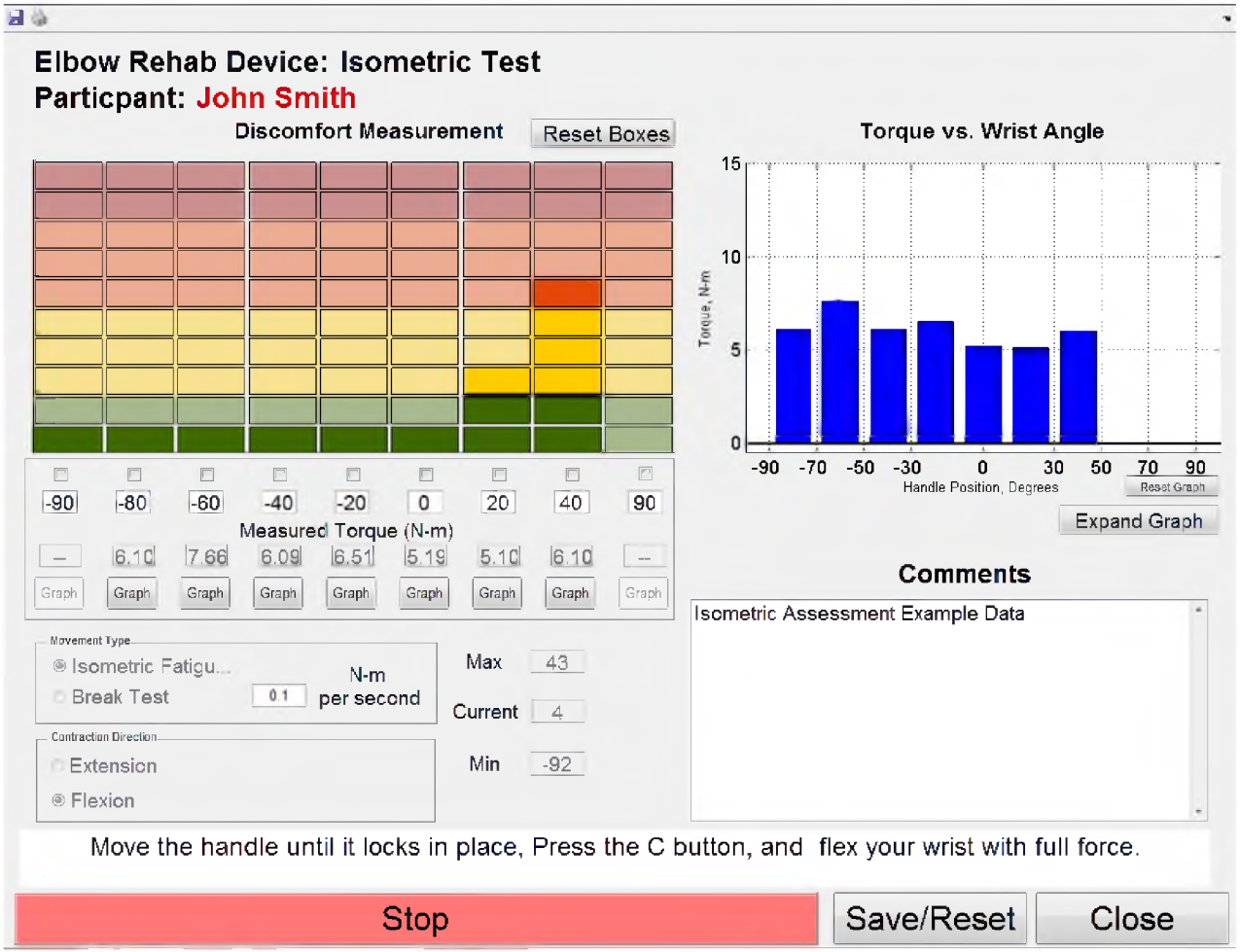

Figure A.6. Example isometric assessment module

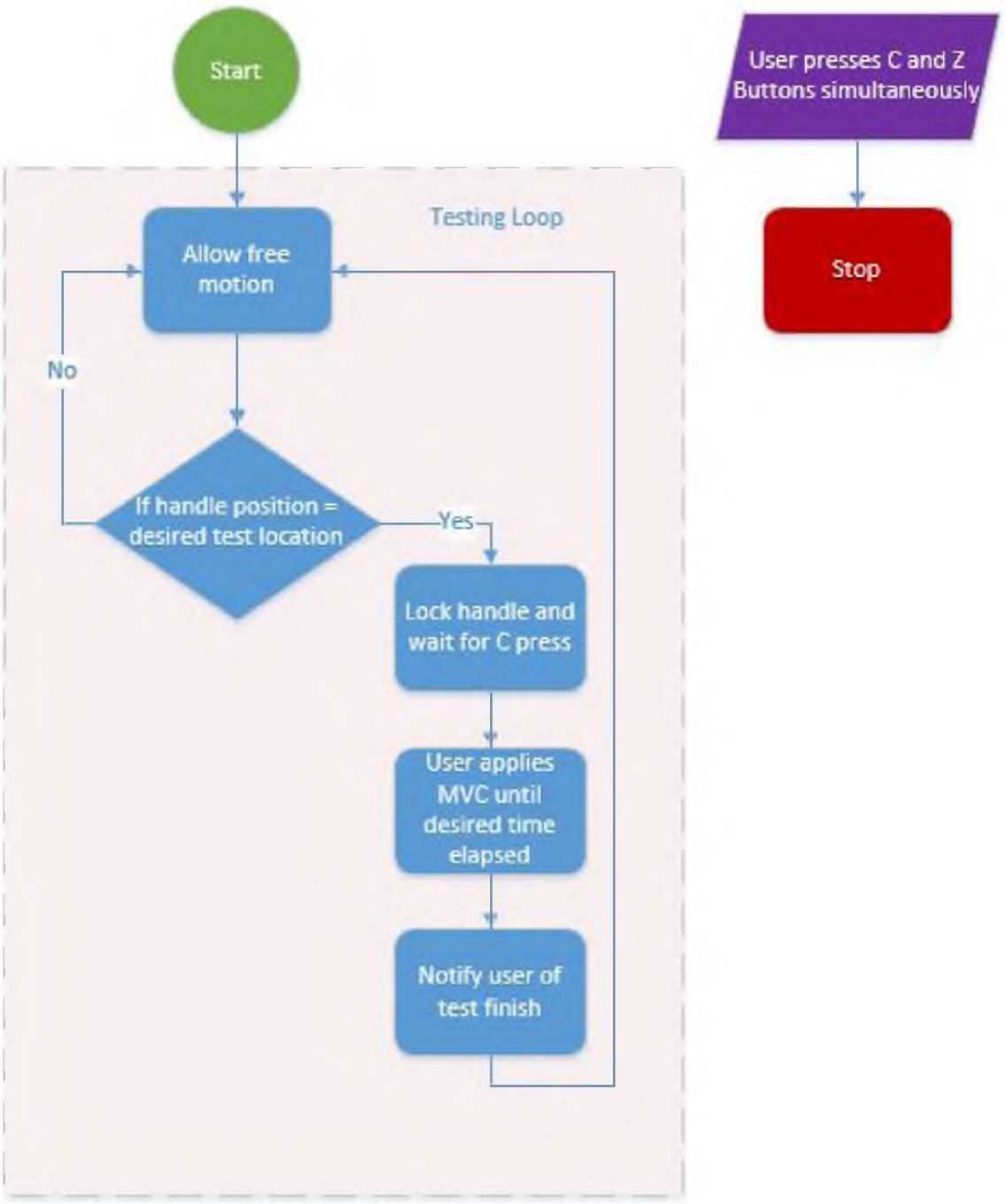

Figure A.7. Isometric fatigue control flow diagram

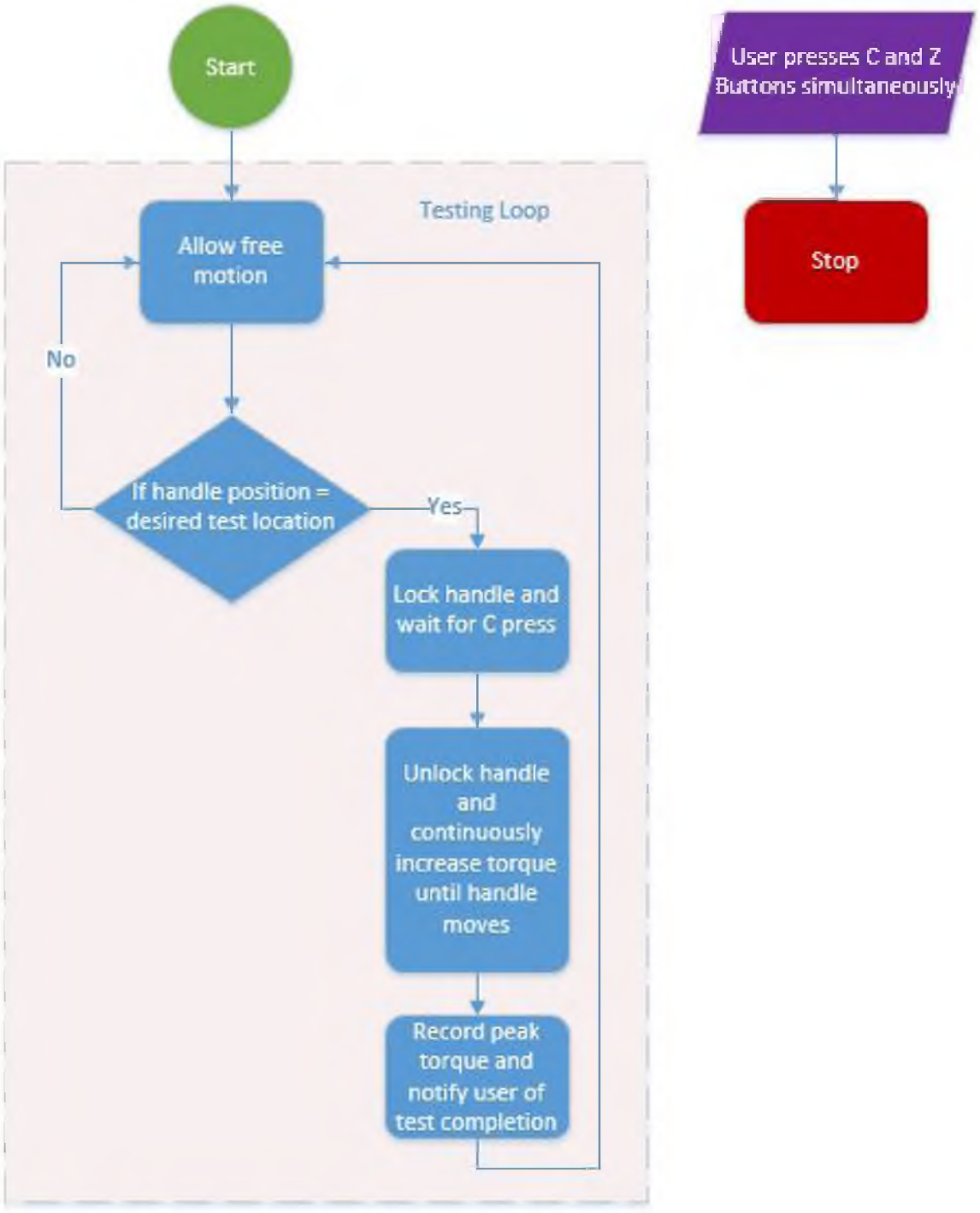

Figure A.8. Isometric break control flow diagram

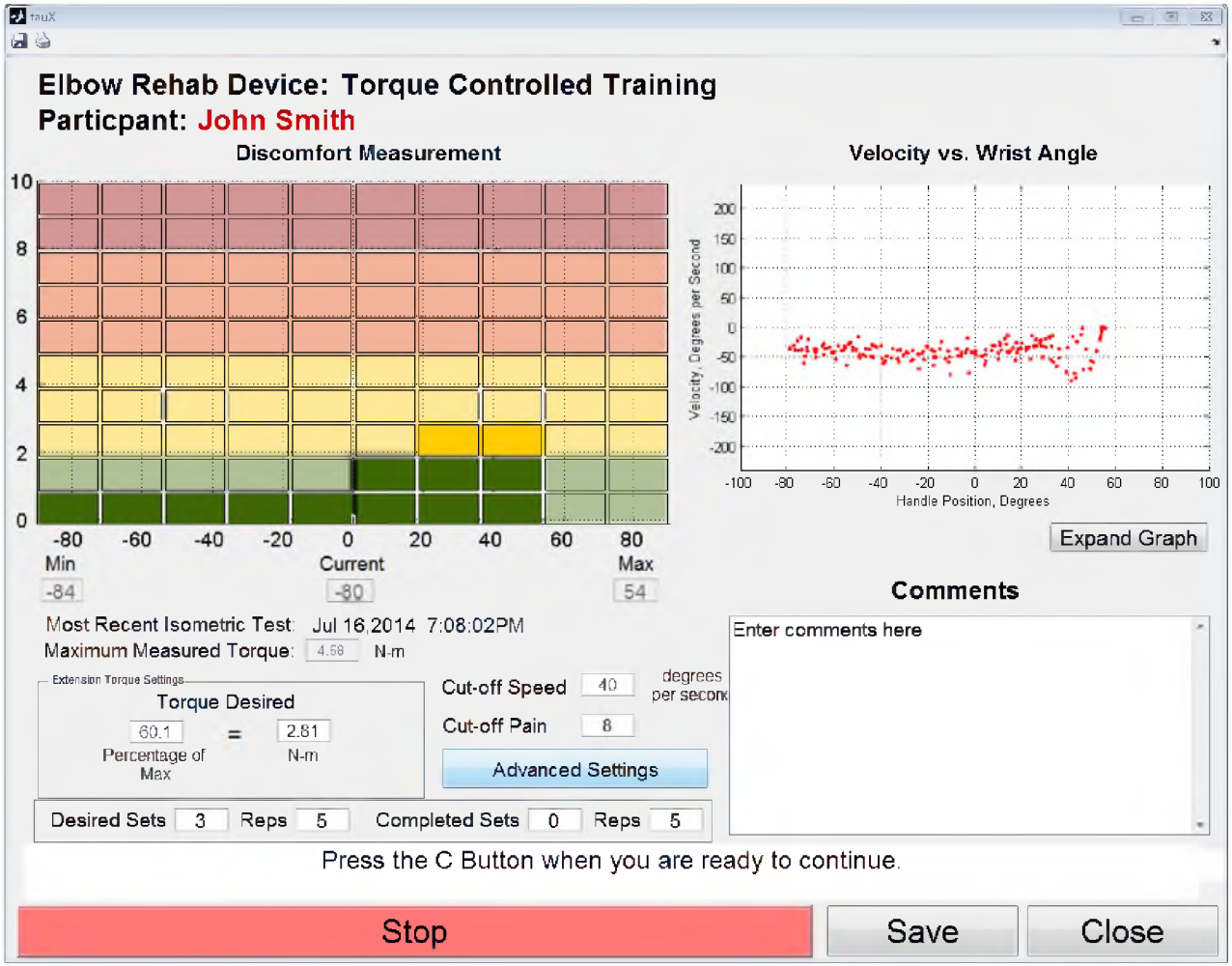

Figure A.9. Example torque-controlled training module

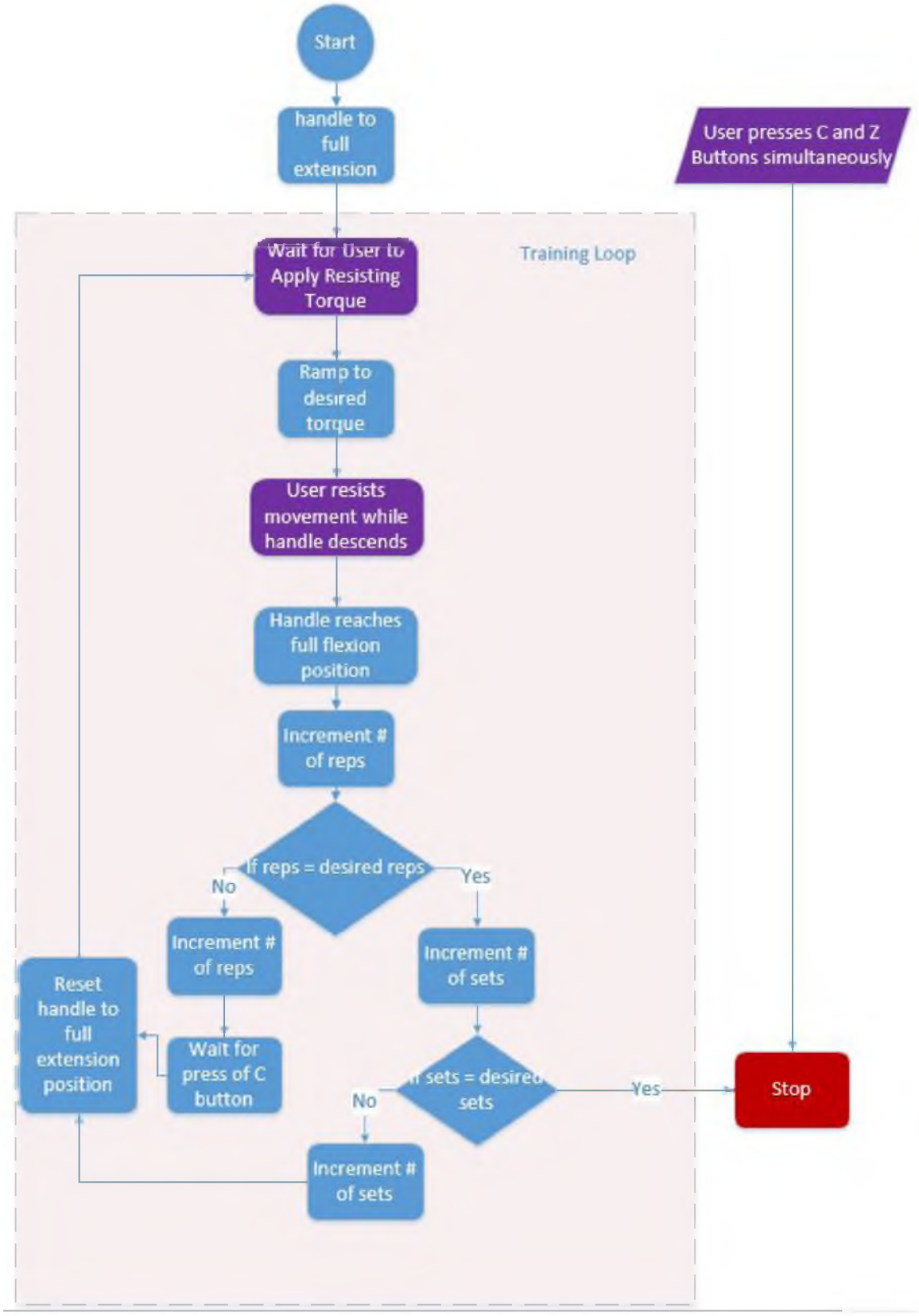

Figure A.10. Torque-controlled training control flow diagram

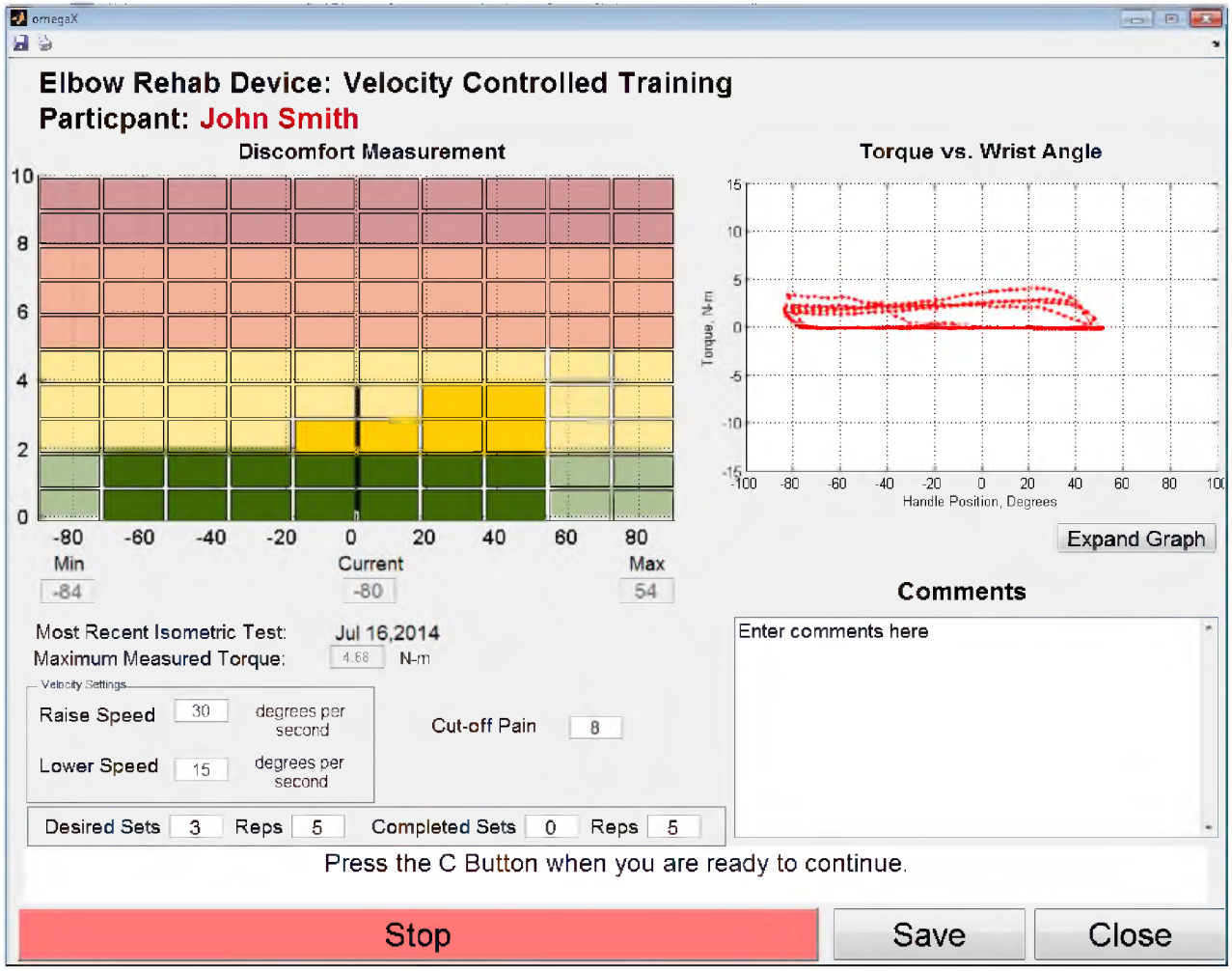

Figure A.11. Example velocity-controlled training module

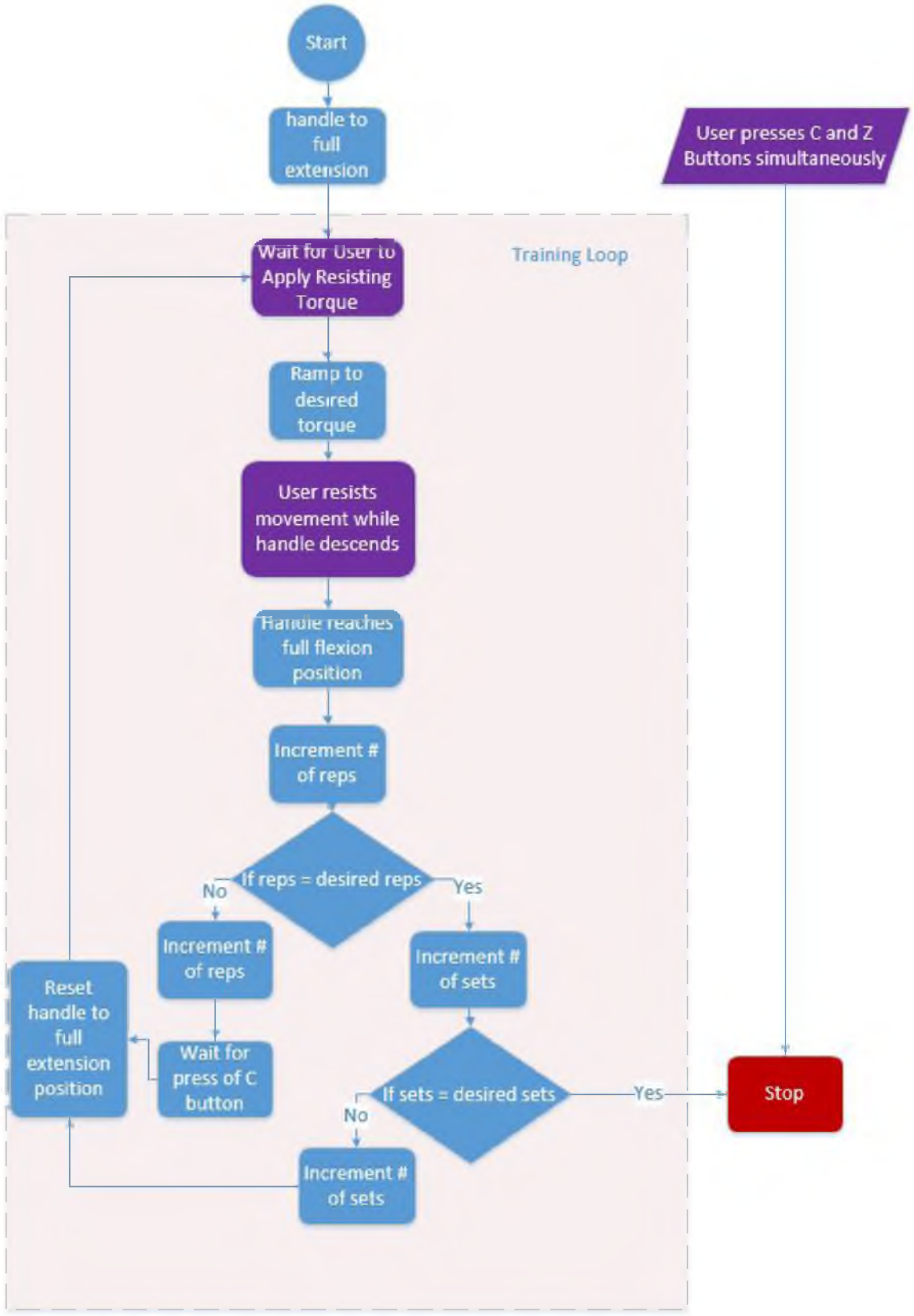

Figure A.12. Velocity-controlled training control flow diagram

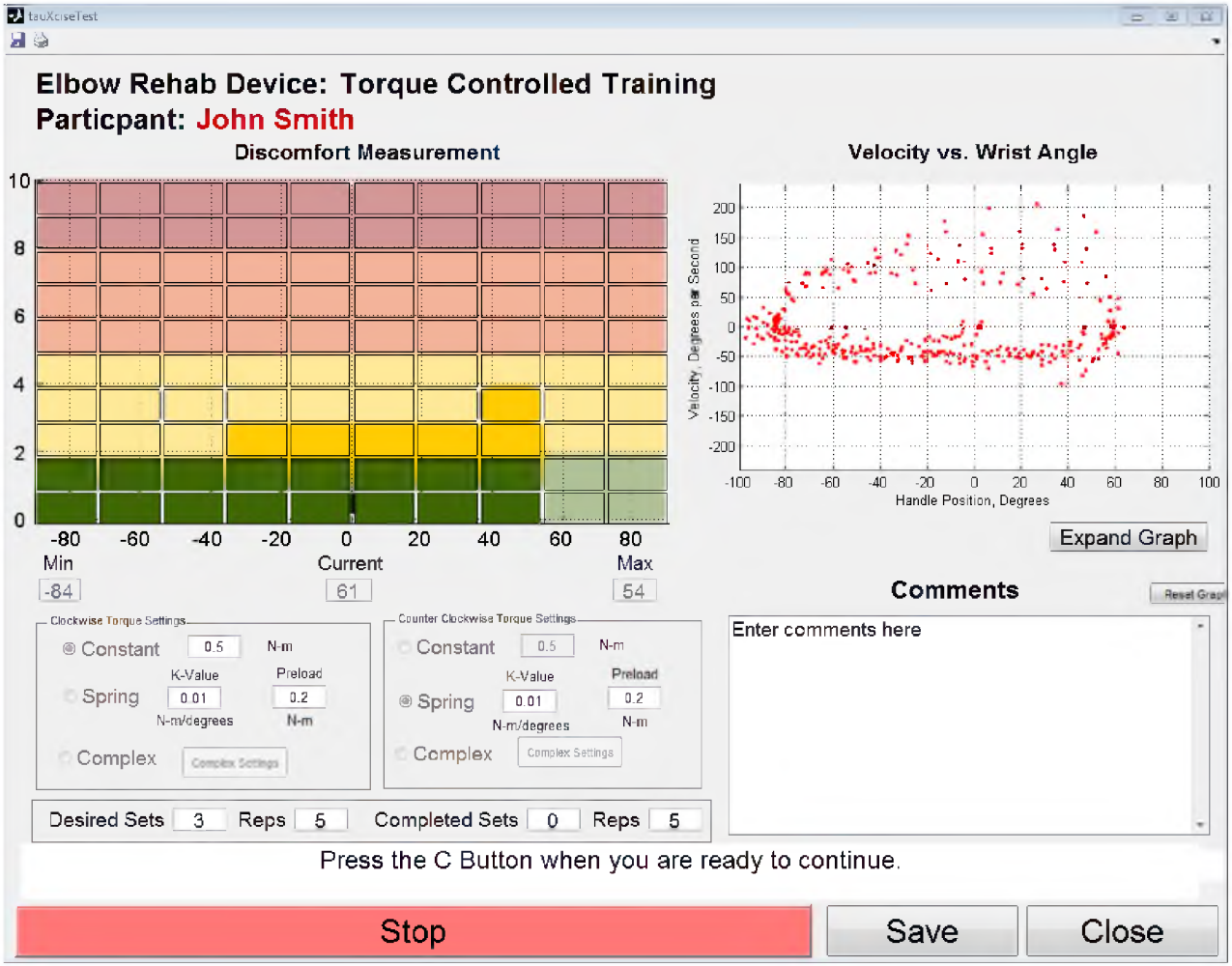

Figure A.13. Example advanced torque-controlled training

Table A.1. Pain input methods and preliminary results

Input method	**Actuation**	**Advantages**	**Disadvantages**
Opposite hand- Thumb joystick	Thumb flexion	-Intuitive mapping to 1-10 pain scale	
Opposite hand- Accelerometer	Wrist ulnar-radial deviation or elbow flexion-extension		-Use of proprioceptive system for pain mapping
Same hand- Thumb button	Thumb flexion	-Intuitive mapping to 1-10 pain scale -Same hand/elbow allows for easier tracking	

REFERENCES

[1] L. Dimberg, "The prevalence and causation of tennis elbow (lateral humeral epicondylitis) in a population of workers in an engineering industry," *Ergonomics*, vol. 30, no. 3, pp. 573–579, 1987.

[2] P. G. Hamilton, "The prevalence of humeral epicondylitis: a survey in general practice," *The Journal of the Royal College of General Practitioners*, vol. 36, no. 291, p. 464, 1986.

[3] J. H. Cyriax, "The pathology and treatment of tennis elbow," *The Journal of Bone & Joint Surgery*, vol. 18, no. 4, pp. 921–940, 1936.

[4] L. Bisset, A. Paungmali, B. Vicenzino, and E. Beller, "A systematic review and meta-analysis of clinical trials on physical interventions for lateral epicondylalgia," *British Journal of Sports Medicine*, vol. 39, no. 7, pp. 411–422, 2005.

[5] H. Labelle, R. Guibert, J. Joncas, N. Newman, M. Fallaha, and C. Rivard, "Lack of scientific evidence for the treatment of lateral epicondylitis of the elbow. an attempted meta-analysis," *Journal of Bone & Joint Surgery, British Volume*, vol. 74, no. 5, pp. 646–651, 1992.

[6] A. B. Leger and T. E. Milner, "Muscle function at the wrist after eccentric exercise," *Medicine and Science in Sports and Exercise*, vol. 33, no. 4, pp. 612–620, 2001.

[7] J. Raman, J. C. MacDermid, and R. Grewal, "Effectiveness of different methods of resistance exercises in lateral epicondylosisa systematic review," *Journal of Hand Therapy*, 2011.

[8] N. Smidt, W. Assendelft, H. Arola, A. Malmivaara, S. Green, R. Buchbinder, D. Van Der Windt, and L. Bouter, "Effectiveness of physiotherapy for lateral epicondylitis: a systematic review," *Annals of Medicine*, vol. 35, no. 1, pp. 51–62, 2003.

[9] K. Hegmann, *American College of Occupational and Environmental Medicine's Occupational Medicine Practice Guidelines 3rd Edition*, Elk Grove Village, IL: ACOEM. 192 pages, 456 references., 2011.

[10] Q. N. Hong, M.-J. Durand, and P. Loisel, "Treatment of lateral epicondylitis: where is the evidence?" *Joint Bone Spine*, vol. 71, no. 5, pp. 369–373, 2004.

[11] P. Nilsson, E. Lindgren, and J. Mnsson, "Lateral epicondylalgia. a quantitative and qualitative analysis of interdisciplinary cooperation and treatment choice in the swedish health care system," *Scandinavian Journal of Caring Sciences*, vol. 26, no. 1, pp. 28–37, 2011.

[12] H. Alfredson, T. Pietil, P. Jonsson, and R. Lorentzon, "Heavy-load eccentric calf muscle training for the treatment of chronic achilles tendinosis," *The American Journal of Sports Medicine*, vol. 26, no. 3, pp. 360–366, 1998.

[13] J. L. Croisier, M. Foidart-Dessalle, F. Tinant, J. M. Crielaard, and B. Forthomme, "An isokinetic eccentric programme for the management of chronic lateral epicondylar tendinopathy," *British Journal of Sports Medicine*, vol. 41, no. 4, pp. 269–75, 2007.

[14] M. Fahlstrm, P. Jonsson, R. Lorentzon, and H. Alfredson, "Chronic achilles tendon pain treated with eccentric calf-muscle training," *Knee Surgery, Sports Traumatology, Arthroscopy*, vol. 11, no. 5, pp. 327–333, 2003.

[15] A. M. Frohm, T. Saartok, K. Halvorsen, and P. Renstrom, "Eccentric treatment for patellar tendinopathy-a prospective randomised short-term pilot study of two rehabilitation protocols," *British Journal of Sports Medicine*, 2007.

[16] N. Mafi, R. Lorentzon, and H. Alfredson, "Superior short-term results with eccentric calf muscle training compared to concentric training in a randomized prospective multicenter study on patients with chronic achilles tendinosis," *Knee Surgery, Sports Traumatology, Arthroscopy*, vol. 9, no. 1, pp. 42–47, 2001.

[17] P. Manias and D. Stasinopoulos, "A controlled clinical pilot trial to study the effectiveness of ice as a supplement to the exercise programme for the management of lateral elbow tendinopathy," *British Journal of Sports Medicine*, vol. 40, no. 1, pp. 81–5, 2006.

[18] J. A. Martinez-Silvestrini, K. L. Newcomer, R. E. Gay, M. P. Schaefer, P. Kortebein, and K. W. Arendt, "Chronic lateral epicondylitis: comparative effectiveness of a home exercise program including stretching alone versus stretching supplemented with eccentric or concentric strengthening," *Journal of Hand Therapy*, vol. 18, no. 4, pp. 411–9, quiz 420, 2005.

[19] P. Nilsson, E. Thom, A. Baigi, B. Marklund, and J. Mansson, "A prospective pilot study of a multidisciplinary home training programme for lateral epicondylitis," *Musculoskeletal Care*, vol. 5, no. 1, pp. 36–50, 2007.

[20] L. Öhberg, R. Lorentzon, and H. Alfredson, "Eccentric training in patients with chronic achilles tendinosis: normalised tendon structure and decreased thickness at follow up," *British Journal of Sports Medicine*, vol. 38, no. 1, pp. 8–11, 2004.

[21] T. T. Pienimki, T. K. Tarvainen, P. T. Siira, and H. Vanharanta, "Progressive strengthening and stretching exercises and ultrasound for chronic lateral epicondylitis," *Physiotherapy*, vol. 82, no. 9, pp. 522–530, 1996.

[22] D. Stasinopoulos and I. Stasinopoulos, "Comparison of effects of cyriax physiotherapy, a supervised exercise programme and polarized polychromatic non-coherent light (bioptron light) for the treatment of lateral epicondylitis," *Clinical Rehabilitation*, vol. 20, no. 1, pp. 12–23, 2006.

[23] B. Svernlöv and L. Adolfsson, "Nonoperative treatment regime including eccentric training for lateral humeral epicondylalgia," *Scandinavian Journal of Medicine & Science in Sports*, vol. 11, no. 6, pp. 328–334, 2001.

[24] B. L. Woodley, R. J. Newsham-West, and G. D. Baxter, "Chronic tendinopathy: effectiveness of eccentric exercise," *British Journal of Sports Medicine*, vol. 41, no. 4, pp. 188–198, 2007.

[25] B. Murtaugh and J. M. Ihm, "Eccentric training for the treatment of tendinopathies," *Current Sports Medicine Reports*, vol. 12, no. 3, pp. 175–182, 2013.

[26] H. Langberg and M. Kongsgaard, "Eccentric training in tendinopathymore questions than answers," *Scandinavian Journal of Medicine & Science in Sports*, vol. 18, no. 5, pp. 541–542, 2008.

[27] T. F. Tyler, G. C. Thomas, S. J. Nicholas, and M. P. McHugh, "Addition of isolated wrist extensor eccentric exercise to standard treatment for chronic lateral epicondylosis: A prospective randomized trial," *Journal of Shoulder and Elbow Surgery*, vol. 19, no. 6, pp. 917–922, 2010.

[28] D. Frost, J. Cronin, and R. Newton, "A biomechanical evaluation of resistance," *Sports Medicine*, vol. 40, no. 4, pp. 303–326, 2010.

[29] D. Reinkensmeyer and M. Boninger, "Technologies and combination therapies for enhancing movement training for people with a disability," *Journal of Neuroengineering and Rehabilitation*, vol. 9, no. 1, p. 17, 2012.

[30] H. I. Krebs, N. Hogan, M. L. Aisen, and B. T. Volpe, "Robot-aided neurorehabilitation," *Rehabilitation Engineering, IEEE Transactions on*, vol. 6, no. 1, pp. 75–87, 1998.

[31] D. J. Reinkensmeyer, L. E. Kahn, M. Averbuch, A. McKenna-Cole, B. D. Schmit, and W. Z. Rymer, "Understanding and treating arm movement impairment after chronic brain injury: progress with the arm guide," *Journal of Rehabilitation Research & Development*, vol. 37, no. 6, 2000.

[32] H. I. Krebs, B. T. Volpe, D. Williams, J. Celestino, S. K. Charles, D. Lynch, and N. Hogan, "Robot-aided neurorehabilitation: a robot for wrist rehabilitation," *Neural Systems and Rehabilitation Engineering, IEEE Transactions on*, vol. 15, no. 3, pp. 327–335, 2007.

[33] T. Nef, M. Mihelj, and R. Riener, "Armin: a robot for patient-cooperative arm therapy," *Medical & Biological Engineering & Computing*, vol. 45, no. 9, pp. 887–900, 2007.

[34] G. Kwakkel, B. J. Kollen, and H. I. Krebs, "Effects of robot-assisted therapy on upper limb recovery after stroke: a systematic review," *Neurorehabilitation and Neural Repair*, vol. 22, no. 2, pp. 111–121, 2008.

[35] J. Y. Park, H. K. Park, J. H. Choi, E. S. Moon, B. S. Kim, W. S. Kim, and K. S. Oh, "Prospective evaluation of the effectiveness of a home-based program of isometric strengthening exercises: 12-month follow-up," *Clinics in Orthopedic Surgery*, vol. 2, no. 3, pp. 173–8, 2010.

[36] J. M. Vanswearingen, "Measuring wrist muscle strength," *Journal of Orthopaedic & Sports Physical Therapy*, vol. 4, no. 4, pp. 217–228, 1983.

[37] S. L. Delp, A. E. Grierson, and T. S. Buchanan, "Maximumisometric moments generated by the wrist muscles in flexion-extension and radial-ulnar deviation," *Journal of Biomechanics*, vol. 29, no. 10, pp. 1371–1375, 1996.

[38] P. W. Fong and G. Y. Ng, "Effect of wrist positioning on isokinetic performance and repeatability of measurement for wrist flexors and extensors," *Physiotherapy Theory and Practice*, vol. 16, no. 3, pp. 169–176, 2000.

[39] R. J. Marley and M. R. Thomson, "Isokinetic strength characteristics in wrist flexion and extension," *International Journal of Industrial Ergonomics*, vol. 25, no. 6, pp. 633–643, 2000.

[40] D. A. Winter, *Biomechanics and motor control of human movement*. John Wiley & Sons, 2009.

[41] F. Valero-Cuevas and C. Small, "Load dependence in carpal kinematics during wrist flexion in vivo," *Clinical Biomechanics*, vol. 12, no. 3, pp. 154–159, 1997.

[42] R. M. Patterson, C. L. Nicodemus, S. F. Viegas, K. W. Elder, and J. Rosenblatt, "High-speed, three-dimensional kinematic analysis of the normal wrist," *The Journal of Hand Surgery*, vol. 23, no. 3, pp. 446–453, 1998.

[43] R. Kaufmann, J. Pfaeffle, B. Blankenhorn, K. Stabile, D. Robertson, and R. Goitz, "Kinematics of the midcarpal and radiocarpal joints in radioulnar deviation: An in vitro study," *The Journal of Hand Surgery*, vol. 30, no. 5, pp. 937–942, 2005.

[44] R. A. Kaufmann, H. J. Pfaeffle, B. D. Blankenhorn, K. Stabile, D. Robertson, and R. Goitz, "Kinematics of the midcarpal and radiocarpal joint in flexion and extension: An in vitro study," *The Journal of Hand Surgery*, vol. 31, no. 7, pp. 1142–1148, 2006.

[45] G. Brigstocke, A. Hearnden, C. Holt, and G. Whatling, "The functional range of movement of the human wrist," *Journal of Hand Surgery (European Volume)*, vol. 38, no. 5, pp. 554–556, 2013.

[46] C. C. Gordon, T. Churchill, C. E. Clauser, B. Bradtmiller, and J. T. McConville, "Anthropometric survey of us army personnel: methods and summary statistics 1988," DTIC Document, Tech. Rep., 1989.

[47] J. W. Garrett, "The adult human hand: some anthropometric and biomechanical considerations," *Human Factors: The Journal of the Human Factors and Ergonomics Society*, vol. 13, no. 2, pp. 117–131, 1971.

[48] J. Ziegler and N. Nichols, "Optimum settings for automatic controllers," *Trans. ASME*, vol. 64, no. 11, 1942.

[49] A. S. McCormack and K. R. Godfrey, "Rule-based autotuning based on frequency domain identification," *Control Systems Technology, IEEE Transactions on*, vol. 6, no. 1, pp. 43–61, 1998.

[50] A. Perotto and E. F. Delagi, *Anatomical guide for the electromyographer: the limbs and trunk*. Charles C Thomas Publisher, 2005.

[51] Z.-M. Li, L. Kuxhaus, J. A. Fisk, and T. H. Christophel, "Coupling between wrist flexion–extension and radial–ulnar deviation," *Clinical Biomechanics*, vol. 20, no. 2, pp. 177–183, 2005.

[52] D. C. Boone and S. P. Azen, "Normal range of motion of joints in male subjects," *Journal of Bone and Joint Surgery (American Volume)*, vol. 61, no. 5, pp. 756–759, 1979.

[53] J. Ryu, W. P. Cooney III, L. J. Askew, K.-N. An, and E. Chao, "Functional ranges of motion of the wrist joint," *The Journal of Hand Surgery*, vol. 16, no. 3, pp. 409–419, 1991.

[54] M. M. Marshall, J. R. Mozrall, and J. E. Shealy, "The effects of complex wrist and forearm posture on wrist range of motion," *Human Factors: The Journal of the Human Factors and Ergonomics Society*, vol. 41, no. 2, pp. 205–213, 1999.

[55] P. Salvia, L. Woestyn, J. H. David, V. Feipel, S. Van, S. Jan, P. Klein, and M. Rooze, "Analysis of helical axes, pivot and envelope in active wrist circumduction," *Clinical Biomechanics*, vol. 15, no. 2, pp. 103–111, 2000.

[56] Z.-M. Li, "The influence of wrist position on individual finger forces during forceful grip," *The Journal of Hand Surgery*, vol. 27, no. 5, pp. 886–896, 2002.

[57] H. I. R. C. Heck, C.V., *Joint motion: method of measuring and recording, American Academy of Orthopaedic Surgeons*, Chicago, IL, 2011.

[58] M. O. Leavitt and B. Shneiderman, "Research-based web design & usability guidelines," *US Department of Health and Human Services*, 2006.

[59] W. O. Galitz, *The essential guide to user interface design: an introduction to GUI design principles and techniques.* John Wiley & Sons, 2007.

[60] M. Bernard and M. Mills, "So, what size and type of font should I use on my website," *Usability News*, vol. 2, no. 2, pp. 1–5, 2000.

[61] V. Ahlstrom and K. Longo, "Human factors design standard," *US: US Department of Transportation Federal Aviation Administration Technical Center*, 2003.